UNIVERSIDADE DE LISBOA

Faculdade de Medicina

Functional role of the Oc2M cortical area in the processing of multimodal sensory inputs in rats

Gonçalo Correia de Oliveira Ferreira

Supervisores: Professor Doutor Armando Miguel Caseiro Pires Remondes

Professora Doutora Luísa Maria Vaqueiro Lopes

Dissertação especialmente elaborada para obtenção do grau de Mestre em Neurociências

2019

UNIVERSIDADE DE LISBOA

Faculdade de Medicina

Functional role of the Oc2M cortical area in the processing of multimodal sensory inputs in rats

Gonçalo Correia de Oliveira Ferreira

Supervisores: Professor Doutor Armando Miguel Caseiro Pires Remondes

Professora Doutora Luísa Maria Vaqueiro Lopes

Dissertação especialmente elaborada para obtenção do grau de Mestre em Neurociências

2019

A impressão desta dissertação foi aprovada pelo Conselho Científico da Faculdade de Medicina de Lisboa em reunião de 17 de Dezembro de 2019.

Agradecimentos

Em primeiro lugar, gostaria de agradecer ao meu orientador Miguel Remondes por me ter aceite como membro na sua equipa de investigação. Obrigado por todo o conhecimento partilhado, por todos os conselhos, e por me ter dado autonomia e liberdade suficientes para tomar as minhas próprias decisões e aprender com os erros. Este projeto foi o maior desafio que alguma vez já tive de superar, e por isso obrigado.

Quero agradecer a todos os meus colegas de laboratório que tanto me ajudaram ao longo desta jornada, e que de alguma forma contribuíram para este trabalho. Tenho orgulho em dizer que muitos destes colegas se tornaram amigos. Em particular, quero agradecer à Ana, Bárbara, Emanuel, e Marcelo. Um muito obrigado.

Por último, quero agradecer aos grandes pilares da minha vida. Aos meus pais José e Ana Ferreira, ao meu irmão Miguel Ferreira, e à minha namorada Débora Falcão. Vocês são as pessoas que me têm sempre apoiado de forma incondicional. Sem vocês nunca teria conseguido chegar até aqui.

Resumo

Quase todos os organismos dotados de um sistema nervoso são confrontados, diariamente, com uma grande variedade de estímulos sensoriais. A forma como os animais (humanos e não-humanos) interagem com o mundo externo, está dependente da capacidade de integração das várias informações sensoriais em seu redor. Esta integração permite formar uma percepção coesa do ambiente envolta, como também possibilita a extração de informação relevante para tomar decisões comportamentais adequadas. Por outro lado, os sistemas sensoriais não processam informação isoladamente, e o conteúdo multissensorial presente nas nossas memórias episódicas sugere que, de alguma forma, o processamento de estímulos sensoriais está intrinsecamente relacionado com a formação e armazenamento de memórias.

O registo electrofisiológico *in vivo* da atividade neuronal em cérebros de modelos animais oferece a possibilidade de correlacionar a atividade cerebral detectada em específicas regiões do cérebro, com determinados outputs comportamentais. Este tipo experiências levaram à descoberta de células presentes no hipocampo, chamadas de 'place cells' (O'Keefe & Dostrovsky, 1971), que se acredita serem responsáveis pela formação de um mapa cognitivo que orienta a navegação no espaço (Keefe, 1976). Estas células podem representar não só a localização atual do animal, assim como localizações anteriores e futuras (Ferbinteanu & Shapiro, 2003; Frank, Brown, & Wilson, 2000). Mais tarde, a descoberta de neurónios com outras propriedades espaciais, tais como as 'células-grelha' (grid-cells, Hafting et al., 2005) células 'head-direction' (Sargolini et al., 2006) ou as células 'border' (Solstad, 2008), contribuíram para um maior entendimento acerca de como o cérebro codifica e organiza informação sensorial à sua volta, na forma de um mapa cognitivo espacial. Contudo, as regiões e os mecanismos subjacentes que levam à formação destes mapas cognitivos, com base na integração de estímulos sensoriais primários, ainda não são conhecidos.

Este projeto explora a região anatómica no cérebro do rato, designada como Oc2M, como um possível local de convergência na integração de

informação multimodal, crucial para a formação de memórias num contexto sensorial. Estudos anteriores mostraram que a região Oc2M, tradicionalmente considerada como uma região visual secundária, está de facto envolvida no processamento de estímulos visuais e auditivos, assim como na sua localização espacial. Para além disso, estudos recentes do nosso laboratório, revelaram que neurónios em Oc2M recebem projeções de todos os córtices sensoriais primários, alguns córtices sensoriais secundários, alguns núcleos do tálamo, e do hipocampo. Com base na utilização de ferramentas de optogenética para a estimulação *in vitro* dos inputs sinápticos em Oc2M, verificou-se que os córtices primários visual e auditivo estabelecem sinapses funcionais com a região Oc2M (Quintino & Remondes, 2017 não-publicado). Evidências preliminares do nosso laboratório de registos extracelulares *in vivo* da região Oc2M, mostraram que esta região responde a estímulos de som e luz, com uma distinta organização temporal (Cardoso & Remondes, 2017, não-publicado).

Neste projeto começámos por desenvolver uma tarefa comportamental com o objectivo de captar – *in vivo* - a dependência funcional entre Oc2M e Hipocampo. Nestas tarefa os animais são colocados num labirinto, e são treinados para associar um determinado estímulo (componente sensorial) com uma específica trajetória (componente de memória). Os resultados comportamentais mostraram que dois, dos seis animais treinados, conseguiram aprender a tarefa. Estes mostraram uma progressão de aprendizagem linear ao longo do tempo, e conseguiram manter de forma consistente uma taxa de acerto acima de 'chance level' (probabilidade de acerto atribuída ao acaso) para cada uma das modalidades sensoriais. Estes animais foram depois sujeitos a um período de interrupção de 33 dias, para serem novamente treinados na tarefa, desta vez com a duração da pista sensorial reduzida para metade (500 milissegundos em vez de 1 segundo). Os ratos conseguiram não só reaprender a tarefa com um nível de dificuldade mais acentuado, assim como ambos precisaram de menos sessões para atingir as performances esperadas.

Os registos eletrofisiológicos foram obtidos através de um dispositivo chamado 'hyperdrive'. A 'hyperdrive' é uma estrutura com 30 tétrodos movíveis, construída no laboratório, e implantada no cérebro do rato através de uma cirurgia estereotáxica, com os vários tétrodos colocados nas regiões de interesse (neste caso, Oc2M e Hipocampo). Cada tétrodo é composto por quatro canais que registam de forma independente a atividade neuronal da região cerebral onde se encontram inseridos. Desta forma, para além de registarmos os valores correspondentes à voltagem extracelular de determinado local (sinal chamado de 'local field potential', LFP), conseguimos também identificar e isolar a atividade proveniente de diversos neurónios representativos do local de interesse, e correlacionar essa atividade com variáveis comportamentais.

No presente trabalho apresentamos dados de eletrofisiologia *in vivo* de 2 ratos implantados, com registo da atividade em Oc2M e Hipocampo, em resposta a estímulos sensoriais num protocolo passivo de estimulação chamado de 'Stimbox'. Neste paradigma experimental, os animais são colocados numa caixa (50 x 30 x 60 cm) onde são sujeitos a 3 condições diferentes de estimulação sensorial: som, luz, e som + luz em simultâneo. Análises realizadas ao LFP revelaram que, após a apresentação do estímulo, apenas as condições de luz e som + luz provocaram uma resposta evidente em ambas as áreas, Oc2M e Hipocampo. O facto de estas duas condições não terem apresentado respostas estatisticamente significativas entre si, sugere que apenas a estimulação visual foi responsável pelos transientes observados na atividade do LFP. Contudo, a identificação de subpopulações de neurónios em Oc2M, e a posterior análise aos potenciais de ação gerados com base na sua frequência de disparos, revelou a existência de células em Oc2M que respondem de forma distinta aos mesmos estímulos sensoriais. Ademais, as respostas observadas por neurónios em Oc2M em resposta à luz e à luz + som em simultâneo, mostraram-se significativamente diferentes, sugerindo assim um efeito modulatório do som na atividade de Oc2M, quando apresentado em combinação com um estímulo visual. Estes resultados suportam a hipótese de Oc2M como uma área de associação multissensorial, possível homólogo do córtex parietal posterior nos seres humanos.

Embora não tenha sido possível realizar, planeamos como futuras experiências o registo simultâneo da atividade neuronal em Oc2M e Hipocampo com ratos a desempenhar a SCTAT. Tal irá ajudar-nos a perceber as computações subjacentes à integração de inputs sensoriais por parte do Oc2M, e como é que essa informação é transferida e utilizada pelo hipocampo numa tarefa de tomada-de-decisão perceptual. Outro objectivo futuro será a supressão seletiva da atividade celular em Oc2M durante sessões da SCTAT, recorrendo a técnicas da engenharia genética tais como *chemogenetics* (Armbruster et al., 2007) ou optogenética (Boyden et al., 2005). Estas experiências permitir-nos-ia testar, de forma causal, a hipótese de Oc2M como um local de convergência no processamento de informação sensorial relevante.

Palavras-chave: Integração Multissensorial, Oc2M, Comportamento, Eletrofisiologia *In Vivo*

Abstract

The hippocampal system has long been associated with episodic memory. The discovery of place cells (O'Keefe & Dostrovsky, 1971) and entorhinal grid cells (Hafting et al., 2005) led to a major insight on how the brain encodes and organizes sensory information in the form of a spatial contextual map. However, little is known concerning the mechanisms underlying the integration of primary sensory stimuli in such a way as to convert it into the hippocampal spatial maps. Previous studies and preliminary data from our lab suggest that the cortical region of the rat's brain Oc2M might play a critical role in the integration of multimodal sensory information in the service of spatial navigation.

We established a behavioral task aimed to test the functional inter-dependency between Oc2M and Hippocampus. In the sensory-cue trajectory association task (SCTAT), rats are required to associate a particular sensory stimulus, sound or light, with a specific trajectory on a modified T-maze. Our results showed that 2 out of 6 animals were able to learn the SCTAT, having reached performance levels of above 80% for both sensory modalities. Additionally, after an interruption period of 33 days, we observed that these two rats were not only able to relearn the task with a shortened stimulus duration (500 milliseconds), but they also needed fewer sessions to achieve performances above chance level.

An 'hyperdrive' array of 30 independently movable tetrodes was built and chronically implanted in the rat's brain, targeted to Oc2M and Hippocampus. Each tetrode comprises four independent channels that record intra-cerebrally the extracellular electrical potential, which allow us to identify single neurons' activity and correlate it with behavior. In the current work, we present in-vivo electrophysiological data from two implanted rats, regarding Oc2M and Hippocampus activity, in response to sensory cues in a passive-stimulation protocol called 'Stimbox'. This protocol is composed by 3 sensory conditions: light stimulation, sound stimulation, and light and sound combined stimulation. Analyses of the local field potential (LFP) activity showed that, after stimulus

onset, only light and sound + light conditions elicited a clear response in both Oc2M and Hippocampus. The fact the light and sound + light conditions were not significantly different, suggests that only light itself was responsible for the observed changes in LFP activity. However, we found neuronal ensembles in Oc2M that exhibited significantly different responses, in terms of firing rate, to the same sensory cues. Importantly, Oc2M neurons' responses to light and sound + light cues were found to be different, thus suggesting a modulatory effect of the sound stimulus once paired with a light cue. Such supports the hypothesis of Oc2M as a multimodal association area, comparable to the human posterior parietal cortex.

As future experiments, neuronal recordings of Oc2M and Hippocampus while rats perform the SCTAT would shed light on how Oc2M integrates sensory inputs, and how it conveys information to hippocampus in a perceptual decision-making task. Furthermore, the use of genetic tools to selectively suppress Oc2M's cellular activity during the SCTAT, such as chemogenetic (Ambruster et al., 2007) or optogenetic (Boyden et al., 2005), would further lead to causally test our long-term hypothesis of Oc2M as a site of convergence to process sensory-relevant information.

Keywords: Multisensory integration, Oc2M, Behavior, In Vivo Electrophysiology

List of Figures

List of Tables

Table of Contents

I. Introduction

Animals strive to survive.

The theory of evolution from Charles Darwin states that "(...) the species that survives is the one that is able to adapt and adjust to the changing environment in which it finds itself." (Megginson, 1963).

This adaptation relies on extracting meaningful features of the environment, process that information and act accordingly (e.g. get food, hide from a predator, find a mate, etc.). At a first glance, it seems a trivial process, but in fact this behavior is only possible due to the existence of a complex communication network called nervous system, which enables an organism to efficiently interact with its surroundings.

Humans and other animals face, on a daily basis, the challenge of processing a multitude of different sensory stimuli. They have to integrate that information in order to be able of making decisions based on such perceptual input. For a long time that scientists have been trying to understand how raw sensory signals are processed in the brain. Also, how and where sensory inputs are converged, further resulting in a unified mental representation of the world. The present work seeks to give a small contribution to this long-sought question.

1.1. Sensory Perception

1.1.1. Unisensory Integration

The ability of our bodies to detect sensory information is an established prerequisite for the phenomenon of sensory experience (Romo & de Lafuente, 2013). This process is based upon the stimulation of receptor cells that transform and convey a specific type of stimulus information into the 'language' of our nervous system: electrical activity flowing in the form of trains of action potentials.

Most of mammalians have four types of sensory receptors: photoreceptors, mechanoreceptors, thermoreceptors and chemoreceptors. They are differently categorized according to the type of stimulus energy they are sensitive to, such as pressure waves, photons, gravity, chemicals, etc. Even within a single sensory system differences are found in the structure and chemistry of these specialized cells, e.g. rods and cones, photoreceptors found in the retina of most vertebrates that respond to electromagnetic radiation of different wavelengths (Squire et al, 2008). The binding of these receptors to its selective molecules leads ion channels to open or close thus changing the membrane potential of the cell. Through the generation of patterns of action potentials, information regarding stimulus intensity and time course[1] can be propagated throughout afferent nerves, reaching then thalamic sensory relay nuclei where the majority of neurons project in a topographic manner to its primary sensory brain regions for an early-stage processing of information (Kandel et al., 2013).

However, as the name suggests, sensory information processing does not end at these primary areas. Brains are capable of doing fast and efficient computations on processing different features within one sensory modality. Such happens due to the fact that information is processed in two manners: through serial and parallel pathways.

[1] Adrian (1926) was the first researcher to demonstrate and describe a cause-effect relationship between stimulus' properties and respective neural response in terms of firing rate patterns.

By performing single and multi-unit recordings in macaques, Pons et al. (1987) demonstrated that, like in the visual system, somatosensory information flows in a sequential way from sensory thalamic nuclei via primary sensory cortices to higher-order sensory regions. In such a way, information flows sequentially by having each brain area carrying certain computations, followed by conveying the treated information to the next area. Nonetheless, the same information can also be processed simultaneously in parallel fashion (Raij et al., 2008). This is corroborated by the existence of ventral and dorsal streams from primary sensory areas that process different aspects regarding stimuli's information (Kandel et al, 2013). There is even evidence showing that higher-order areas receive direct input from thalamus bypassing primary sensory cortices, and that can actually respond to stimuli earlier than those primary regions (Liang, Mouraux, & Iannetti, 2013).

To some extent, sensory integration can be seen as independent by considering receptor cells' specificity and the way information flows through functionally specialized pathways. However, in the real-world environment, such view reveals to be insufficient, once we take into account the large number of multiple stimuli sources that the nervous system has to process simultaneously. In fact, recent findings have challenged the old assumption that perception is a modular function with the different sensory modalities operating independently (Ghazanfar & Schroeder, 2006; Shimojo & Shams, 2001). In order to understand the phenomenon of how perception arises, it is crucial to unravel the mechanisms and regions by which the brain integrates multisensory information.

1.1.2. Multisensory Integration

Our brain is naturally prompted to match cross-modal sensory information. As McGurk & McDonald (1976) demonstrated, such predisposition might not always be beneficial and can actually lead to multisensory illusions. They showed for the first time ever that the auditory perception of a sound could change when an incongruent visual cue is simultaneously presented. Another example is the experiment conducted by Botvinick & Cohen (1998), where participants reported to feel tactile sensations on a fake limb. In this study, the participant's real hand was hidden inside a box out of sight, whereas a rubber hand was placed in front of the participants lined up with the shoulder. The effect is accomplished by simultaneously stroking the participant's real hand and the fake limb. More than a perceptual illusion, it shows how the combination of visual and tactile information can override proprioception information, to a point where people actually feel an external fake limb as their own.

On the other hand, Cherry (1953) showed that the brain is also capable to process simultaneous information in a selective manner. Cherry (1953) found that while participants listened, at the same time, one message to the left ear and a different message to the right ear, they were able to separately understand the content of the two messages, and even shift the focus between the two. This phenomenon became known as the 'Cocktail Party effect', and outlines the capacity of our brain to discriminate a target signal from background noise. Besides, literature has shown that such ability is enhanced in a multisensory context, when an auditory input is paired with congruent visual information (Sumby & Pollack, 1954; MacLeod & Summerfield, 1987).

Benefits

Recent evidence corroborates Sumby & Pollack (1954) and MacLeod & Summerfield (1987) studies, showing that synchronous presentation of audiovisual stimuli enhance speech recognition, in comparison to unimodal conditions (Eramudugolla, Henderson, & Mattingley, 2011; Liu et al, 2013; Ross et

al, 2007). It has also been shown that when an input from one sensory modality is ambiguous, adding a congruent cross-modal cue is enough to increase the attentional control over the ambiguity (van Ee et al, 2009), or even alter the whole perceptual experience (Sekuler et al, 1997).

In comparison to unimodal stimulation, congruent multisensory conditions result in more accurate responses in decision-making perceptual tasks, an effect seen across rodents, non-human primates and humans (Gleiss & Kayser, 2012; Raposo et al., 2012; Raposo, Kaufman, & Churchland, 2014; Siemann et al., 2015). Furthermore, the behavioral benefits of combining sensory information from more than one modality seem to generalize to other tasks, such as target detection (Cappe et al., 2010; Frassinetti, Bolognini, & Làdavas, 2002; Lovelace, Stein, & Wallace, 2003; Odegaard, Wozny, & Shams, 2015; Seitz, Kim, & Shams, 2006), fastest response times (Diederich, Colonius, Bockhorst, & Tabeling, 2003; Doyle & Snowden, 2001; Noel, Modi, Wallace, & Van der Stoep, 2018; Schröger & Widmann, 1998; Stevenson et al, 2012), or sensorimotor integration (Buchholz et al., 2012; Elliott, Wing, & Welchman, 2010).

Also, some studies conducted over recent years have provided robust evidence on how multisensory contexts can improve memory on object recognition tasks (Lehmann & Murray, 2005; Matusz et al., 2015; Murray, Foxe, & Wylie, 2005; Thelen, Talsma, & Murray, 2015). For example, in the paradigm used by Matusz, Wallace, & Murray (2015), human subjects are presented with a set of pictures coupled with a semantic congruent noise, a meaningless tone (e.g. 'beep' tone), or a semantically incongruent sound. Based on these cues, they must judge whether they saw the given object for the first time or not. The overall effect was clear: participants were significantly better on recognizing repeated pictures that were initially paired with congruent auditory information, than images paired with either a meaningless or incongruent tone. This suggests that multisensory contexts have a significant impact on memory performance (for review, see Matusz et al, 2017; Shams & Seitz, 2008)

Principles and Influencing Factors

The seminal principles of the effectiveness of multisensory integration arose from neuronal recordings in the superior colliculus (SC) of cats (Meredith & Stein, 1983; Stein et al, 1989). This influential work reported the existence of multisensory neurons: cells that responded to, or were influenced by, stimuli more than one sensory modality (see fig.1). Based on correlations between these neurons' activity and different behavioral conditions, researchers postulated three general principles by which multisensory integration happens.

The "spatial" and "temporal" rules state, respectively, that the magnitude of the integrated response is greater when physical signals occur approximately at the same location, and time. Each neuron has a receptive field defined by the sensory area that can trigger neuronal responses when stimulated. In the case of multisensory neurons, the number of receptive fields is proportional to the number of modalities to which they respond. According to the 'spatial' and 'temporal' principles, in order to elicit a response from a multisensory neuron, cross-modal stimuli should derive from the same location in space ('spatial' rule) and within a short time-window ('temporal' rule), so that the receptive fields of the neuron are stimulated simultaneously. Additionally, the "principle of inverse effectiveness", predicts that the degree to which a multisensory response is enhanced, is inversely related to the effectiveness of the modality-specific cues being paired. In other words, two combined signals are likely to produce a multisensory enhancement[2] if they are poorly captured when presented alone. On the opposite, if one sensory stimulus in isolation evokes a strong response, its combination with a congruent stimulus from a different modality will not significantly increase the neuron's response (reviewed in Stein & Stanford, 2008). According to these principles, multisensory integration can be defined as 'the

[2] It is important to mention that, within this framework, an enhanced response can take different forms: *superadditive*, *additive*, or *subadditive*. *Superadditivity* is characterized by a multisensory response in which its activity is larger than the arithmetic sum of the responses to the stimuli in isolation (see for example fig. 1.1). The *additive* effect is seen when the multisensory response statistically equals the arithmetic sum of the responses to the stimuli components, whereas in a suba*dditive* multisensory response, the sum is smaller than the response to the stimuli separately (see Stein & Stanford, 2008).

neural process by which unisensory signals are combined to form a new product' (Stein et al, 2010).

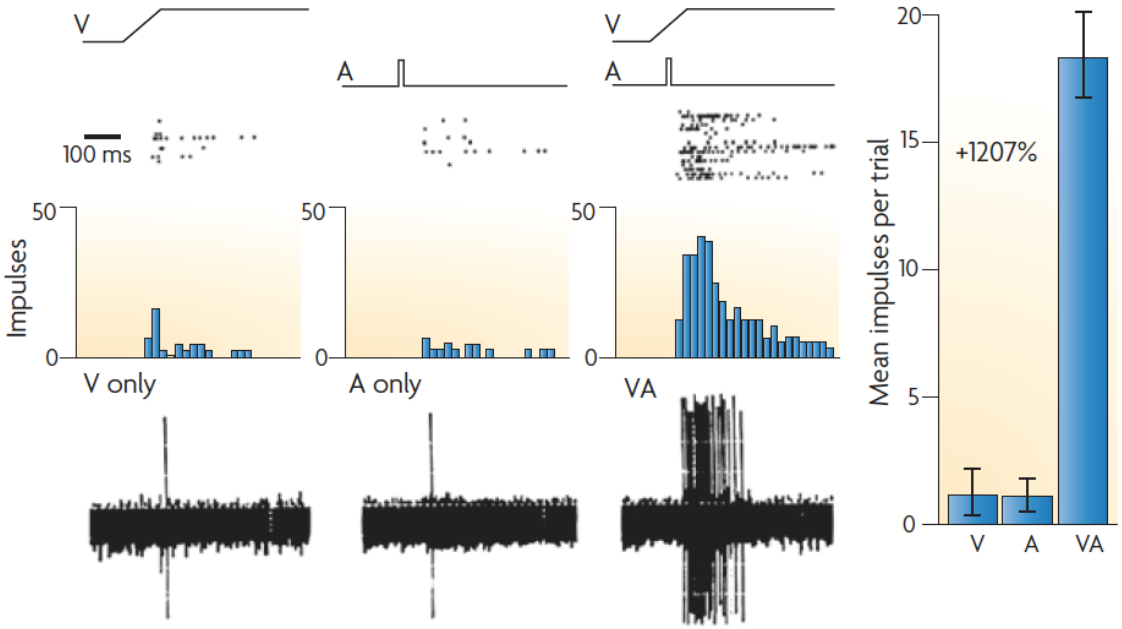

Fig 1.1 – Representation of a multisensory neuron in the superior colliculus.

The figure shows a clear enhancement of the neuron's firing rate in response to the visual + auditory (VA) condition compared to the visual (V) and auditory (A) conditions. In fact, not only the response in the multisensory condition is stronger than the responses to both sensory cues in isolation, as it also exceeds the sum of both unisensory responses combined. Retrieved from Stein & Stanford (2008), for the original work see Meredith & Stein, 1986.

Importantly, the activity observed in multisensory neurons was in accordance with the behavioral output exhibit by the animal (i.e. combined stimuli that elicited an increased response in terms of firing rate, were also more effective at driving behavioral detection of the stimuli (Stein et al, 1989). Nevertheless, there are a few considerations that should be taken into account. First, the phenomenon of superadditivity is mostly observed in neurons in which the responses to unisensory trials are weak (Stanford & Stein, 2007). Therefore, the effect that was thought to be the neurophysiological evidence of multisensory integration, does not contemplate the integration of combination of stimuli that

vary in its intensity spectrum. Second, the principles described lack an explanation concerning the underlying computations and mathematical rules of neuron's activity. Third, the works of Meredith & Stein (1983) and Stein et al., (1989) try to address how multimodal information is integrated and merged across senses, but fails to describe how to deal with the 'causal inference problem': how does the brain decides which sensory inputs come from the same source and hence should be combined, and which are originated from different sources so that signals are processed separately. Finally, why not all deep SC neurons are multisensory given that multisensory neurons are also responsive to unisensory stimulation? In fact, in the cat, only approximately half of deep SC neurons were found to be multisensory, whereas in the monkey just about one quarter (Wallace & Stein, 1996)

More recently, aimed to fit the findings at the level of single neurons with the descriptions of multisensory integration perceptual tasks (Alais & Burr, 2004; Ernst & Banks, 2002; Gu, Angelaki, & DeAngelis, 2008), researchers have been developed models within the framework of Bayes' theorem. Briefly, according to Bayes' theorem, an organism estimates the probability of an event (e.g. the location of a specific object) based on prior knowledge/experience related to the event (e.g. the number of times we found the object on that particular place), and the current incoming information (e.g. the combined sensory information captured by our senses). In other words, one infers the posterior probability - the *likelihood* of the object's location – given its prior beliefs and the updated sensory inputs (see fig. 1.2). It is also assumed that an organism tries to perform in an optimal way, in the sense that expected cost is always minimized and the final estimate has the lowest degree of uncertainty. Given that sensory information is intrinsically noisy (Faisal, Selen, & Wolpert, 2009), Bayesian models predict that, gathering complementary information from multiple senses, will reduce the uncertainty of a sensory estimation.

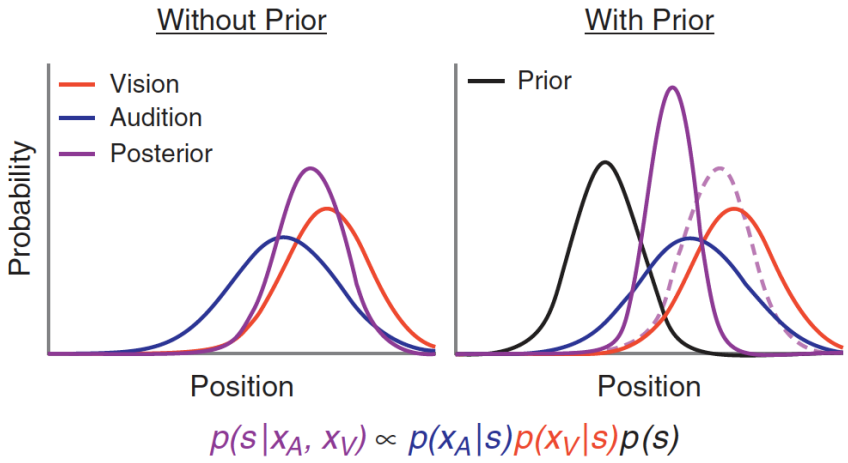

Fig 1.2 – Multisensory cue integration according to Bayes theorem.

Consider the example of localizing a bird in a tree (s). P(S \ X_A, X_V) represents the posterior probability of a subject to see the bird at a specific location, where X_A and X_V stand for auditory and visual information, respectively. P(X_A \ S) and P(X_B \ S) mean, in a probabilistic manner, the representation of brain's response to each sensory cue, whereas P(S) represents the subjects' prior knowledge/experience related to the event. Both graphs represent the position of the bird on the x-axis and its associated probability on the y-axis.
On the left plot, the posterior probability of bird's location (purple) is the result of the product of the likelihood functions for each sensory stimulus (blue and red). This means that only current sensory information is being considered (called maximum-likelihood estimation). On the right plot, we see that the estimated location moves further to the left along the x-axis, once prior information is added to the equation (called Bayesian estimation). Retrieved and adapted from Seilheimer, Rosenberg, & Angelaki (2014).

In conformity with Bayes' law assumptions, Anastasio, Patton, & Belkacem-Boussaid, (2000) put forward a possible explanation regarding the physiological properties of SC multisensory neurons. The main idea is that each of these neurons computes the probability of the presence of a stimulus source in its receptive field, given all sensory inputs it receives. The model described by these authors demonstrates the principle of inverse effectiveness in a probabilistic manner. According to them, as neuron's activity to unisensory inputs decreases, the target probability rapidly increases from the combination of two or more modalities. Nevertheless, as Colonius & Diederich (2002) pointed out, the model proposed by Anastasio, Patton, & Belkacem-Boussaid (2000) does not take into account the decision making process that an organism faces when confronted with sensory information. In a natural environment, one has to be

able to detect sensory inputs, but also to process that information as relevant or irrelevant, so that 'false alarms' to irrelevant stimuli are minimized.

The previous works were developed with the goal of providing a mechanistic explanation of the neural computations carried by deep SC single neurons. An important limitation is the fact that they do not consider multisensory perception at the level of the neural population. Besides, these models share the assumption that neurons respond with the same firing rate whenever stimuli are captured in neuron's receptive field, regardless stimuli features, like intensity or frequency. As such, and still under the framework of Bayesian probability, Ma et al., (2006) proposed a theory attempted to tackle such limitations. According to these authors, probability distributions over stimulus can be represented by neurons at the population level. At first sight, the Poisson-like variability[3] observed in cortical activity (London et al., 2010; Moreno-Bote, 2014) makes this idea unlikely. For example, in a paradigm where the same sensory cue is presented over trials, one can observe that the number of spike counts in cortical neurons varies from trial to trial (Tolhurst, Movshon, & Dean, 1983). However, as stated by Mat el (2006), such neuronal variability reflects the always-present degree of uncertainty of an animal when confronted to sensory information, whether he has to integrate or perform a causal inference. The model introduced by these authors – called probabilistic population code - predicts that the simple linear summation of population activity (i.e. the sum of the conditional probability distributions of a neuronal response given a specific input) can result in the Bayes-optimal combination of multiple sensory cues. It provides a straightforward solution on the way neural circuits represent optimal-cue integration through biologically plausible computations. Moreover, it matches neurons' activity (seen as encoders of probability distributions) with behavioral evidence that shows the process of cue integration as probabilistic (Körding, 2007; Ernst & Banks, 2002).

[3] Briefly, a Poisson distribution represents a series of discrete events where the average time between those events in a given fixed interval is known, but the exact timing of events is random. Such probabilistic distribution fits the findings in the literature since that, in many brain regions, the variability observed in neural responses is proportional to its mean.

In 2012, Fetsch, Pouget, Deangelis, & Angelaki (2012) tested macaque monkeys in a multisensory heading discrimination task with conflicting visual and vestibular cues, while neural activity in the dorsal medial superior temporal (MSTd) area was being recorded. Even though multisensory neuronal responses were well predicted by the weighted linear sum of unisensory responses, corroborating Mat et al (2006), they also found that the neural weights placed in each cue varied as a function of its reliability. Specifically, multisensory responses reflected the manipulations implemented on the reliability of sensory information (e.g. variations on the intensity of a light cue). On the other hand, the theoretical framework of probabilistic population codes assumes that the brain does not explicitly represent cue reliability. Instead, different neuronal populations represent probability distributions over stimuli regardless its strength. Ohshiro, Angelaki, & Deangelis, (2011) proposed a solution that accounts for the neurophysiological findings in the MSTd area (Fetsch et al., 2012), called divisive normalization. This model states that inputs from primary sensory units feed forward sensory information into a population of multisensory neurons. However, besides the linear weighted sum of inputs carried by the multisensory neuron, the response is normalized by the summed activity of all other multisensory neurons present in that population. This model not only accounts for the empirical principles of multisensory integration at the cellular level, as it also provides a computational explanation at the network population level, considering the observed changes of the neural weights as a function of cue reliability.

It is noteworthy that the way the brain interprets and acts upon cross-modal stimulation is greatly influenced by bottom-up and top-down modulation. Some of the factors that influence perception on a bottom-up manner were already mentioned and are related to inherent properties of sensory stimuli (e.g. timing, spatial location, intensity, etc.) and established pathways according to the anatomy of the mammalian nervous system (see previous section 'Unisensory Integration'). What about top-down signaling?

The process of learning a sensory-cue association task can lead to differences in the brain's physiological responses. Memory is often implicated, as there is accumulated evidence from in-vivo cellular recordings in different mammalian species showing enhanced responses to sensory stimulation in primary cortices after learning (Makino & Komiyama, 2015; Polley, 2006; Yan et al, 2014). Cortical improvements are found to predict to a great extent behavioral outcomes in trained animals (Caras & Sanes, 2017; Yamashita & Petersen, 2016; Yan et al, 2014) and sensory-evoked signals are also present in the higher cortex contributing directly to task's performance (Le Merre et al, 2018). Attention is also an example of top-down control that seems to modulate perception both at the unisensory (Atiani et al, 2014; Downer, Niwa, & Sutter, 2015) and multisensory (Fairhall & MacAluso, 2009; Talsma, Doty, & Woldorff, 2007) level.

The previous studies outline the functional and anatomical interdependency between the sensory and memory system. How neural activity patterns change in response to multisensory stimuli, further leading to specific changes in behavior, have become a central question in the neuroscience field (Burnett et al, 2004; Hirokawa et al, 2008; Raposo et al, 2014; Sheppard, Raposo, & Churchland, 2013). The present project seeks to explore how multimodal sensory information is integrated in the brain during contextual memory formation, and we will focus on two regions from the rat's brain: Hippocampus and Oc2M.

1.2. Regions of Interest

1.2.1. Hippocampus

In 1953, Henry Molaison (widely known as patient H.M.) underwent a surgery called bilateral medial temporal lobotomy, in which parts of the hippocampal formation and amygdala were removed from both hemispheres. As a consequence, H.M. started showing symptoms of severe anterograde amnesia. He was able to remember specific personal events well before surgery, yet he displayed a complete loss of memory of any episodic events since his procedure, and also showed a partial retrograde amnesia for the 3 years leading up to his operation (Milner & Scoville, 1957)[4]. Researchers began studying H.M. and they found that he was able to retain information for short-time periods, as long as he could stay focused on the task. Additionally, he showed significant behavioral improvements over days in complex motor tasks, even though he had no recall of having learned it (see for review Dossani, Missios, & Nanda, 2015). Together, this evidence suggested the existence of multiple memory systems placed at different locations in the brain, so that different types of memory also rely on different neural circuits. Such findings inevitably shaped the way human memory research was conducted for the following years until nowadays.

On the other hand, most of the rodent literature has focused on the role of the hippocampus in spatial navigation. Space is considered to be a key concept within the definition of episodic memory, as it is related to happenings at particular times in particular places (Clayton & Dickinson, 1998). Spatial navigational tasks have been widely used as a proxy to study memory mechanisms in rodents. In a similar manner to humans, in these paradigms, rodents are also required to encode and storage information from specific trajectories or places, and later retrieve such information (Ergorul & Eichenbaum, 2004; Zhou & Crystal, 2009).

[4] The paper *Loss of recent memory after bilateral hippocampal lesions* from Milner & Scoville (1957) is one of the most cited and important ones in the history of neuroscience.

Using methods developed for recording hippocampal neural activity in freely–behaving animals, researchers have been able to link neural activity from different brain regions, with specific behaviors (Moser, Rowland, & Moser, 2015). Such experiments led to the discovery of place cells in the hippocampus (O'Keefe & Dostrovsky, 1971), which are believed to store a cognitive map that guides navigation (O'Keefe, 1976), representing not only the current location of the animal, but also previous and upcoming locations (Frank et al, 2000; Ferbinteanu & Shapiro, 2003).

Additionally, the discovery of entorhinal cortical grid cells (Hafting et al, 2005), head-direction cells (Sargolini et al, 2006), and border cells (Solstad et al, 2008), have contributed to a major insight on how the brain encodes and organizes sensory information in the form of a spatial contextual map.

However, little is known concerning the mechanisms underlying the integration of primary sensory stimuli in such a way as to convert it into these spatial maps.

1.2.2. Oc2M

The cortical area located anterior to the rat's primary visual cortex and posterior to parietal cortex, named occipital cortex 2 medial (Oc2M), is believed to be an association cortex that integrates sensory inputs of multiple modalities (Chen & Nakamura, 1998; Nakamura, 1999). As illustrated in fig. 2.1, Oc2M is a brain region located between 3.8 mm and 5.8 mm posterior to Bregma, and between 1.4 mm and 3.1 mm lateral to Bregma.

Several anatomical studies have been conducted over time and brain's regions nomenclature has also been subject to change to some extent. Oc2M is no exception as it overlaps with Krieg's area 7 (Krieg, 1946; see fig. 6.1 in VI. Supplementary figures), considered as a homologue of primate posterior parietal cortex (Redish, 1999; Palomero-Gallagher & Zilles, 2004), with the Caviness's area 18b and partially 17 (Caviness, 1975; fig. 6.1), or the area anteromedial

(Olavarria & Montero, 1981). As Lyamzin & Benucci (2019) pointed out, "(...) a large part of PTLp reported in the Allen atlas corresponds to the rostral parts of V1, V2M, and V2L in the Paxinos atlas." where PTLp stands for posterior parietal association area. This represents a problem and might lead to misconceptions as scientists are studying the same brain regions by using different names[5].

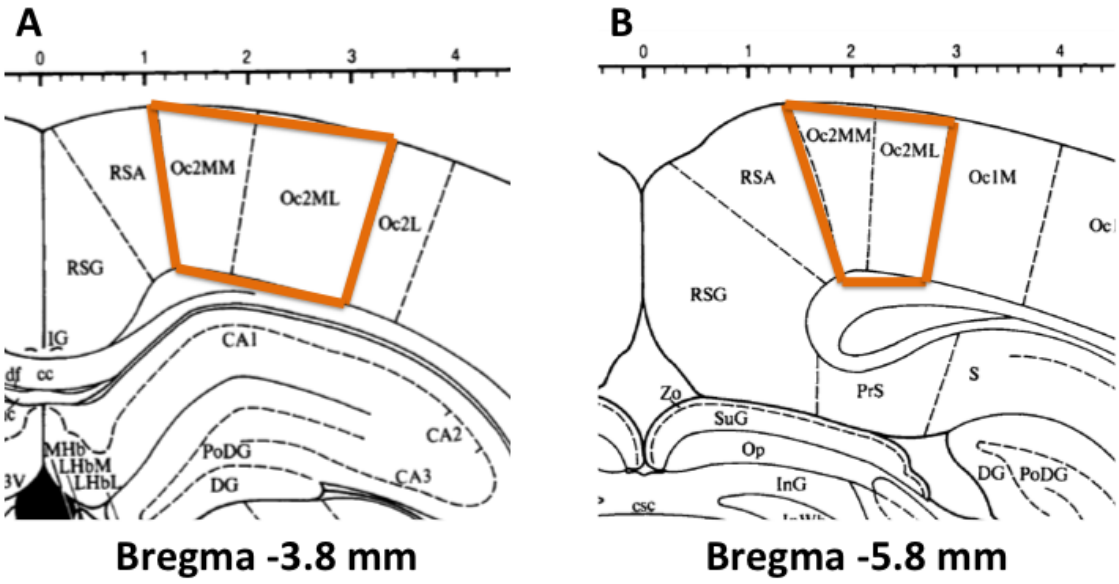

Fig. 1.3 – Localization of Oc2M's region according to Paxinos & Watson (1986).
(A) Most anterior coordinates of Oc2M relative to Bregma at -3.8 mm.
(B) Most posterior coordinates of Oc2M relative to Bregma at -5.8 mm.

Lesions in Oc2M region result in behavioral impairments related to multimodal stimuli perception, namely the ability of rats to perform a location discrimination task, when such discrimination involves light sources located at vertically distinct positions (Sánchez et al, 1997). Such lesions also result in greater latencies to swim towards a hidden platform inside a pool of water - the Morris water-maze - showing the importance of this region for the processing of allocentric visuospatial cues (Espinoza et al, 1999).

[5] The recent studies of Licata et al. (2017), Mohan et al., (2018), David Raposo et al. (2014) and Schiffino et al., (2014) are perfect examples of the aforementioned problem. They highlight the multisensory properties of Oc2M but the authors refer to it as Posterior Parietal Cortex, which corresponds to the rostral Oc2M.

Also, Pinto-Hamuy, Montero, & Torrealba (2004) assessed the retention of performance in the Lashley III maze in blind rats, after partial Oc2M lesions. The behavioral apparatus consists in a labyrinth with a start and a goal box where food reinforcement is provided. The animal has to learn to accurately run through it and avoid errors, such as entering into blind alleys. The results showed that Oc2M area, but not the visual information per se, is needed to perform the task, suggesting its critical role in long-term spatial memory, independently of visual information processing. Finally, Nakamura (1999) found that Oc2M contains cells that encode the spatial source of acoustic information, suggesting the processing of allocentric auditory information.

Recent studies have indicated that the most anterior region of Oc2M might play a causal role in sensory decision-making tests, suggesting again its importance on integrating multisensory information. According to Raposo et al. (2014), "(...) neural responses in PPC seem likely to reflect a process of transforming ambiguous sensory information into action". It seems to be the case in visual (Licata et al, 2017; Raposo et al, 2014) and auditory (Akrami et al, 2018; Hanks et al, 2015; Raposo et al, 2014) decision-making tasks, but the neural mechanisms and the circuits implicated in this process are still debatable.

For instance, Licata et al. (2017) trained rats in a sensory discrimination task, where they had to judge whether the overall rate of a repeating visual or auditory stimulus, was higher or lower, compared to a previously learned baseline. They found that rostral Oc2M neurons were more strongly driven by individual visual events than by auditory events, even though both sensory stimuli were shown to be equally effective in driving behavior. Importantly, by measuring trial-to-trial variability in neural responses (Churchland et al, 2011), a clear decrease was shown for both sensory cues. Based on these results, Licata et al. (2017) proposed that rostral Oc2M integrates visual inputs but that sensory evidence over time must be accumulated at a different site, which feeds back to Oc2M. Similarly, Akrami et al. (2018) trained rats in an auditory parametric working memory task, where rats were presented with two auditory stimuli, and

had to correctly report the loudest tone. From electrophysiological recordings at Oc2M while rats performed the task, they found that Oc2M neurons carried more information about the sensory stimuli of previous trials than the current. As such, they proposed that Oc2M is a critical locus to represent and sustain prior auditory stimuli information over time (as opposed to Licata et al., 2017). Nevertheless, it should be noted the two studies came to different conclusions based on the findings of Oc2M's processing of different sensory modalities, and using different behavioral tasks (even though in the Licata et al. (2017) experiment auditory information was also present).

Previous work from our lab has shown that Oc2M neurons receive projections from all primary sensory cortices, some secondary sensory cortices, some nuclei of the thalamus and hippocampus. Optogenetic stimulation in vitro of both **visual** and **auditory synaptic inputs** locally in Oc2M generates bona fide synaptic responses to both inputs (Quintino & Remondes, 2017, *unpublished*). Furthermore, extracellular in vivo recordings have revealed that **light** and **sound stimuli trigger Oc2M responses** with a distinct temporal organization (Cardoso & Remondes, 2017, *unpublished*).

1.3. Aims

The main goals of the present MSc project are:

- Establish a behavioral protocol in which rats learn to perform a **sensory-cue trajectory association task** (SCTAT) with auditory and visual stimuli.

- Build a **multielectrode array platform** (see Methods section) and implant it on the rat's brain regions of interest (Hippocampus and Oc2M).

- Replicate previous results on Oc2M's response to multimodal sensory information by using a passive-stimulation behavior protocol (called 'Stimbox Protocol', see 4. Methods section).

- Analyze Local Field Potential (LFP), Multi-Unit Activity (MUA) and Single-Unit activity between Oc2M and Hippocampus in different behavioral tasks.

II. Methods

2.1 Subjects

All animal experiments were performed according to the European Union guidelines and under approval of DGAV AEC_2015_03_MR_Synapses.

In total, 9 male Long-Evans rats were used in this project and were all acquired from Charles Rivers Laboratories France. Animals arrived to iMM facilities with different ages but were never older than 2 months old. All of them underwent through an acclimatization period of 48 hours and were further moved to an animal house facility with controlled temperature, humidity, 12 hours light/dark cycle, provided with food and water *ad libitum*. They are kept in this room until needed for experiments.

Rats had to go through an initial process of handling carried by the experimenter in order for them to get used to the human presence and contact. If handling is not properly done, animals might develop anxiety and show defensive behaviors towards people. Such can lead to variations in behavioral and electrophysiological data and potentially add to results a confounding variable. Additionally, the experimenter provided chocolate milk (the reward used in the behavior sessions) during handling so that they could associate the human presence with a positive/rewarding feeling.

2.2. Behavior Room and Set-up

The behavior and electrophysiological data were acquired by making use of two separate rooms: the behavior room and the 'control/computer room' (see fig. 2.1).

The behavior room contains a 1.5m by 1.9m maze, a camera over it, the electrophysiology acquisition system, and different stimuli sources used in the tasks. In order to minimize the human interference, the experimenter stays in a different room where all the recorded data is displayed in real time by the open-

source Bonsai software, which shows both the video file and the raw neural data of the ongoing session. Each behavioral paradigm requires a personalized Bonsai script according to its specific behavior constraints.

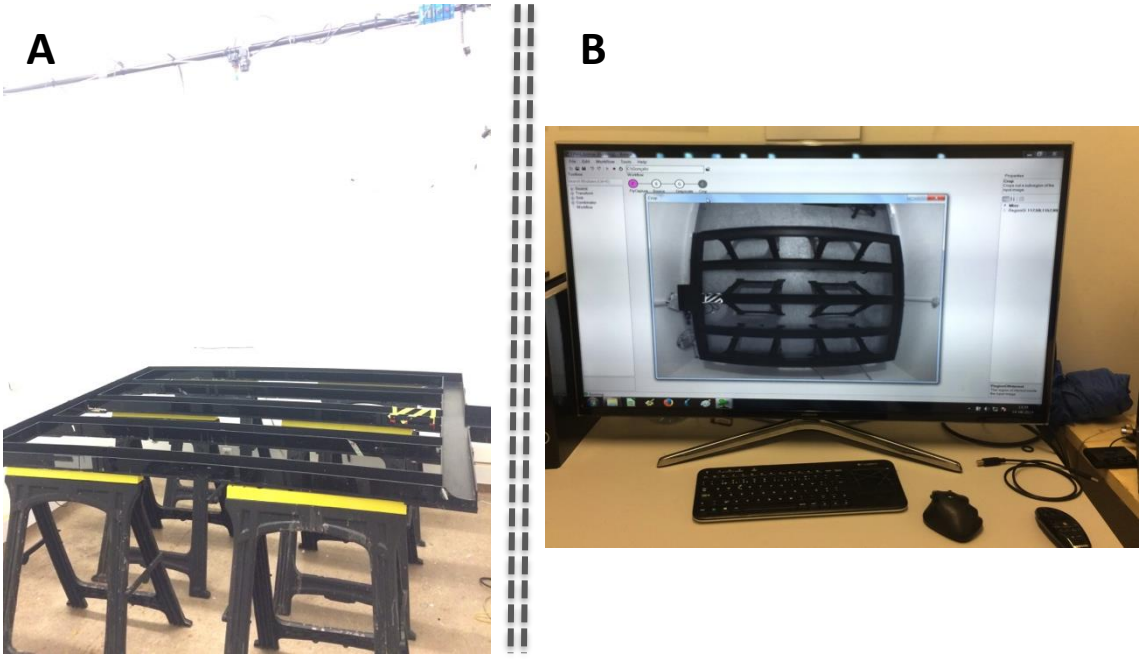

Fig. 2.1. Behavior room facilities.
(A) Inside view of the behavior room showing the adjustable 4-choice maze.
(B) Inside view of the 'control' room representing the researcher's point of view when experiments are running.

2.3. Behavior Protocols

2.3.1. Sensory-cue trajectory association task (SCTAT) - 4 conditions

The SCTAT comprises the association of a specific sensory cue with a particular spatial trajectory. In the 4-conditions SCTAT, two blue led lights of different intensities and two tones of different frequencies compose the stimuli setup. Given that each cue corresponds to one spatial trajectory, this protocol has a total of 4 conditions (i.e. 4 different cue-trajectory associations, see fig. 2.2).

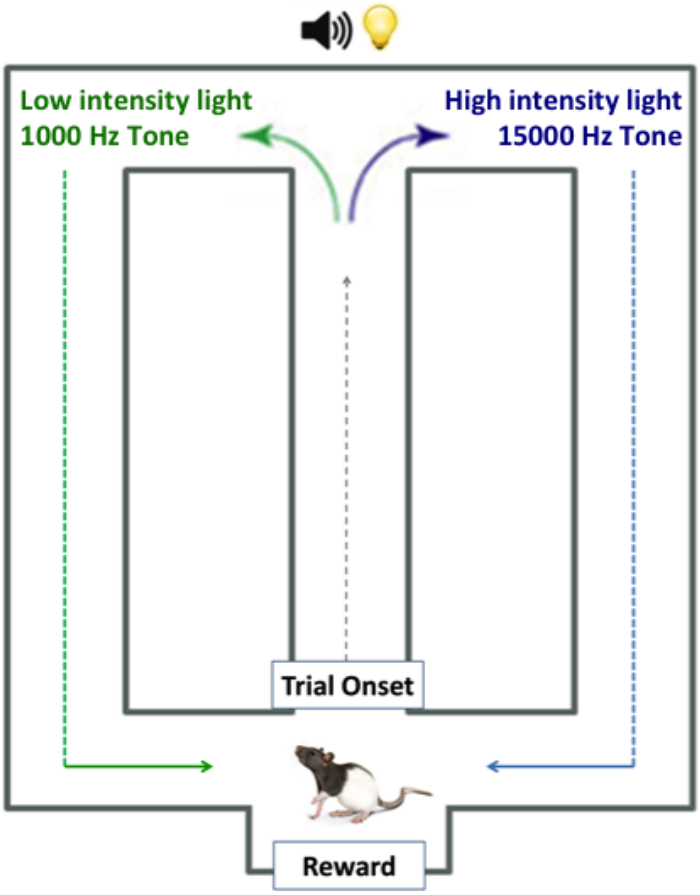

Fig. 2.2. Sensory-Cue Trajectory Association Task (4 conditions). Rats are trained to associate a 1000Hz tone and a low intensity light cue with the left trajectory, and a 15000 Hz tone and a high intensity light cue with the right trajectory. Both stimuli are set to the duration of 1 second and placed at the end of the central arm.

To build the stimuli set for the visual conditions, a low and high resistance (100 Ω and 3000 Ω) were welded to two led light bulbs in order to get, respectively, a high and low intensity lights clearly distinguishable. Both led lights were connected to one Arduino board and its activation was dependent upon Bonsai software commands. For the auditory conditions we used the open-source software Audacity to upload a low-frequency tone (1000 Hz) and a high-frequency tone (15000 Hz), and both tones were controlled directly through Bonsai.

Both stimuli sources were intentionally located at the end of the central arm to avoid biases based on their spatial location (as represented in the schematic fig. 2.2).

In this protocol the trial begins once rats enter the central arm and a stimulus of 1-second duration is immediately triggered. Animals have to choose the correct turn at the decision point and are rewarded accordingly at the end of the trajectory. The 4 conditions were distributed as follows:

- Low intensity light cue / Left trajectory
- High intensity light cue / Right trajectory
- Low frequency tone / Left trajectory
- High frequency tone / Right trajectory

This task was designed with the purpose of testing **unisensory trials** (one stimulus at a time) and **multisensory trials** (two stimuli at a time). Multisensory conditions are supposed to be tested as probe trials. They are divided between **congruent audiovisual trials**, in which both cues indicate one single trajectory (e.g. low intensity light paired with a low frequency tone), and **incongruent audiovisual trials**, where conflicting cues are presented (e.g. low intensity light paired with a high frequency tone).

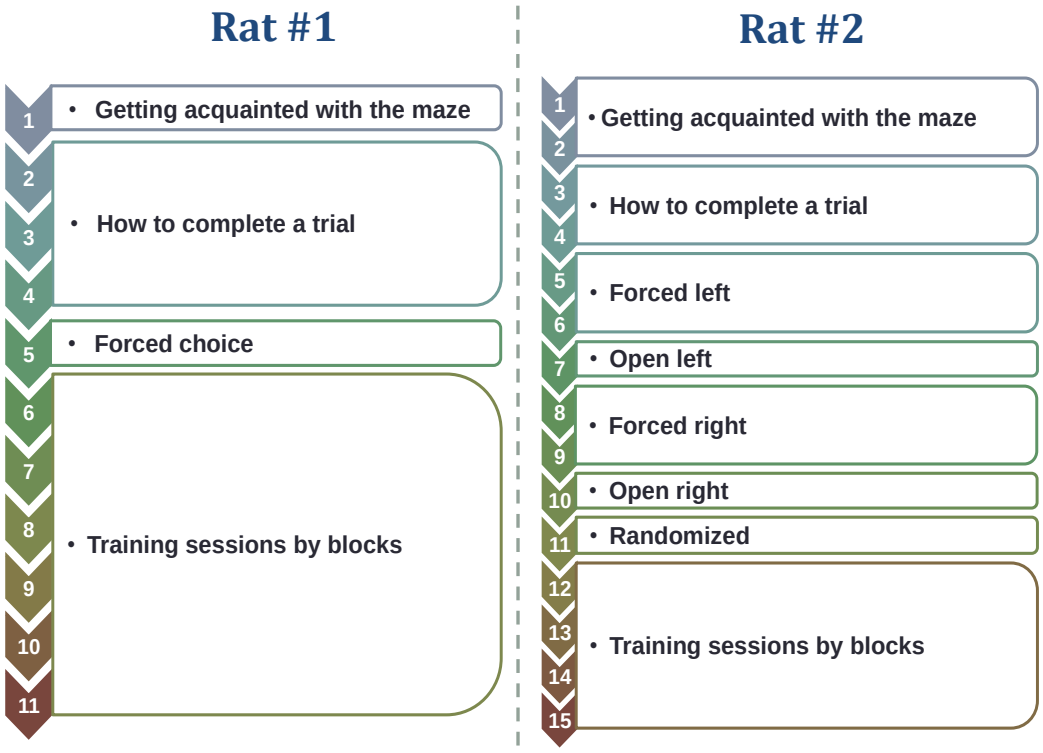

Fig. 2.3. Training progression of two rats from the implementation of the SCTAT and respective number of sessions on each stage (column numbers).

The first behavioral sessions did not contemplate the presentation of the sensory cues. Since animals were naive to the constraints and goals of the task in the beginning, we conducted an introductory protocol for them to get comfortable in the behavior room and learn how to move around the maze.

The fig 2.3 shows the overall training progression before rats reached the randomized / final version of the task. The record of behavior during shaping was animal-specific.

In the first session(s) we spread chocolate milk throughout the maze for rats to get acquainted to it and create a positive feeling towards the new environment. We then introduced the reward's port location and animals were only rewarded after performing a correct trial. At this stage, we consider a correct trial every time the animal enters the central arm, turns left or right at the decision point, and comes back to the reward location through one of the lateral arms (i.e. they have to complete accurately the full trajectory).

Once subjects got proficient in performing laps, they were then introduced to forced choice trials, in which only one turn is available at the decision point. At this point, stimuli are presented for the first time and given according to the trajectory available.

The rat #1 had one forced choice session for both trajectories followed by training sessions by blocks of consecutive trials (i.e. it is established before each session a specific number of consecutive repetitions of the same. For example, a session comprising 10 trials per block for both sound conditions, would mean that the low frequency tone would be triggered for 10 consecutive times, followed by 10 trials with the high frequency tone, and so on). The 'trials per block' method allows us to gradually increase the difficulty of the task over sessions until the desired behavior is reached.

The rat #2 received a different protocol. We implemented more forced sessions, and those were followed by an open left/right session in which both trajectories were available but only one cue was presented.

The described training protocol lasted for a month and only sound conditioning was tested. No progression whatsoever was observed across sessions and performance never went above chance level. Instead of the usual chance level cutoff of 50%, here we consider that the animal is behaving randomly when he shows overall performances between 40% and 60%. This was decided given the average number of trials per session, and the fact that, in every trial, one out of two possible outcomes is always correct.

2.3.2. Sensory-cue trajectory association task (SCTAT) – 2 conditions

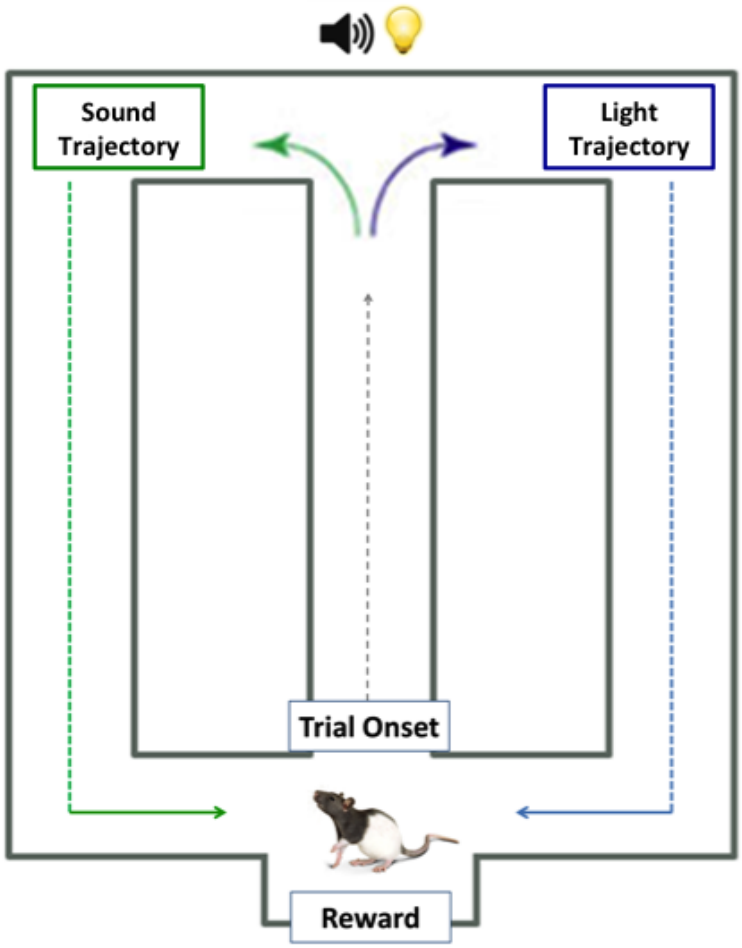

Fig. 2.4. Sensory-Cue Trajectory Association Task (2 conditions). Rats are trained to associate a 1000Hz tone with the left trajectory and a visual cue with the right trajectory, both set to the duration of 500 ms and placed at the end of the central arm.

As it is shown in fig. 2.4, the subsequent protocol had only 2 distinct conditions: sound and light. Since we carried on with the same group of animals, we took advantage of the previous training by maintaining the condition of the low frequency tone (1000 Hz) / left trajectory, adding only the novel condition of light cue/right trajectory. In this case, a different pair of lights was used and they were set to exhibit the same luminous intensity. This time both cues were being activated through the same Arduino board.

Each output pulse sent from the Arduino resulted in either a sound or light stimulus 500 milliseconds long. Such duration allows animals to clearly perceive the cue, although still having a silent period between halfway the central arm and its end (decision point). In this manner, the animal is required to maintain sensory information in memory, and act later accordingly by turning to its associated trajectory.

2.3.3. 'StimBox' Protocol

The StimBox is a behavior protocol previously used in our lab where rats' neural activity is recorded while sensory stimuli are delivered. The box itself is a black container (50 x 30 x 60 cm) where animals can move freely. The fact that rats are not required to produce any behavioral response is an advantage of this protocol, as there is no need for pre-training. In this setup, two led lights were fixed on opposite walls of the box and a sound speaker was placed externally. Stimuli were randomly presented and controlled by the experimenter from a separate room (see fig. 2.1), while animal's behavior and brain activity were being displayed.

Subjects were tested in 3 different conditions: light, sound and light+sound (simultaneously activated). In all sensory conditions, stimuli were 2 seconds long in order to match previous data from our lab. Each session lasted on average 45 minutes.

2.3.4. Open-field stimulation protocol

The open-field protocol coupled with sensory stimulation was developed in this project as an alternative to the previously described SCTAT. We use a circular field with a diameter of 105 cm, surrounded by a wall 35 cm tall. Two regions of interest (ROI) are defined in the Bonsai software and, each time the animal crosses it, a sensory stimulus is randomly presented (we have exactly the same 3 conditions as in the StimBox protocol). ROIs are usually located close to the field's surrounding wall, but its location changed from session to session so that animals don't form undesired habits over time (see schematic representation in the fig. X).

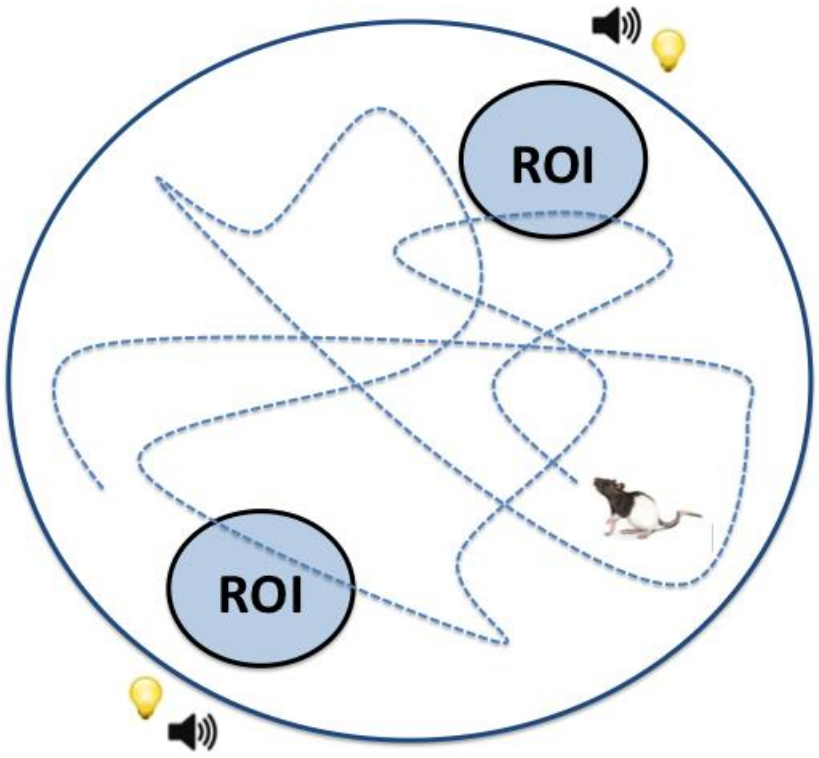

Fig. 2.5. Open-field Stimulation Task.
While animal's neural activity is recorded, rats explore a circular arena (illustrated by the dashed blue line). The two 'ROI' circles represent the regions of interest that trigger sensory cues each time the animal crosses it. Despite the led lights fixed near the ROI, the animal does not have any other cue regarding ROI's location.

In the SCTAT protocol rats are required to integrate sensory stimuli and rely on memory so a correct decision is made. In this open-field protocol, the decision-making component is not present and that represents a disadvantage when comparing to the SCTAT. On the other hand, in theory, we would still be able to disentangle sensory and spatial coding and check for neural correlates of memory and sensory systems interdependency. For instance, we might find place cells that fire in one specific ROI but others that are sensory coded and will fire independently of the animal's location, taking advantage of having more than one single ROI. Besides, pre-training is not required as correct/incorrect trials do not exist, like in SCTAT. In order to guarantee simultaneous recordings from the two target regions, this task started once tetrodes reached hippocampus.

2.4. Multielectrode Array Platform (Hyperdrive)

The hyperdrive is a structure composed of 30 independently adjustable tetrodes that we use to monitor and acquire the activity of neurons in freely behaving animals (Liang et al., 2017). Its design allows us to record neural activity from two or more regions simultaneously according to our needs. These drives are built in the lab and this section highlights some of the steps involved in its construction.

2.4.1. Main-body Structure

The main structure of the hyperdrive is 3D-printed using the material acrylonitrile butadiene styrene, a rigid and dense thermoplastic although still flexible enough to make it bend without easily breaking it.

As it is shown in fig. 2.6, the hyperdrive is composed of four main support posts (EIB holders) converging on the top on a flat surface with two screw holes where the Electrode Interface Board (EIB) is further fixed on a later stage. The guiding posts between the EIB holders support the microdrive units (a spring and

screw mechanism used to adjust the respective tetrode). The designed hyperdrive has a circular open tube at the bottom where the assembled polyimides bundle is fixed with epoxy glue.

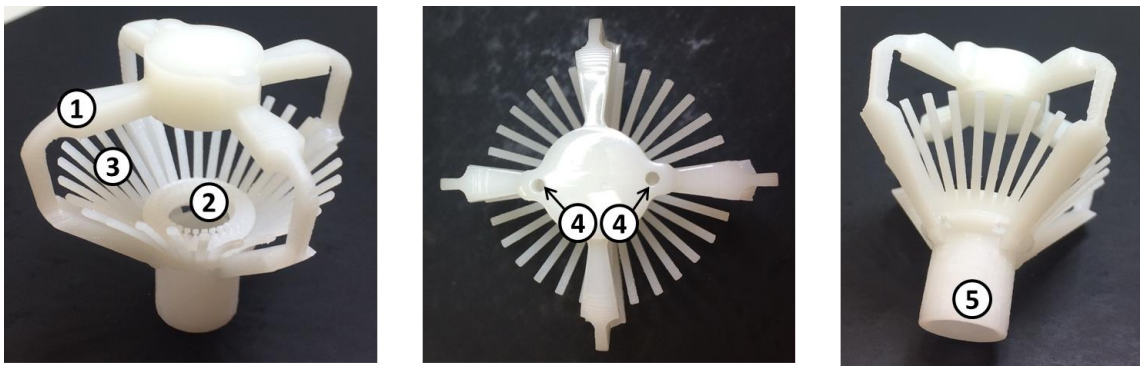

Fig. 2.6. Hyperdrive's main structure from different perspectives.
(1) One of the four EIB holder posts. **(2)** Inner circle before microdrives' holes perforation. **(3)** Microdrives' guide posts. **(4)** Top flat surface of the hyperdrive highlighting the holes used to fix the EIB. **(5)** Bottom part of the drive where the array bundle is fixed inside and all polyimides and tetrodes converge.

2.4.2. Medium polyimides bundle

In the designed hyperdrive we use a set of polyimide tubing (i.e. a polymer thermoset plastic) and its function varies according to its respective size. The bottom piece of our hyperdrive is composed by a bundle of medium polyimides (outer diameter of 294.64 µm and inner diameter of 180.34 µm) in which both the size and design of the array is settled according to the target regions' brain coordinates. Based on our target regions' anatomy and the size of each medium polyimide, we ended up with a bundle of 5 by 7 layers thus resulting in an array of 1.7 mm medium-lateral by 2.5 mm anterior-posterior (see figs. 2.7 and 2.8).

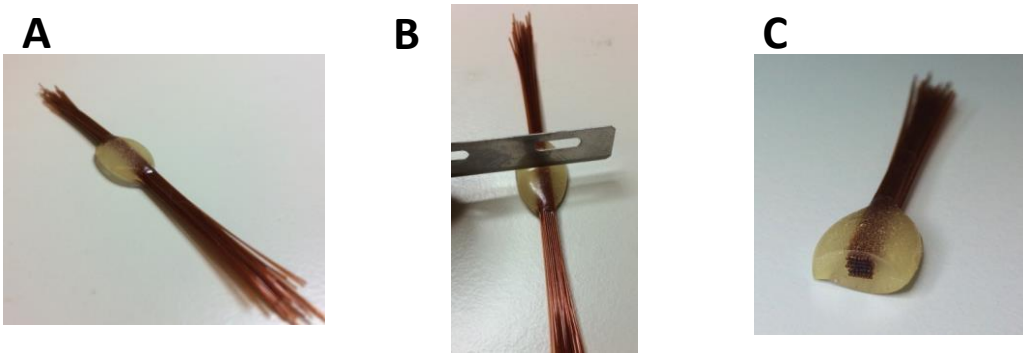

Fig. 2.7. Bundle array cut.
(A) Medium polyimides bundle after fixation with epoxy glue. **(B)** Cutting the collector cannula with a sharp razor blade. The blade and the set of polyimides must form a 90º degrees angle. **(C)** Cross-section view of the bundle after the cut showing the array's format.

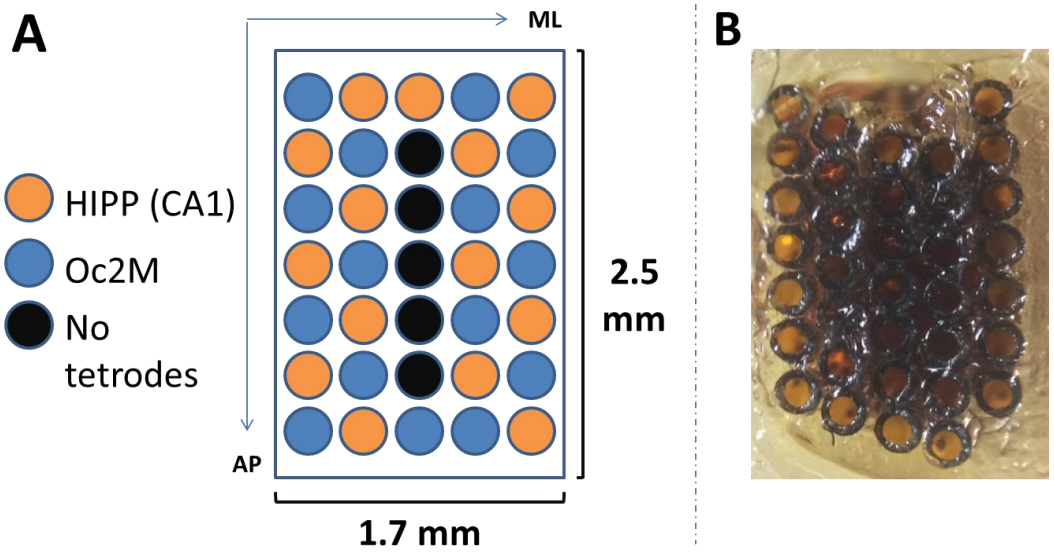

Fig. 2.8. Hyperdrive's bundle array.
(A) Cross-section representation of the tetrode array. **(B)** Magnified bottom view of the array.

2.4.3. Map medium polyimides to the corresponding brackets

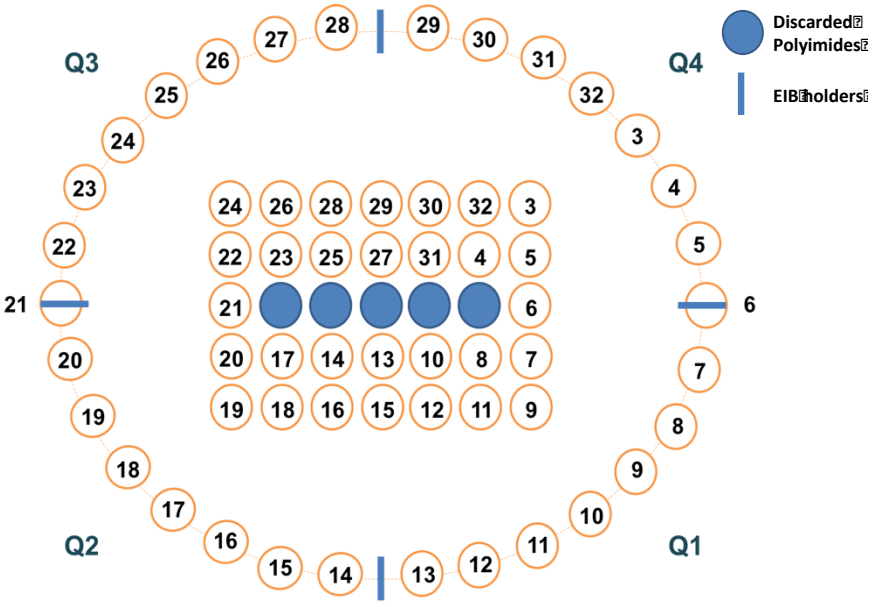

Fig. 2.9. Top view of a schematic representation of the guide tubes mapping.
The middle rectangle shows the designed array and each number represents one single medium polyimide. The outer circle stands for the 30 guiding posts of the hyperdrive's main body. By corresponding the equal numbers we get the destination sites of the guiding tubes. The EIB holders divide the hyperdrive into 4 quadrants (i.e. Q1, Q2, Q3, and Q4).

Medium polyimides work as guiding tubes that conduct thinner polyimides and respective tetrodes from the bottom array to the EIB. Polyimides are matched to the available brackets in a way to minimize as possible their curvature and overlapping (fig. 2.9). The polyimides placed in the middle line of the array are the most distant ones to the brackets, which result in a more

accentuated curvature if connected (fig. 2.9, blue circles). Therefore, these polyimides were discarded. Thick polyimides were cut into several small pieces within a range of 2-2.20 millimeters and slid over the medium size tubes (fig. 2.10, B, 2). They help fitting the guiding tubes into the brackets in order to provide more stability.

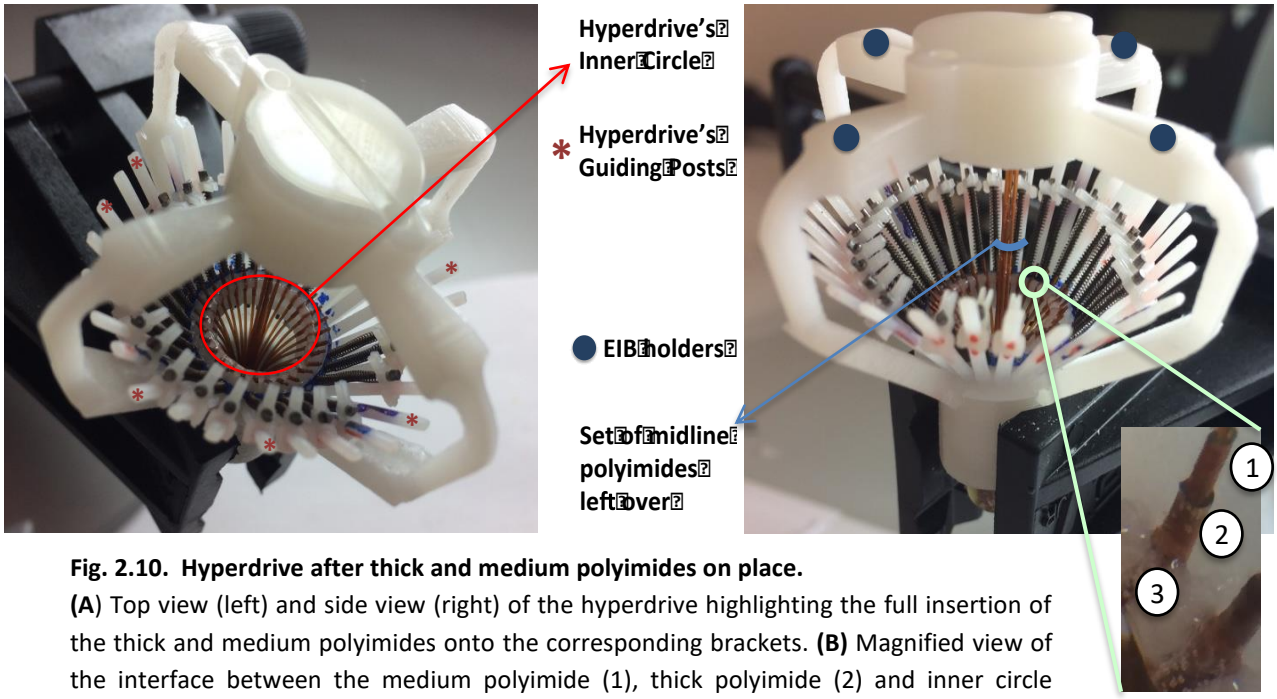

Fig. 2.10. Hyperdrive after thick and medium polyimides on place.
(A) Top view (left) and side view (right) of the hyperdrive highlighting the full insertion of the thick and medium polyimides onto the corresponding brackets. **(B)** Magnified view of the interface between the medium polyimide (1), thick polyimide (2) and inner circle structure filled with epoxy (3).

2.4.4. Top piece, half-moon microscrew and drive spring

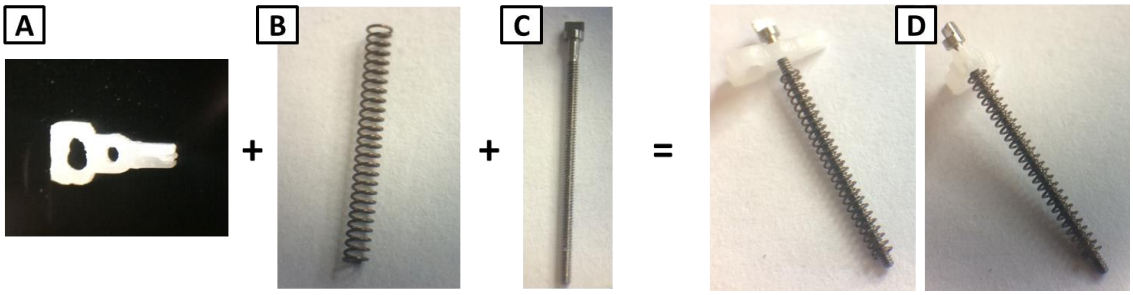

Fig. 2.11. Microdrive components responsible for the up and down movement of tetrodes.
(A) Top-piece tool showing two hand-made holes of different sizes. The hyperdrive's guide post will fit into the larger hole whereas the smaller one is meant the microscrew. **(B)** Microdrive's spring. **(C)** Half-moon microscrew used to move up and down all microdrive's components. During electrophysiology recordings, the number of microscrew turns will indicate how deep tetrodes are in the brain. **(D)** Picture of these components assembled before its attachment to the hyperdrive (see fig. 4.8 in the previous section for a view of the multiple microdrives (without tetrodes) already added to the main structure).

2.4.5. Thin polyimides

The thin polyimides will later receive tetrodes. They are cut into 30 equally sized portions, inserted inside the medium ones from the bottom of the hyperdrive, and fixed to the top pieces (fig. 2.12).

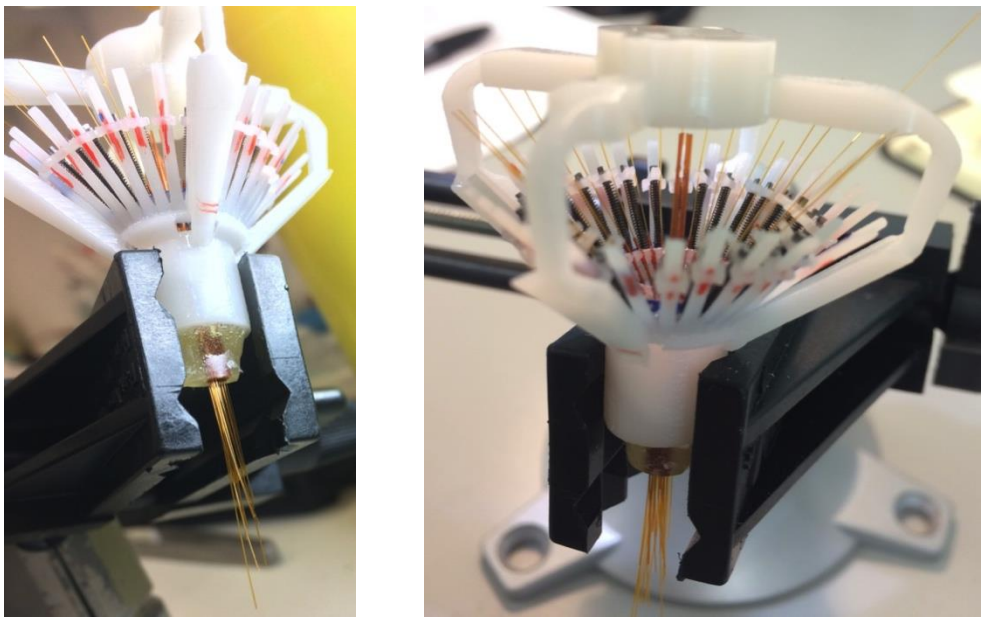

Fig. 2.12. Hyperdrive from two different perspectives after thin polyimides insertion and fixation.

2.4.6. Tetrodes

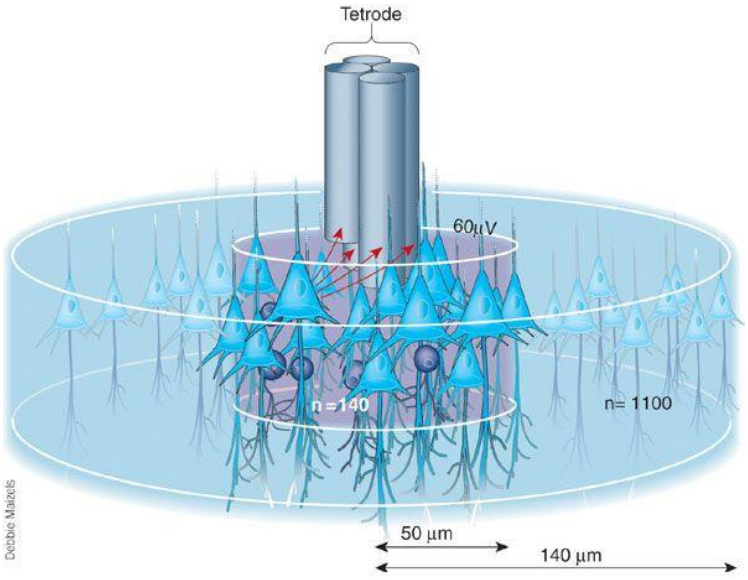

Fig. 2.13. Representation of neural recordings using tetrodes. Retrieved from Buzsáki (2004).

The activity of the surrounding neurons is recorded by tetrode wire implanted on the brain tissue. Each of the four red arrows represents the distance between the cell and the respective tetrodes' channel. Due to their different lengths, the neuron's activity recorded at a given timestamp will show different waveform shapes across the four channels thus allowing the identification of specific neurons.

What they are

All the electrophysiological data was acquired by using tetrodes (fig. 2.13). Each tetrode comprises four channels that independently record extracellular field potentials. The existence of multiple channels in a single wire enables to identify the activity of single neurons and correlate its activity with behavior outputs.

How they are made

Tetrodes are made in the lab using insulated electrode wire (inner diameter of 12.7 µm). We begin the process by getting a 40/50 cm long portion of wire and we fold it in half. The wire is folded back again and we cut the non-looped end.

As illustrated in fig. 2.14, the wire goes through a twisting process programmed in the motorized device in which 100 clockwise turns are applied followed by 40 counter clockwise turns. Once finished, the wires are fused using a heat gun (420º) from 3 different angles along the whole tetrode (fig. X - B) and as a result we get a stiff bundle of four microwires.

Fig. 2.14. Turning four separated wires into one single tetrode.

(Left) View of the folded wire hanged and clamped to the motorized twister machine **(Bottom)** After twisted, wires' insulation is melted by applying hot air flow (420º) from 3 different angles along the tetrode.

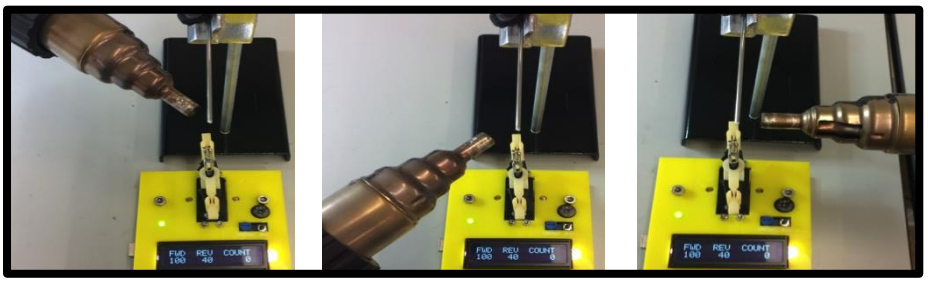

How they are loaded

Before start loading the tetrodes to the hyperdrive, the EIB (green circular structure in fig. 2.15, A) is fixed on the top of the main body structure using two custom-made screws and epoxy.

Tetrodes are inserted into the thin polyimides using a microscope with 3x magnification (fig. 2.15, C). Once inside the polyimide, the tetrode is slowly pushed down and a quick cut is performed in the middle of the looped end (i.e. the top remaining portion of wire with a circular shape). The cut splits the twisted electrode wires thus leaving their tips available to be inserted into the EIB holes. The electrical connection between the wire and the EIB is established by fitting in a gold pin (fig. 2.15, B).

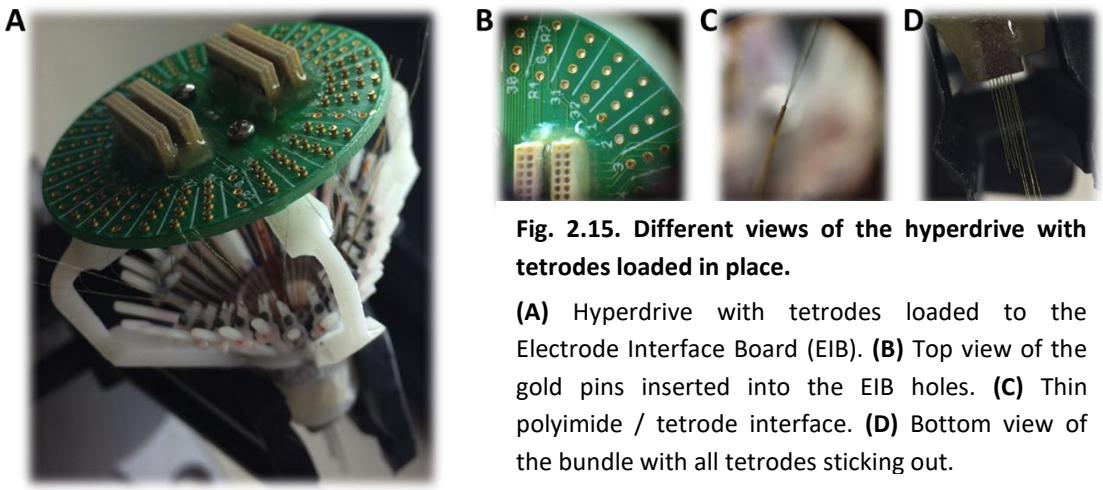

Fig. 2.15. Different views of the hyperdrive with tetrodes loaded in place.

(A) Hyperdrive with tetrodes loaded to the Electrode Interface Board (EIB). **(B)** Top view of the gold pins inserted into the EIB holes. **(C)** Thin polyimide / tetrode interface. **(D)** Bottom view of the bundle with all tetrodes sticking out.

2.4.7. Gold Plating of Tetrodes

The gold plating is a process that uses electrical current to deposit a thin layer of gold onto the tips of all tetrodes (fig. 2.16). This process aims to reduce tetrodes' long-term corrosion and decrease its electrical impedance. Low-impedance electrodes increase the signal-to-noise ratio and allow us to record and analyze signals of small amplitudes.

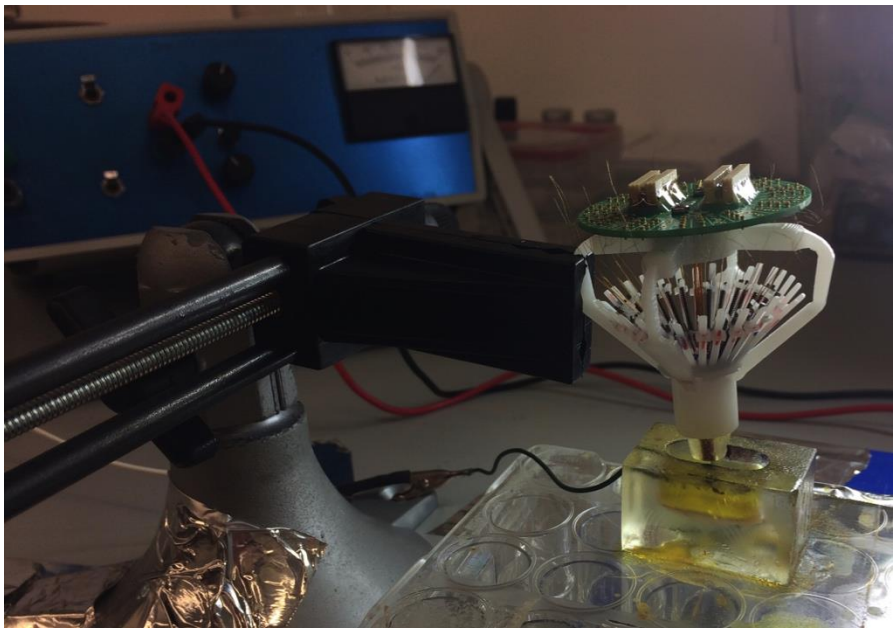

Fig. 2.16. View of the hyperdrive during tetrodes' gold plating process.
One of the four EIB holder's posts is clamped to the panavise. We down-expose the tetrodes about to be plated and immerse them in the electroplating solution.

We setup a stimulus isolator and an electrode impedance tester. The positive and negative leads are connected, respectively, to the gold plating solution and the EIB gold pin. Once established the electrical circuit, brief bursts of current pulses are generated ranging between 1 μA and 3 μA until impedance levels of 200 to 300 kΩ are achieved. Tetrode electroplating leading to values below than 100 – 150 kΩ might cause a short circuit meaning that channels become no longer independent of each other.

2.4.8. Protective Cone and Ground Wires

The different components of the hyperdrive are highly exposed and its probability of damage increases significantly by having it on an implanted living animal. To guarantee the long-term stability of the whole structure equipment, a shielding cone from a sheet of aluminum foil was hand-made in the lab and added to the hyperdrive (fig. 2.17).

The last step comprises the soldering of two grounded wires to the EIB. The shortest one (about 5 cm long) is connected to the protective cone and the other one (about 15 cm long) to the animal's skull. They serve as reference points from which voltages are measured.

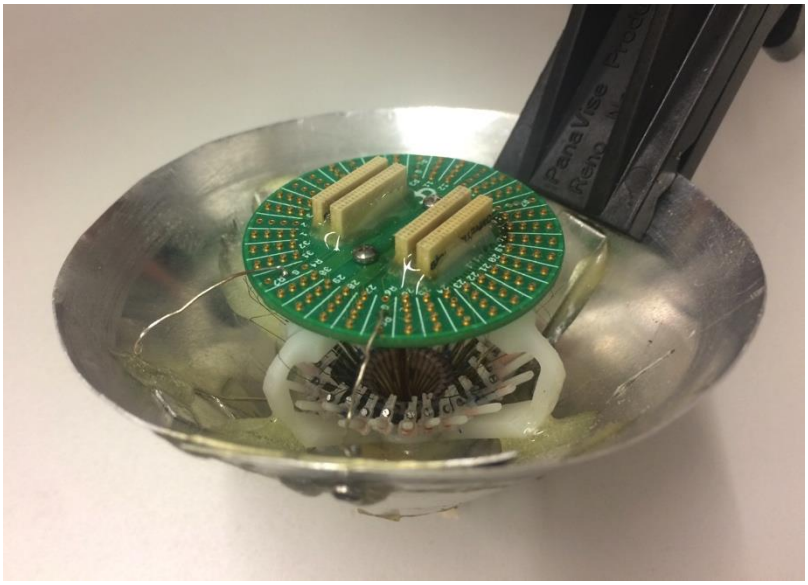

Fig. 2.17. Hyperdrive on its final stage ready for implantation.

2.5. Implant Surgery

We performed a stereotaxic surgery for implantation of the hyperdrive (for a detailed description, see VI. Supplementary Information – Methods). The size and location of the craniotomy window were defined based on the coordinates of the target regions and the size limits of the bundle array. The full recovery of the animals occurred approximately within a week, during which rats had access to *ad libitum* solid food and high nutritional water-gel. Animal's welfare was checked on a daily-basis and any illness symptoms were treated according to the standard medical procedures.

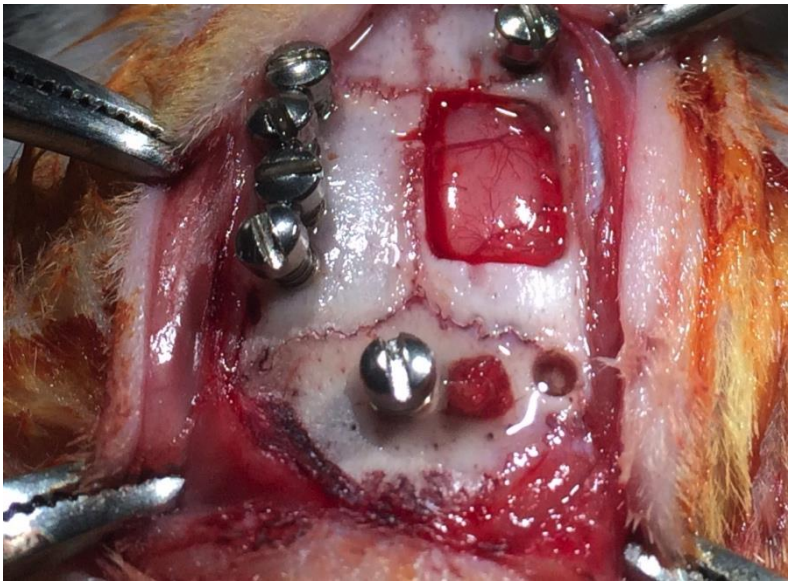

Fig. 2.18. Top view of the surface of the skull after craniotomy and screws fixation performed on a training surgery session.

The figure highlights the correct placement of the fixation screws close to the temporal crest on the left side of the skull. One should avoid driving the screws right on the sutures, as represented by the screw placed right on the top of the craniotomy. It is also possible to see the screw aimed for the ground electrical connection placed posterior to the lambdoid suture. This picture was taken from a surgery test performed in a young Sprague Dawley rat so the size of the craniotomy does not necessarily corresponds to the measures used in the implant surgery.

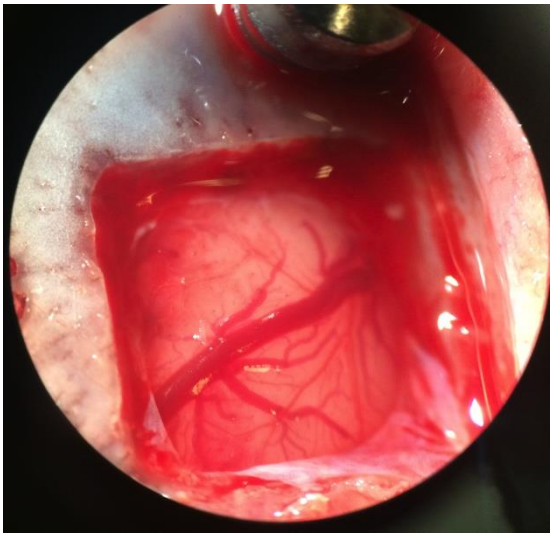

Fig. 2.19. Magnified view of the surface of the brain after craniotomy and durotomy performed on a training surgery session.

For durotomy, a tip of a small needle is used to puncture and cut the dura mater carefully enough to not touch the brain tissue underneath. The membrane should be then pushed aside towards the margins of the craniotomy area leaving the brain surface fully exposed. It is possible to see in this picture remaining fragments of dura mater around the craniotomy after its lateral extraction, especially at the bottom right corner (the whitish tissue).

2.6. Perfusion and Histology

After all experiments with the implanted rats are done, they are sacrificed via isoflurane inhalation overdose and perfused with 300 ml of phosphate-buffered saline (PBS), followed by 500 ml of 10% formalin solution. Discoloration of lungs and muscle, paws' contraction and tail twitching are good indications of a successful perfusion meaning that formalin is reaching the whole body. Animals are further decapitated, the brain is carefully extracted and placed inside a falcon tube containing a postfix 4% PFA solution, where is kept overnight at 4ºC. The day after, the brain is soak into a 30% sucrose solution made with PBS where is once again kept overnight at 4ºC. The brain is then embedded in gelatin for 4 hours at 37ºC and frozen in liquid nitrogen.

Coronal brain slices of 40 µm were obtained using a cryostat (Leica, CM3050 S). By comparing the atlas of the rat brain with the appearance of the slices, we discarded samples correspondent to very posterior or anterior coordinates from the target regions. Brain tissue sectioned from the regions of interest (or close enough) were mounted on slides right away or, in case slices golt folded, were put in a multi-well culture plate. All selected samples were subject to Nissl staining, a procedure conducted by the Histology Facility of iMM.

2.7. Tetrodes tracks imaging

High-detailed images of pre-processed brain slices were obtained using a digital slide scanner (NanoZoomer-SQ, C13140-01). We used a 20x magnification and performed single layer scan with a bright-field profile. The scan covered the entire slice and the focusing points were manually selected (preferentially over the identified target regions).

2.8. Data analysis

Results regarding SCTAT behavioral data were analyzed and plotted using

the integrated development environment (IDE) PyCharm for Python programming language. Electrophysiological data was analyzed in Matlab (MathWorks, version R2015b) and raw data extraction was carried out using code written by Miguel Remondes. The code for Local field potential (LFP) analysis was adapted from available scripts written by Mike X Cohen (Cohen, 2014), whereas multi and single-unit activity was analyzed using the software package UltraMegaSort2000 (Hill, Mehta, & Kleinfeld, 2012).

Position data was acquired by tracking a light source connected to the animal's head that generates values of x and y coordinates (as also time values) at the sampling rate of the video file acquisition system (30 frames/s). However, such does not happen at a constant rate since it is entirely dependent on light detection by the system[6]. Despite the tracking system, time vector values could also be obtained directly from the video file (it takes time values at a constant sampling rate independently of tracking detection), or simply by converting the number of ephys data points assuming a linear sampling rate acquisition of 30k samples per second. Bonsai software was also encoded to take stimuli timestamps and save it accordingly. In the end, all data outputs are interpolated and combined so that behavioral data can be correlated with neural activity.

Time series data derived from a particular brain area was computed by signal averaging all tetrodes that were targeting the respective area at the time. Therefore, in LPF analyses, electrophysiological data from Hippocampus and Oc2M are each represented by one single vector of data points. There is just one caveat: one must be sure that all tetrodes contributing for the average are actually on place[7]. To come up with a reliable estimation of tetrodes position over days, we used different sources of information, such as the number of turns in each microdrive adjustment, the alignment of the tetrodes at the time of the surgery, the signal trace and, ultimately, the post-mortem histological verification of

[6] For instance, the animal sometimes moves to the corners of the SimBox and stays in a certain position that light can no longer be detected. Additionally, since tracking system is encoded by Bonsai software to take the largest binary region, when light stimulus is triggered, its source 'competes' with the light on the rat which lead the considerable variations on x and y values. This problem is further addressed in the Discussion section.

[7] This verification is also vital for further conclusions regarding single and multi-unit post-hoc analyses.

tetrode tracks. Short sleep sessions were recorded everyday after behavior, to later plot and compare the signal trace along the different tetrodes (fig. 2.20). Such strategy allows us to estimate how far tetrodes are (or not) from the target and to prepare the next day adjustments accordingly. Indeed, events such as sharp-wave ripples (SPW_Rs, see for review Buzsáki, 2015) and high-frequency oscillations, widely known as 'ripples' (110-200 Hz), are unique neural hippocampal signatures that, once you see it on the trace, serve as confirmatory evidence that activity is being recorded from the hippocampus (fig. 2.20).

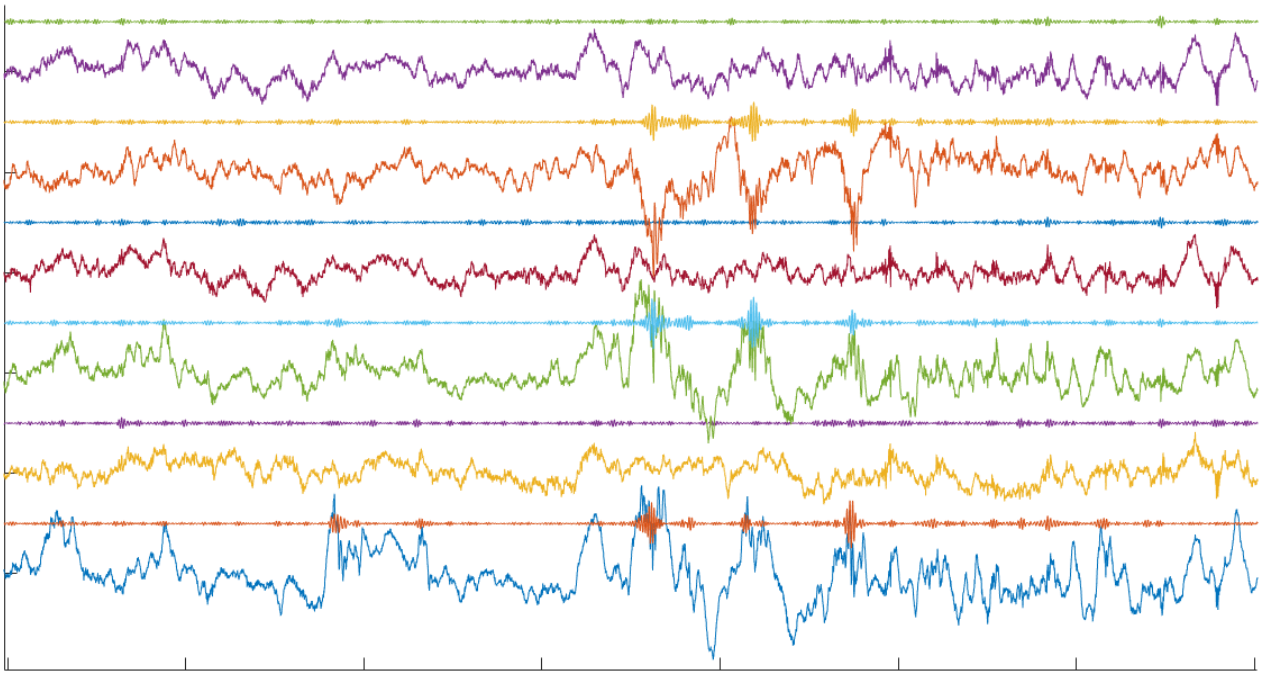

Fig. 2.20. Two seconds of LFP data highlighting the differences between cortical and hippocampal activity.

Each LFP trace corresponds to the recorded activity from one single channel of a chosen tetrode. From top to bottom, the first (purple), the third (red) and the fifth (yellow) trace represent cortical activity, whereas the remaining ones (orange, green and blue trace) represent LFP activity recorded from hippocampus. Right on the top of each LFP trace, the respective filter for the sharp-wave ripple band (between 150-250 Hz) is also plotted, in which its increase in amplitude is proportional to the frequency increase of the signal. The figure clearly shows a ripple component captured by the high-frequency filter only on 3 of the 6 tetrodes. As expected, those 3 correspond to hippocampal channels.

For LFP analyses data were band-pass filtered between 0.1 Hz and 300 Hz and resampled at 3 kHz to optimize computational time. In ERPs, each trial is time-locked, as we take 500 milliseconds of data before stimulus onset, followed by the 2 seconds stimulus duration, plus 500 milliseconds after stimulus offset,

thus resulting in a 3 seconds epoch. All trials over sessions were concatenated. Time-frequency representation of the ERP was calculated through a mathematical method called continuous wavelet transform. A complex Morlet wavelet was created multiplying a Gaussian window with a complex sine wave. The resulting wavelet is composed by a real and imaginary part, and its length corresponds to a four seconds window (i.e. it was defined by -2:1/sampling rate:2, zero padding both sides). The wavelet 'slides' throughout the whole signal (looping over different frequencies) giving us frequency information at each point in time, as opposed to the Fourier transform that only give us the overall frequency representation of a time varying signal[8] (see fig. 6.2, in section VI. Supplementary Figures). This method works as a band-pass filter since we define beforehand the number of wavelets of different frequencies that convolute the signal. Additionally, working with complex functions enable us to extract phase and power information from the input signal.

The process of action-potentials extraction starts by computing a common-average of all tetrodes' signal and subtract it to each channel individually. As a result, general noise is subtracted to itself thereby partially removing it. Such subtraction does not eliminate putative spike-trains present in the signal given that those are channel-specific. The resulting data were then band-pass filtered between 700 Hz and 8 kHz. A set of built-in functions from UltraMegaSort2000 (Hill et al., 2012) were used to automatically detect and sort single-unit spikes from the filtered data[9]. The software comes with a graphical user interface (GUI) that allows us to manually inspect and correct the previous sorting based on specific metrics displayed on graphical tools (e.g. refractory period during interspike interval, temporal stability over time, estimated missing spikes, etc. See Hill, Mehta, & Kleinfeld, 2011). In the end of spike sorting process, each cluster should be assigned to a single neuron or to multi-unit activity (in case waveform shapes can't be separated because of a low signal-to-noise ratio).

[8] Even though the main underlying mathematical operation of wavelet convolution (i.e. transforming a signal in time-domain to frequency-domain) comes from the Fourier transform technique.

[9] One could expect beforehand which tetrodes will show single-unit spike trains in the UltraMegaSort2000 framework, as Bonsai shows in real-time spike activity detected below a predefined threshold along the 4 channels of a single tetrodes (fig. 2.21).

Based on animal's position tracking we computed speed by taking the distance covered by the animal as a function of time. Only trials in which the animal was detected during the whole epoch were included in the analysis (i.e. where the total number of x, y and t values per trial is equal to 60, since that trials are 2 seconds long and camera's acquisition rate is 30 frames per second). Solely sound trials were suitable for this analysis. Next, we took all detected trials and separated them into two different groups: stationary and non-stationary trials. We consider that the animal is motionless if speed is below 5 cm/second, so stationary trials were defined as trials where at least 80% of all speed values (45 out of 60) were below the threshold of 5 cm/s. If such criterion was not met, trials were included in the non-stationary group.

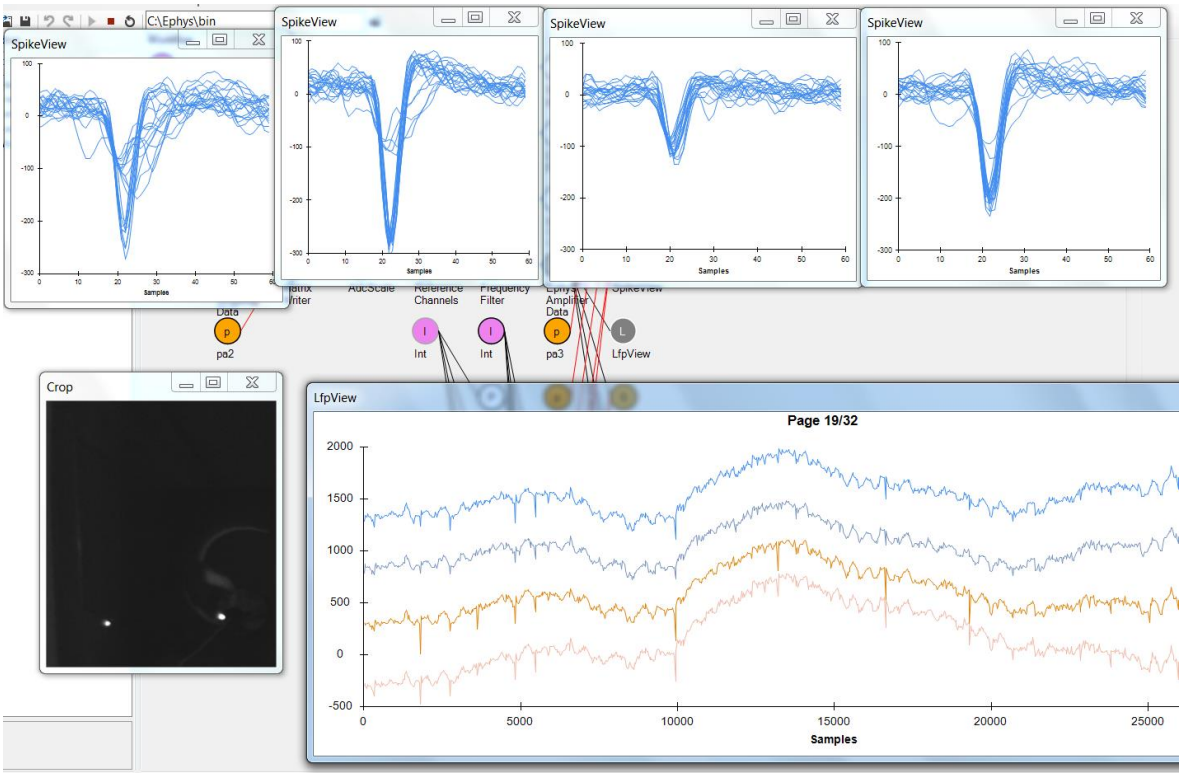

Fig. 2.21. Bonsai software view during StimBox electrophysiological recordings.

On the top, 4 SpikeView windows are displayed corresponding respectively to the 4 channels of the selected tetrode (in this case, the tetrode number 19). On the bottom there are two open windows: the left is showing the video file being transmitted from inside the behavior room, and the right window is displaying the LFP trace of each channel of the chosen tetrode. A threshold of -80 mv is defined in the Bonsai software and whenever an electrophysiological event is detected below that threshold, the corresponding waveform is shown in the SpikeView windows. In this picture it is possible to see the activity of at least one neuron being captured, given the different amplitudes across channels and the physiological waveform shape. Such spikes can also be seen on the LFP trace.

III. Results

3.1. Behavior – SCTAT (2 Conditions)

We were able to successfully implement the SCTAT (2 conditions) protocol with the first group of animals used (fig. 3.1). The plots show that both rats achieved good performance levels within a relatively short number of sessions. According to our criteria, chance level is between 40% and 60% of correct trials (represented by the grey squares in fig. 3.1 and 3.2), and we evaluate a behavior session as 'good' when animals are able to perform above 70% in both sensory conditions. For instance, only taking into account the average performance of the animal (represented by the blue line in fig.3.1) might lead to biased interpretations of the behavior. Take the example of fig. 3.1, where the average performance of both animals on the session number 5 is above chance level. A more careful evaluation of this data lead us to conclude that rats were actually biased to the right trajectory, meaning that they were behaving independently of the triggering cue.

Caution is important when interpreting behavioral results from a 'blocks increment' approach. For example, good performances from sessions with a high number of consecutive trials per block, do not necessarily mean that the animal is responding to the conditioning. In this sense, repetitive choices have a high likelihood of being rewarded and rats can just adopt the strategy of deciding based on the outcomes of previous trials, independently of stimuli. Such strategy might partially underlie the good results observed at the very first session in fig. 3.1 (especially in 3.1-A), given the small difference between the defined number of trials per block, 20, and the total number of trials performed, 30. As such, sensory condition was switched only once. Additionally, it is also possible that rats have retained information from the previous training composed by forced and open choice sessions.

The overall average number of trials per session in rats #1 and #2 were, respectively, 58 and 56 trials (fig.3.1 and 3.2). The number of trials per block was also equally pre-defined so that data could be compared across animals.

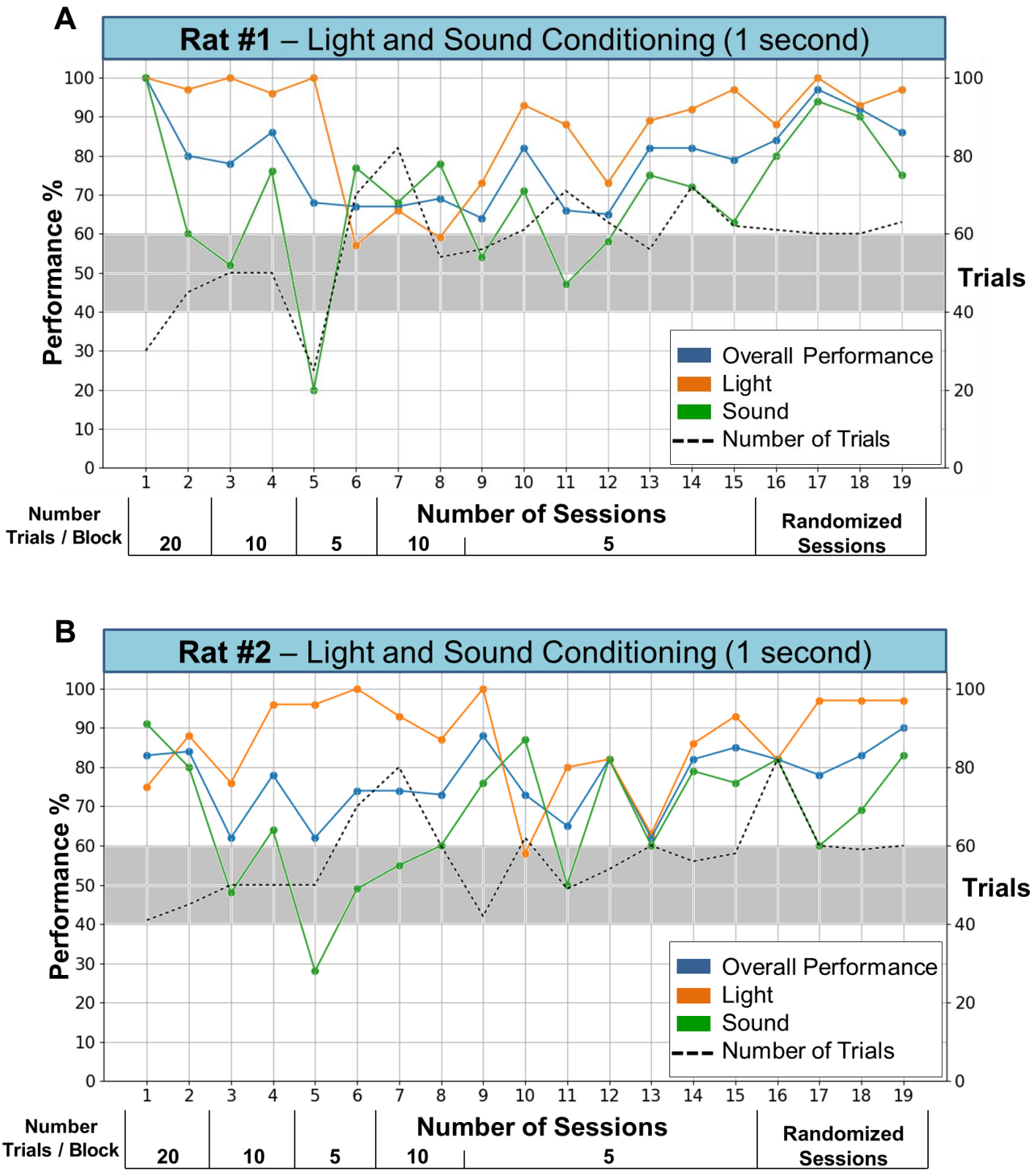

Fig. 3.1. (A) and (B). Rats do associate a particular sensory stimulus with a specific trajectory.

Within 2/3 weeks they were able to reach a consistent performance above 70% for both stimuli. On the bottom of each plot it is represented the number of trials per block at a given session. The number on its axis represents how many consecutive trials of the one single sensory modality were triggered before present the other sensory cue (see II. Methods section).

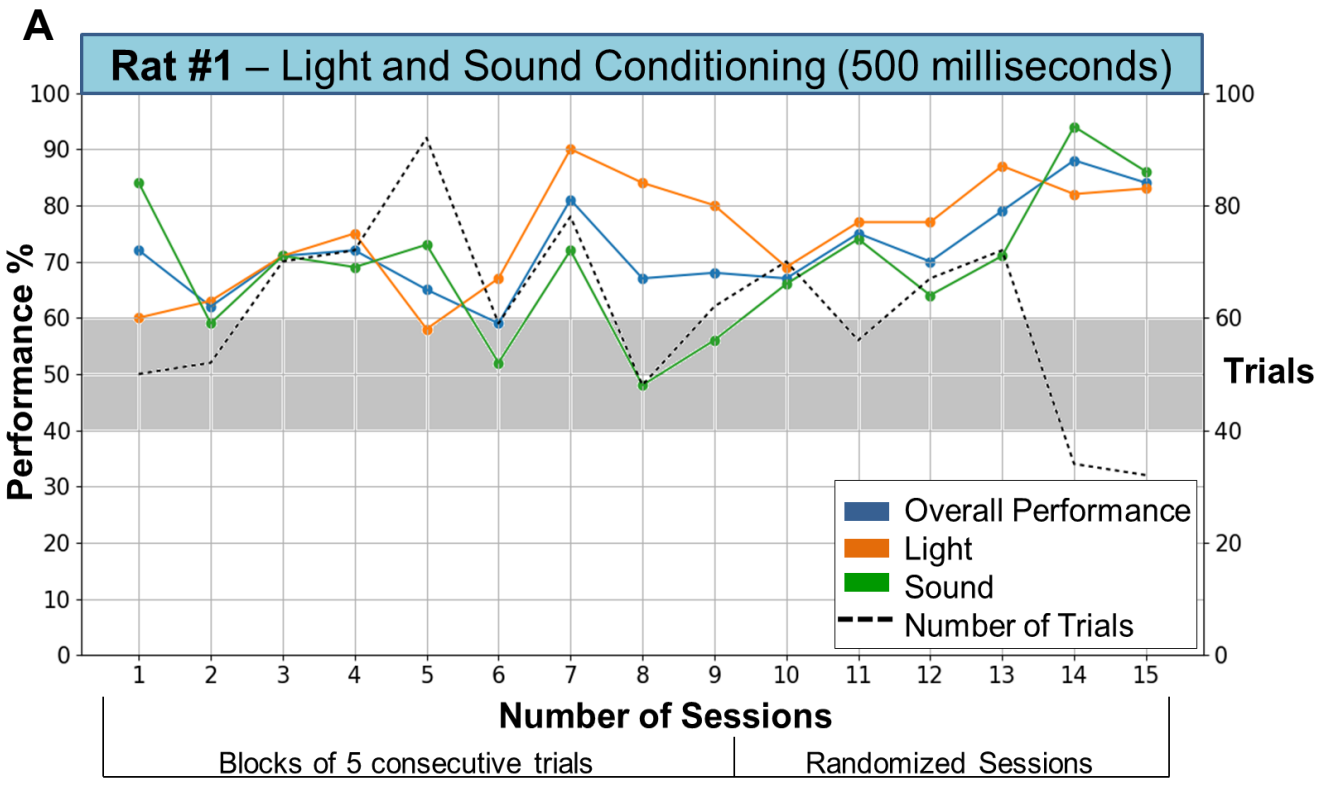

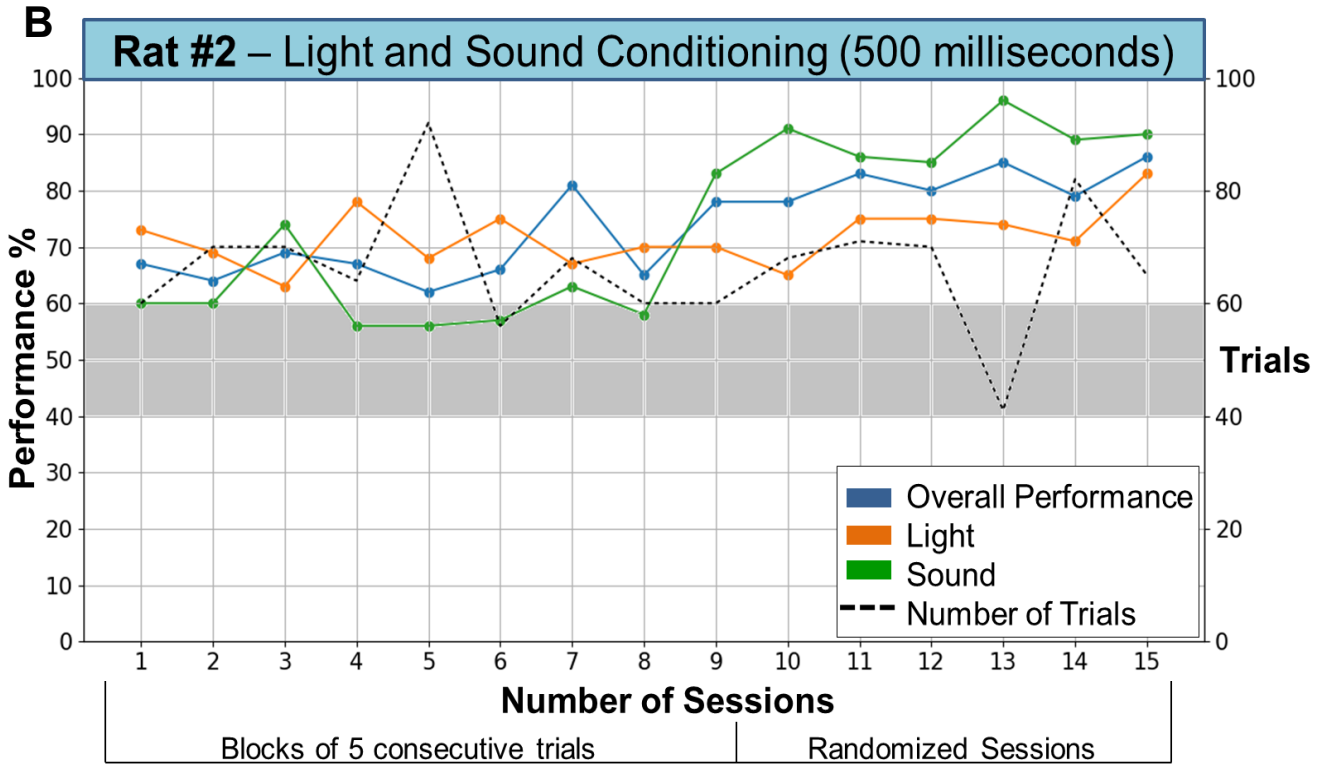

Fig. 3.2. (A) and (B). Rats are able to recall the SCTAT after a long period without training.

Even with a shortened duration of stimuli (500 ms instead of 1 second), they took fewer sessions to reach the expected performance.

After 19 sessions, the protocol was discontinued and animals were only tested again 33 days after. They were then trained under the same principles but with some added variations: stimuli duration were 500 milliseconds long, instead of 1 second, and both rats immediately started with the 5 trials per block protocol. Despite the more demanding constraints of the task, only 9/10 sessions were needed for rats to recover the good performance levels. The fig. 3.2 highlights the fact that both subjects showed a percentage of correct trials significantly above chance level during the randomized stage. Besides, one can observe that such difference is stable over time and balanced across stimuli[10].

Interestingly, there was an increase of performance once rats were tested for the first time in the randomized version of the task (exception for fig. 3.2, B). By a better performance, one can define it as the overall improving in terms of percentage of correct trials (fig. 3.1-A), or simply a more equal response to both modalities (represented by the approximation between the orange and green dots at the given session, figs. 3.1-B and 3.2-B).

The total number of trials across sessions varied in a non-constant manner[11]. Such observation could not be attributable to rats' deprivation, since their body weight was regulated to never go less, or above, than 85% of the initial body weight. We tested if the number of trials performed in a session was correlated with the interval (in days) between sessions. The fig. 3.3 shows a statistically significant negative correlation between these two variables, where 28% and 44% of the variance observed in the number of trials is explained by the inter-sessions interval, respectively, for rats #1 ($r = -0.53$, $p < 0.01$) and #2 ($r = -0.66$, $p < 0.001$).

[10] The otherwise would be suggestive of a possible bias towards a specific trajectory.
[11] Although it hasn't always affected performance values, is it crucial to get a reasonable number of trials per session. This is especially important during electrophysiological recordings, so we can have enough statistical power for single and multiunit analyses.

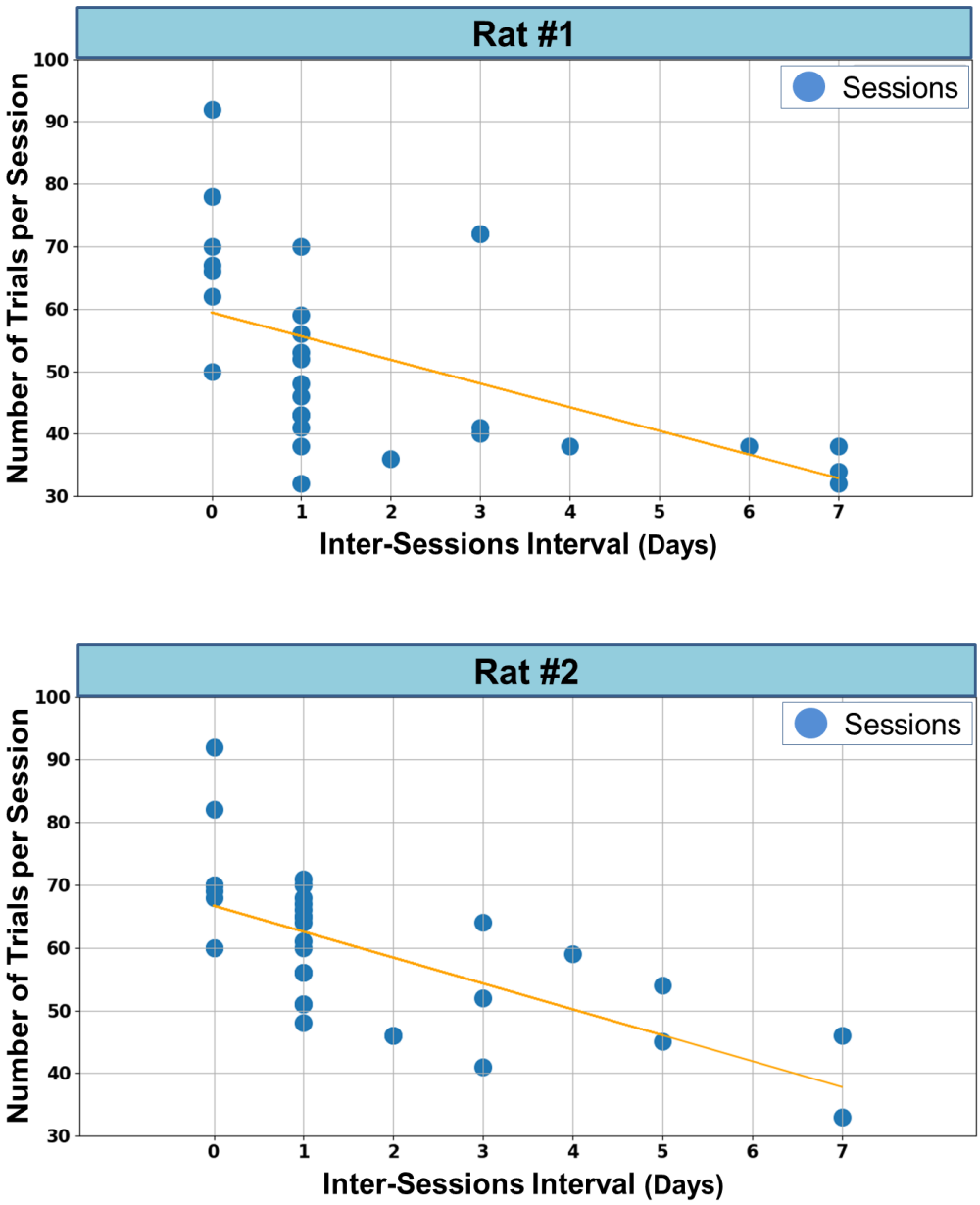

Fig. 3.3. Number of trials performed in a session is negatively correlated with the interval (in days) between sessions.

Each blue dot represents one single session. The y-axis gives the total number of trials performed by the animal in a given session, whereas the x-axis represents how much time has passed between that session and the previous one. In this sense, an inter-session interval of value 0 (zero) means that the respective session and the previous one happened on the same day.
It was found a statistically significant negative correlation between the two variables (rat #1: $r = -0.53$, $p < 0.01$; rat #2: $r = -0.66$, $p < 0.001$) meaning that, as the time gap between sessions increases, the number of trials performed by the animals decreases.

The fig.3.4 represents the performance plots of all sessions conducted with rats #1 and #2, from the time 500 milliseconds conditioning started. Behavior progression can be divided in two different stages (represented by the vertical

blue line): a first period, corresponding to the establishment of the SCTAT, and a second period, composed by a less intensive training schedule where the goal was only to maintain the task in animals' memory.

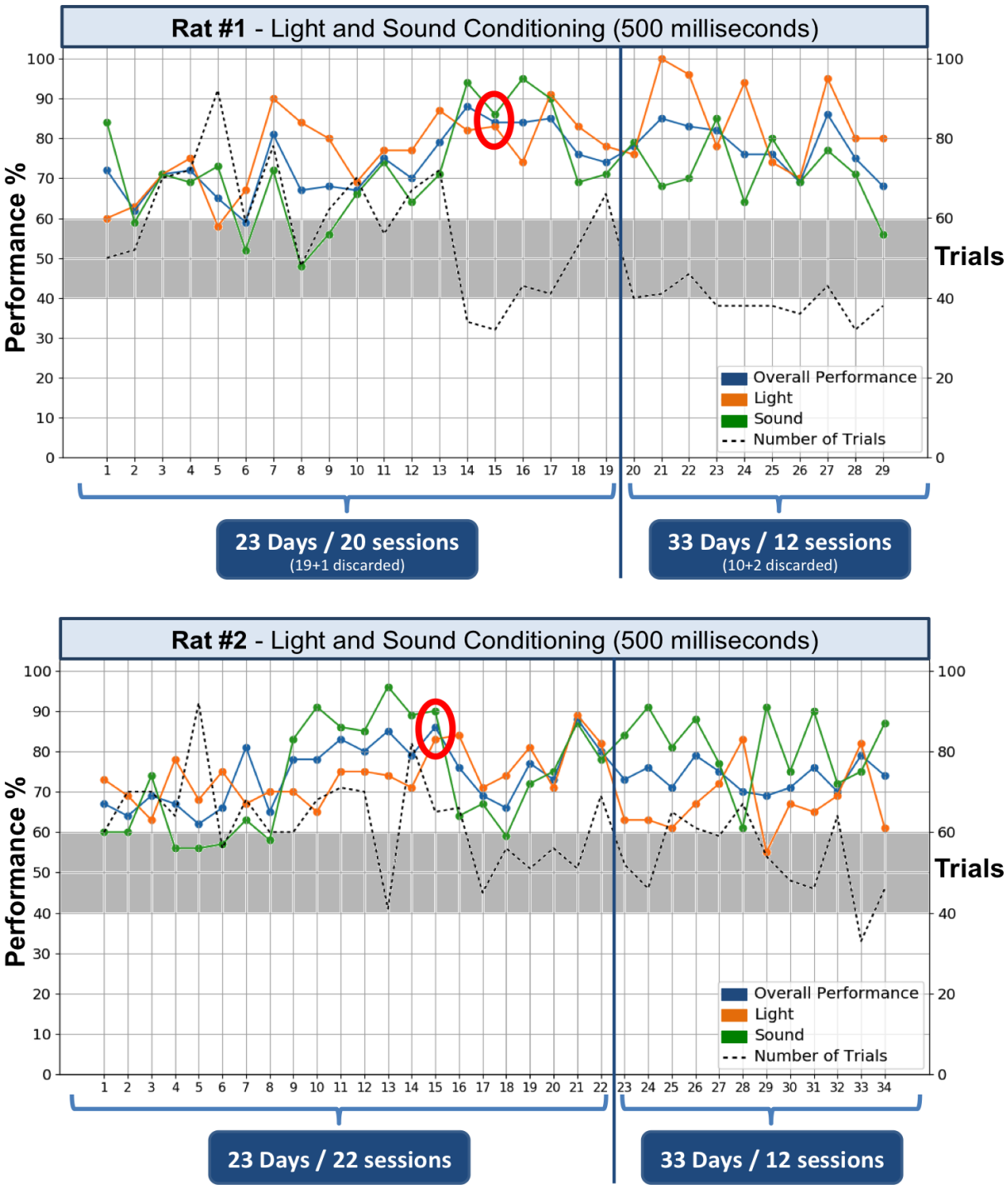

Fig. 3.4. All behavioral sessions conducted with rats #1 and #2 using 500 milliseconds conditioning.

The red circle in the middle of each plot marks the last session represented in fig 3.2 A and B, respectively. The vertical blue line along the plots divides two different training periods. On the left side, we see the behavior progression until expected performance was achieved (red circle) followed by a few more sessions; on the right, we have the correspondent performance values resulted from a flexible and low-intensity training schedule. On the bottom of each graph one can see the ratio of the number of sessions to the total number of days from both periods.

Despite the decrease in number of trials during this second period (especially in rat #1, fig. 3.4), performance stability over time seemed to decay (even though overall performance stayed always above chance level). Indeed, one can observe an increase in the number of sessions in which the difference in performance between sensory modalities is higher (i.e. worst performance). Such evidence outlines the importance of establishing a rigorous training schedule comprising, preferably, two sessions per day, in order to get the desired behavioral outputs.

Based on our data we decided to do the surgical implantation on the rat #2. The surgery lasted approximately 6 hours[12] and we left the animal recovering according to the recommended procedures. Despite the absence of any signs of illness, the animal ended up dying about 4 hours after surgery. Consequently, the hyperdrive had to be partially reconstructed during the following weeks and a new batch of animals arrived for behavioral training to start.

These new rats had a common problem regarding their initial behavior progression: a small number of trials per session. Such does not only have implications for post-hoc statistical analyses, as we previously mentioned. Importantly, the assumption that an animal adjusts behavior according to the outcomes of the task (i.e. reward correct trials and not reward incorrect responses) falls apart if a reasonable sample of trials does not exist. In other words, a good number of trials is needed when shaping behavior. The fig. 3.5 exemplifies this problem, since we had to do 24 pre-training sessions with the rat #3, before starting the actual protocol[13]. Note we took a step back after the 14th session, by implementing once again sessions in which animals were only required to perform laps without any sensory cues.

[12] It should be noted that at the time of this surgery we did not have the chance to use the isoflurane anesthesia system as described in section II. Methods. In this surgical procedure, instead of maintaining general anesthesia by inhalation of isoflurane, we administered each 1:30h a Ketamine (1ml) + Saline (2ml) injection. Even being a perfectly valid protocol, the risk of overdose is higher when compared to the usage of a precision vaporizer for isoflurane delivery (especially considering that this type of surgery lasts, at least, 5 hours).

[13] Considering that pre-training plots of all animals don't differ much between them, we only show one from rat #3 as an example.

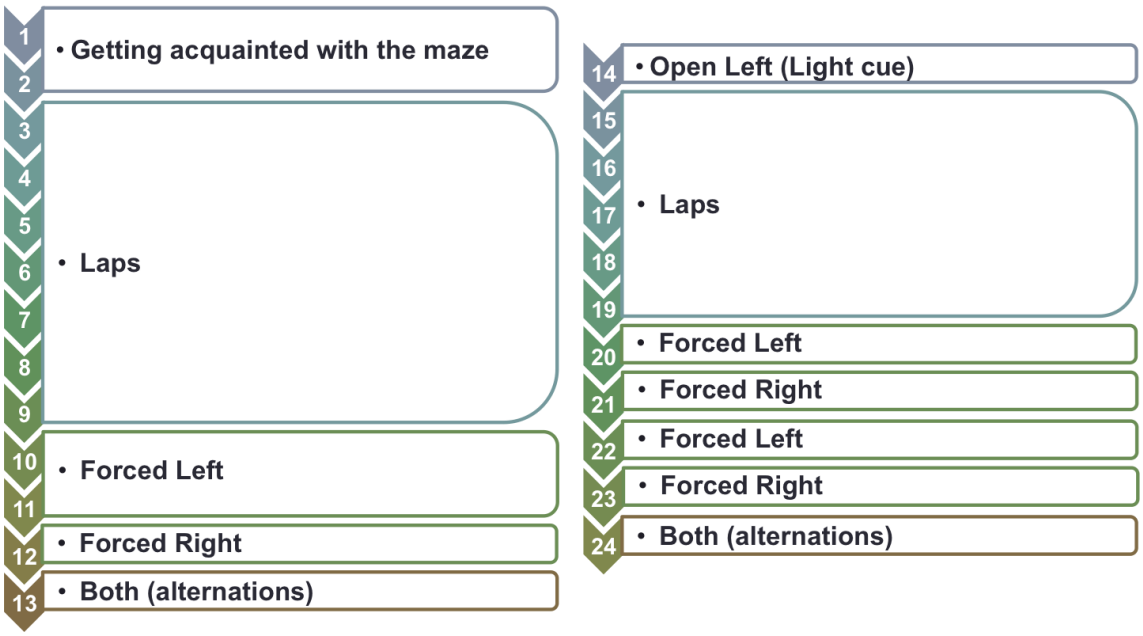

Fig. 3.5. Pre-training progression of rat #3.

The 24 sessions represented here were prior to the beginning of the 'trials per block' training approach. A 'Both (alternations)' session is when forced right and left trials are done within the same session (see II. Methods section for remaining nomenclatures).

In total, 4 more animals were trained in the SCTAT (2 conditions) and the fig. 3.6 illustrates the behavior results obtained from 3 of those rats (one was excluded since he never reached the conditioning stage of trials per blocks). The total number of sessions (pre-training sessions + sessions in the task itself + chosen discarded sessions) performed by rats #3, #4 and #5, were, respectively, 39, 43 and 44. Unfortunately, we did not get the desired results.

Animals never showed a consistent performance above chance level. Actually, in some cases, the best sessions in terms of performance also registered the lowest number of trials (e.g. see in fig. 3.6 the 6th session of rat #4 and the 4th session of rat #5). The tendency of an increase in performance once randomized trials start (see figs. 3.1 and 3.2) was not observed among the new group of animals. The rat #4 looked promising as exhibited an initial positive progression, but it soon decayed and got worse during the final version of the task. Additionally, as opposed to rats #4 and #5 who responses to both stimuli were somewhat balanced, the rat #3 had always been biased to the right trajectory regardless of sensory cue (fig. 3.6).

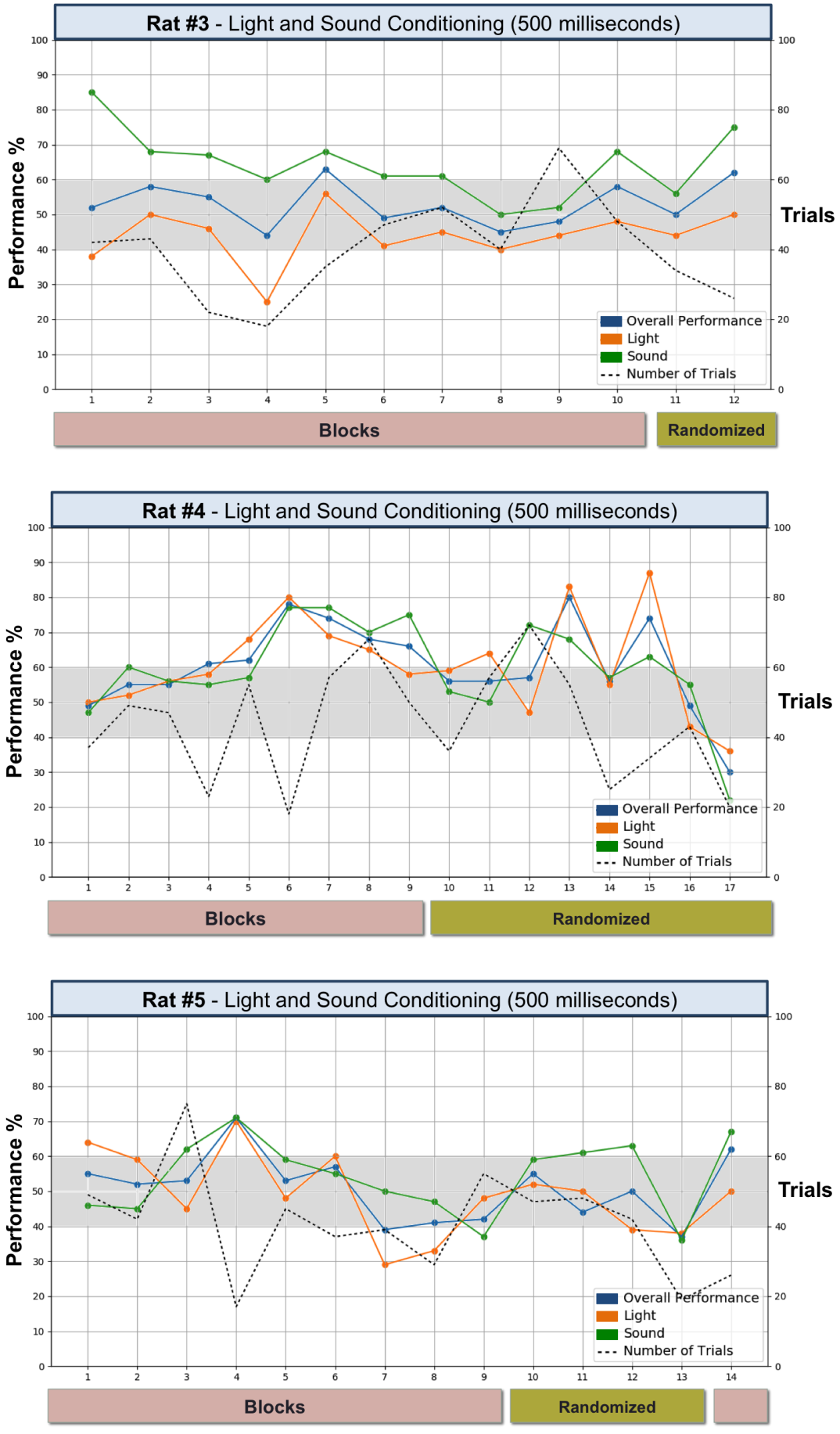

Fig. 3.6. Behavior results of rats #3, #4, and #5 on SCTAT implementation after pre-training.

3.2. In Vivo Electrophysiology

In the current section we present the results of electrophysiological recordings from two implanted rats under the StimBox protocol (see previous II. Methods chapter). The Open-Field protocol was only tested in one of the rats, in which LFP analyses were also conducted. However, the same ERP's components were found in both protocols. The main difference observed was a higher standard deviation of the signal in the Open-Field protocol, which is expected, given the lower signal-to-noise ratio due to an animal's movement. As such, we present just one example from the Open-Field to illustrate this difference (see VI. Supplementary Figures, fig. 6.3).

3.2.1. LFP responses – Stimbox Protocol

All following graphs, regarding LFP responses respective to rat's brain region and sensory condition, share the same core features. The displayed signals were computed via the same methodology (see 2.8. Data Analysis, in II. Methods section). Therefore, the description in the legend of figure 3.7 serve as a reference to all remaining LFP plots.

Rat #1 – 'Fausto'

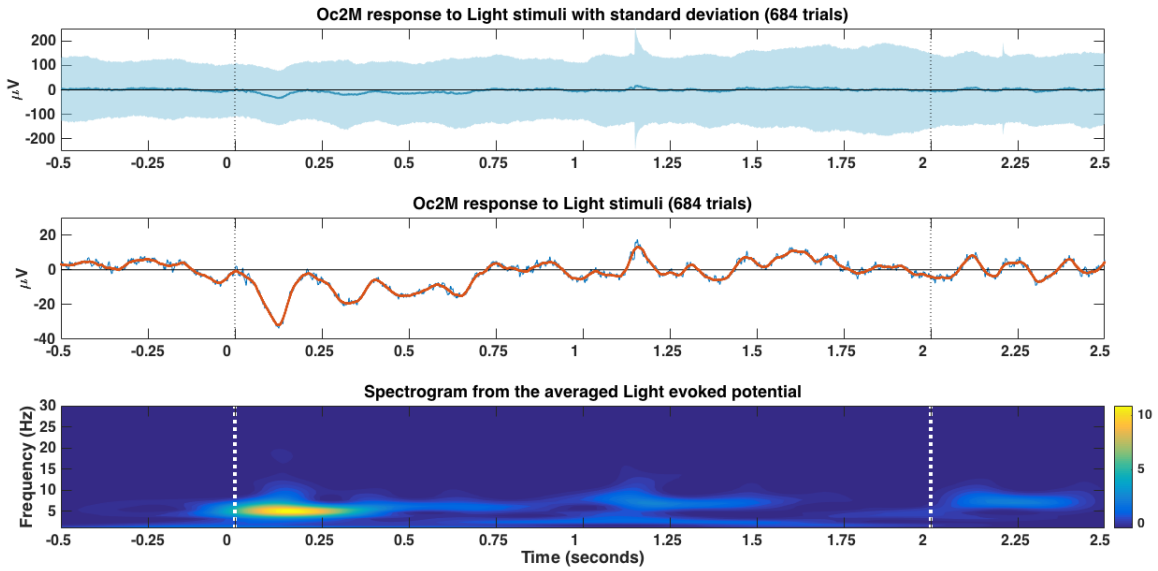

Fig. 3.7. Fausto's Oc2M response to light stimuli in the Stimbox protocol (n=684 trials).

The plots displayed here show the same signal represented in different ways. They share the same x-axis, where stimulus onset is at t=0 seconds and offset at t=2 seconds. 500 milliseconds of pre and post-stimuli are also displayed. **(Top)** Event-related potential with standard deviation around the trace. **(Middle)** Close-up view of the LFP trace displayed above. A Savitsky-Golay filter (red trace) was applied to smooth the averaged raw trace. **(Bottom)** Z-scored power spectral density of the averaged signal.

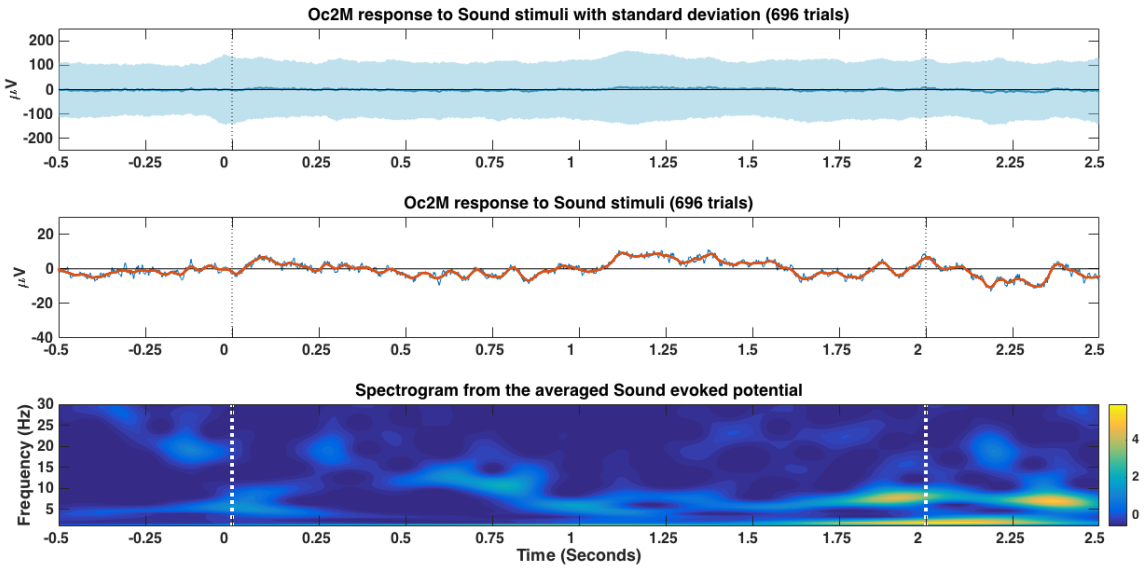

Fig. 3.8. Fausto's Oc2M response to sound stimuli in the Stimbox protocol (n=696 trials).

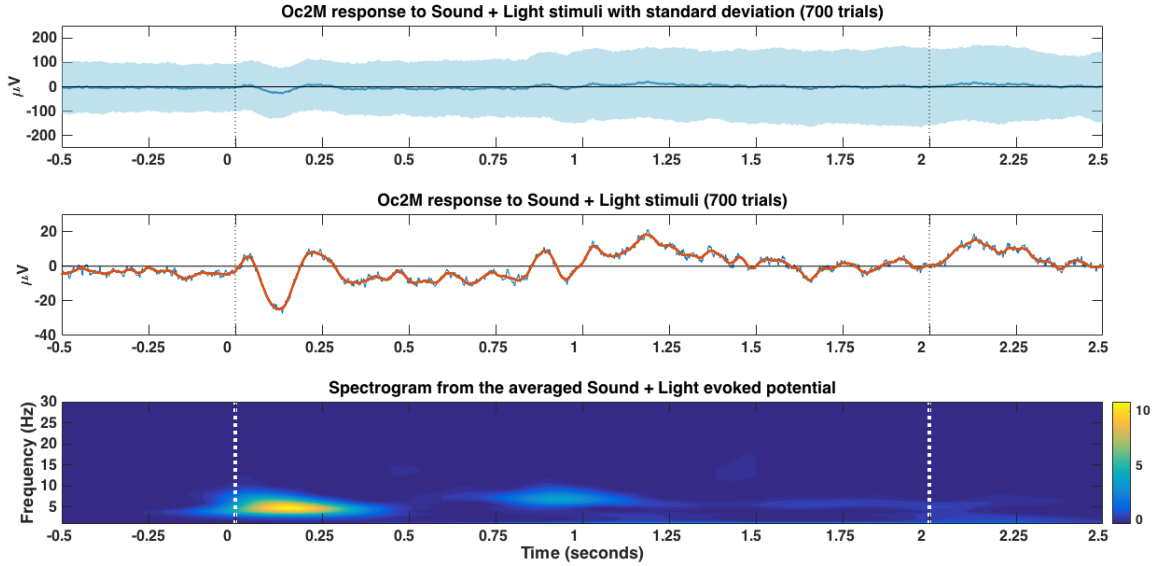

Fig. 3.9. Fausto's Oc2M response to sound + light stimuli in the Stimbox protocol (n=700 trials).

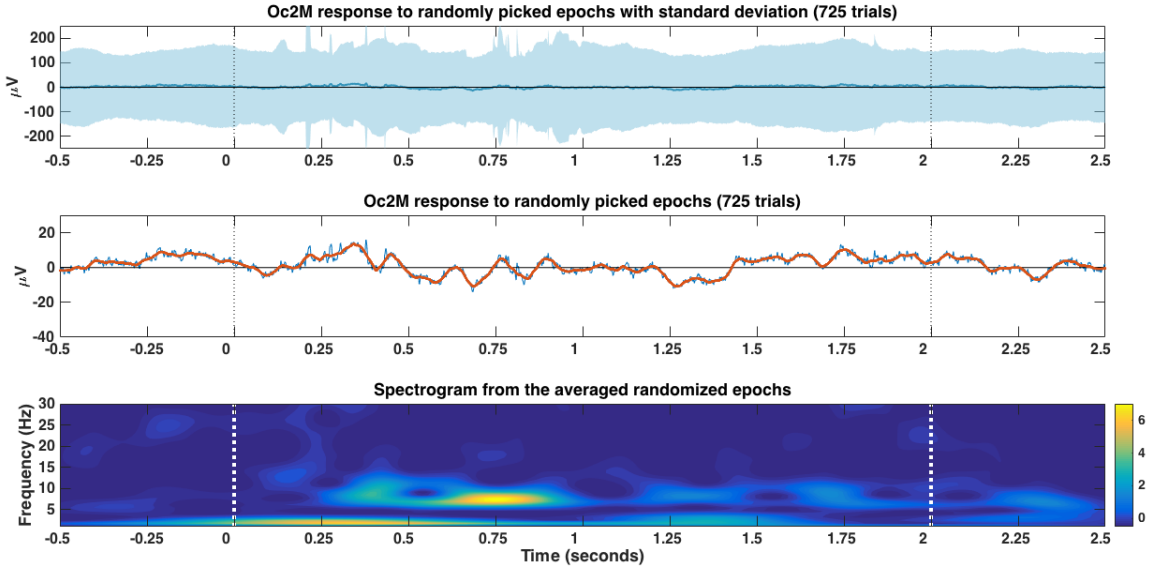

Fig. 3.10. Fausto's Oc2M response to randomly picked epochs in the Stimbox protocol (n=725 trials).

The figures above show a standard deviation within the expected range of 100 – 150 µV. Yet, the fig. 3.9 displays some shifts in the values of standard deviation. Such might be explained by the contribution of noisy epochs, since trials were randomly chosen from all recorded sessions.

The standard deviation displayed around the LFP trace helps to distinguish actual event-related potentials (ERPs) from noise. For instance, take the examples of fig. 3.6 and fig. 3.8, where the signal shows a negative fluctuation at approximately t=0.1 seconds, to values below than 20 µV. In both conditions the corresponding standard deviation follows the trend of the responses (see top panel of figs. 3.6 and 3.8, at t=0.1 seconds). Besides, the extracted signals resulted from the average of 684 trials (light condition) and 700 trials (sound + light condition). Therefore, both ERPs likely represent bona fide responses.

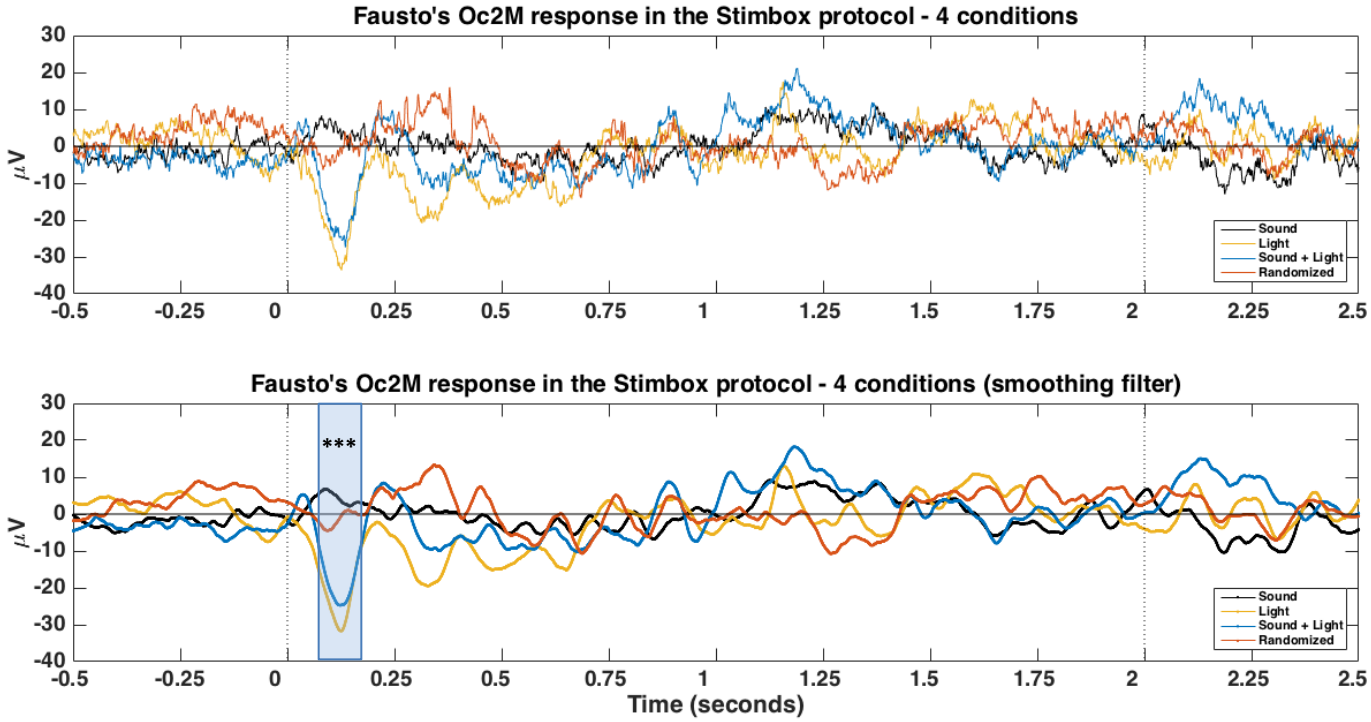

Fig. 3.11. Averaged LFP traces of Fausto's Oc2M responses to all sensory conditions in the Stimbox protocol.

This figure highlights the differences between the LFP responses from each sensory condition. Both plots have represented time (in seconds) on the x-axis, whereas voltage values are represented along the y-axis. Similar to previous figures, -0.5 to 0 seconds represents baseline activity before stimulus is triggered; the vertical dashed lines at t=0 seconds and t=2 seconds represent stimulus onset and stimulus offset, respectively. The interval between 2 to 2.5 seconds represents post-stimuls activity. **(Top)** Averaged raw traces from different conditions plotted together. **(Bottom)** Shows the same signals as above after applying a Savitsky-Golay filter to smooth the data. The blue rectangle between t=0.076 seconds (76 milliseconds after stimulus onset) and t=0.176 seconds (176 milliseconds after stimulus onset) represents the window of statistical analysis for the chosen ERP. An analysis of variance showed that the effect of sensory stimulation on Oc2M's LFP response was statically significant, $F_{(3,2801)}$ = 11.1, $p < .001$.

The spectrograms previously showed (bottom plot in figs. 3.6, 3.7, 3.8, and 3.9) represent how the power spectrum of frequencies of a signal changes over time. The power spectral density values were normalized to the whole window of analysis, in this case, from t = -0.5 seconds to t = 2.5 seconds (x-axis), and from 0 Hz to 30 Hz (y-axis), looping over 40 frequencies. The z-score values enable us to detect along the signal when the strongest response is elicited, and compare it across conditions. Based on that, we identified the time value corresponding to the peak amplitude value of the most robust response. In the case of Fausto's Oc2M responses, the defined time-window of our analysis is 100 milliseconds long, as it goes from 76 milliseconds after stimulus onset (time of the peak minus 50 milliseconds) to 176 milliseconds (time of the peak plus 50 milliseconds).

A one-way ANOVA was conducted to compare the effect of different types of sensory stimulation on Oc2M's LFP responses in the chosen ERP. We found a statistically significant effect of sensory stimulation on Oc2M's responses at the $p < .05$ level for the four conditions tested ($F_{(3,2801)} = 11.1$, $p < .001$).

Compared Conditions	Difference between estimated group means	95% Confidence Interval for the true mean difference		P-Value
		Lower Bound	Upper Bound	
Light x Sound	-26.9	-41.2	-12.6	**< .001**
Light x Mixed	-3.8	-18.1	10.5	0.903
Light x Rand	-21.1	-35.3	-6.9	**< .001**
Sound x Mixed	23.1	8.9	37.3	**< .001**
Sound x Rand	5.8	-8.3	19.9	0.716
Mixed x Rand	-17.3	-31.4	-3.2	**.008**

Table 3.1 Pairwise multiple comparisons using the Tukey-Kramer test between each pair of stimulus condition relative to Fausto's Oc2M.

The multiple comparisons analysis suggested that light sensory cue was the main responsible for the changes observed in the LFP activity in Fausto's Oc2M. The Tukey-Kramer test indicated that the mean score for the light condition (M = -22.65, SD = 3.96) was significantly different than the sound (M = 4.25, SD = 3.92) and randomized (M = -1.55, SD = 3.85) conditions. Similarly, the sound + light condition ('mixed', M = -18.85, SD = 3.91) was significantly different

than sound and randomized conditions. However, no statistically differences were found between the light and sound + light conditions, and between the sound and randomized conditions. Such suggests that sound stimulus did not modulate Oc2M's LFP responses, either when presented together with light or in isolation.

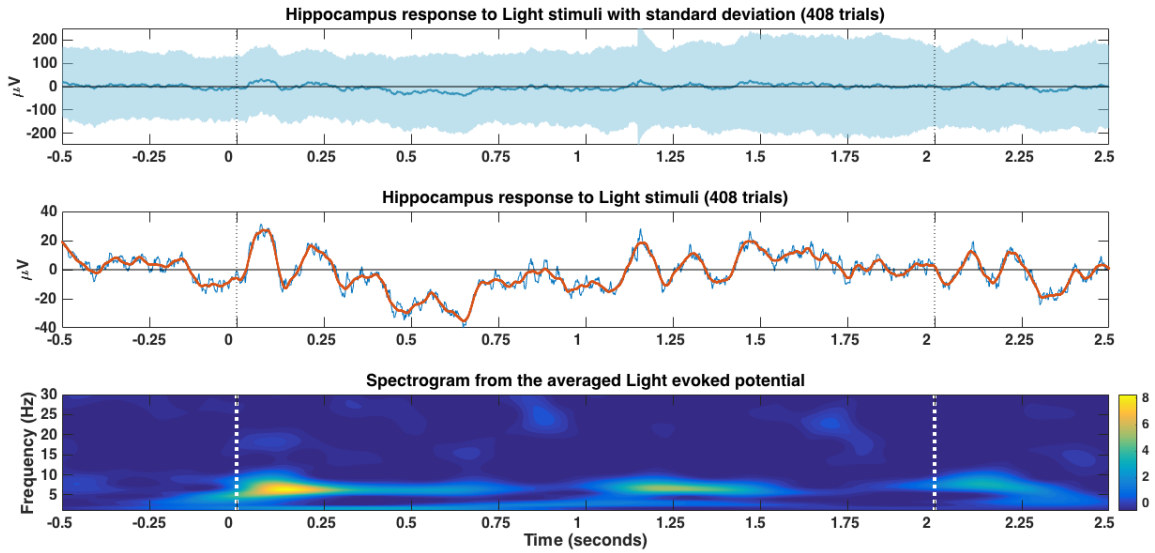

Fig. 3.12. Fausto's Hippocampus response to light stimuli in the Stimbox protocol (n=408 trials).

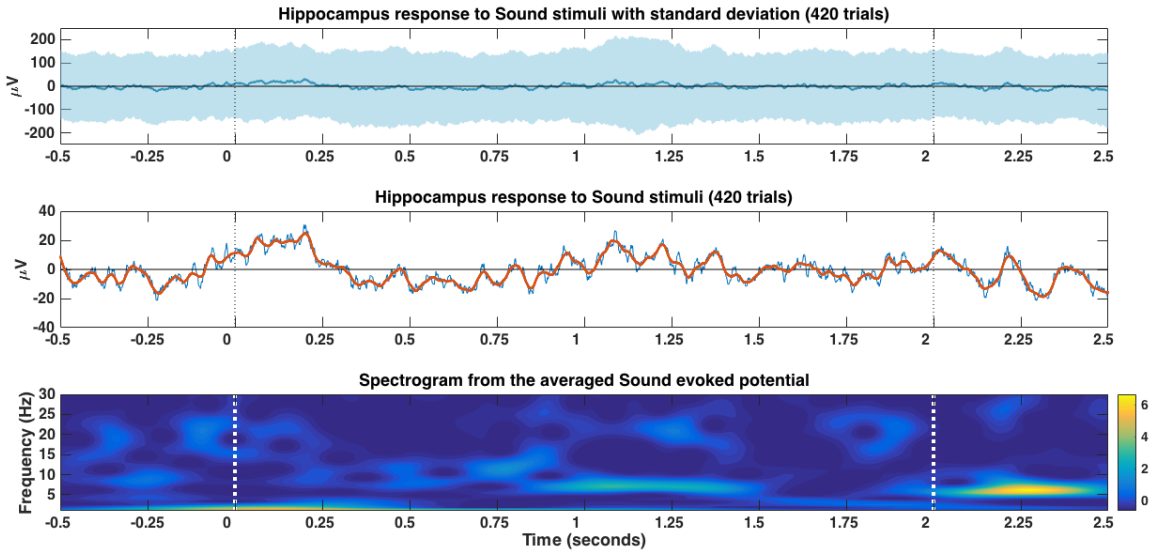

Fig. 3.13. Fausto's Hippocampus response to sound stimuli in the Stimbox protocol (n=420 trials).

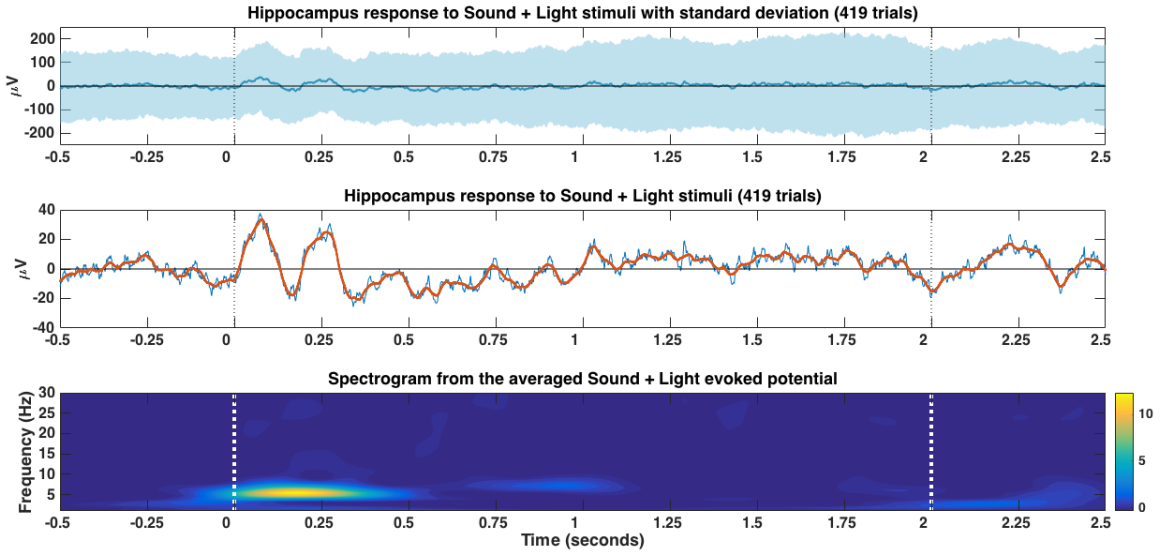

Fig. 3.14. Fausto's Hippocampus response to sound + light stimuli in the Stimbox protocol (n=419 trials).

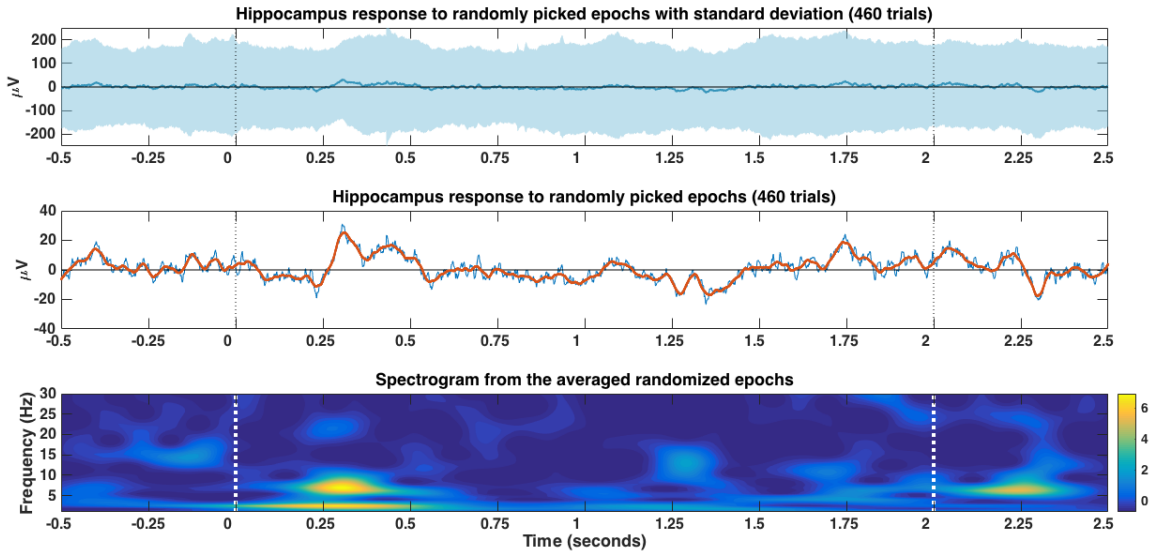

Fig. 3.15. Fausto's Hippocampus response to randomly picked epochs in the Stimbox protocol (n=460 trials).

Note that the number of trials accounting for hippocampal LFP activity from Fausto (figs. 3.11, 3.12, 3.13, and 3.14) is lower than in Oc2M results. As described in the section II. Methods, tetrodes were daily adjusted and by tracking the number of turns given, we could come up with an estimation of tetrodes' location. Additionally, data sets were analyzed on a daily-basis in order to look for prototypical neural hippocampal signatures (SWR_Rs and high frequency

oscillations, see fig. 2.20 in II. Methods section). We only included tetrodes in the analyses of hippocampus activity once we could confirm that they were on target. None of the tetrodes were at hippocampus in the first recording sessions of Stimbox. That explains the different number of trials between Hippocampus and Oc2M datasets.

Identical to what was observed in Oc2M responses, light cue evoked a prominent response of hippocampus right after stimulus is triggered. Although it is not clear in the figures above, the positive peak of the hippocampal response in the light condition (x = 0.070 seconds) was detected 56 milliseconds before Oc2M's response to the light stimulus (x = 0.126 seconds). A similar delay was observed in the sound + light condition, where the positive peak of the hippocampal response (x = 0.077 seconds) was detected 58 milliseconds before Oc2M's response (x = 0.135 seconds).

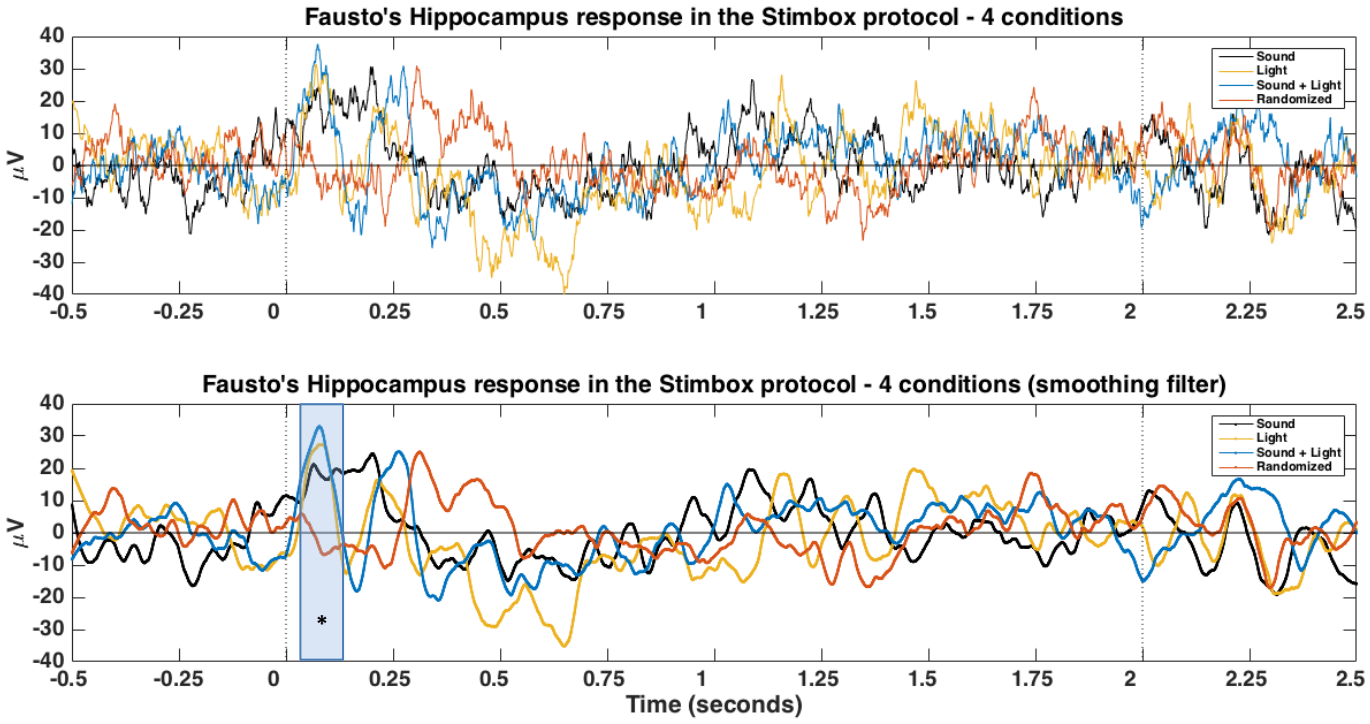

Fig. 3.16. Averaged LFP traces of Fausto's Hippocampal responses to all sensory conditions in the Stimbox protocol.

(Top) Averaged raw traces from different conditions plotted together. **(Bottom)** Shows the same signals as above after applying a Savitsky-Golay filter to smooth the data. The blue rectangle between t=0.027 seconds (27 milliseconds after stimulus onset) and t=0.127 seconds (127 milliseconds after stimulus onset) represents the window of statistical analysis for the chosen ERP. An analysis of variance showed that the effect of sensory stimulation on Hippocampus's LFP response was statically significant, $F_{(3,1703)} = 3.58$, $p = .013$.

Using the same methodology as before, a one-way ANOVA was conducted to compare the effect of different sensory conditions on Hippocampus' LFP responses in the selected ERP. We found a statistically significant effect of sensory stimulation on Hippocampus responses at the $p < .05$ level ($F_{(3,1703)} = 3.58$, $p = .013$).

Compared Conditions	Difference between estimated group means	95% Confidence Interval for the true mean difference		P-Value
		Lower Bound	Upper Bound	
Light x Sound	0.6	19.6	20.8	0.999
Light x Mixed	-3.2	-23.8	17.5	0.979
Light x Rand	20.2	-0.4	40.9	0.057
Sound x Mixed	-3.8	-23.8	16.3	0.963
Sound x Rand	19.6	-0.4	39.7	0.057
Mixed x Rand	23.4	2.9	43.9	**0.017**

Table 3.2 Pairwise multiple comparisons using the Tukey-Kramer test between each pair of stimulus condition relative to Fausto's Hippocampus.

Pairwise multiple comparisons using the Tukey-Kramer test showed that only the sound + light condition (M = 20.81, SD = 5.65) was found to be statistically significant different than the randomized condition (M = .2.59, SD = 5.64).

Hippocampus LFP shows larger standard deviation values (figs. 3.11, 3.12, 3.13, and 3.14) than Oc2M's (figs. 3.6, 3.7, 3.8, and 3.9). Hippocampus often elicits high frequency power oscillations above 100 Hz (Buzsáki & Silva, 2012), resulting in larger amplitude values within short-time windows, in comparison to cortical activity. Consequently, such amplitude variations are likely to be present in baseline activity (pre-stimulus onset), which can lead to considerable differences between conditions at the time stimulus is triggered (t = 0 seconds). In fig. 3.15, one can see that both averaged traces of hippocampal activity in light and sound + light conditions, show a mean amplitude value of around -10 μV at stimulus onset. On the contrary, in the sound condition, hippocampus LFP has an averaged amplitude value of approximately 10 μV at the time stimulus is triggered. The point here is that baseline activity differences can either enhance or mask differences in ERPs' activity across conditions. However, it should be

noted that the LFP traces displayed in the fig. 3.15 derived from the averaged activity of more than 400 trials per condition, meaning that drawing out conclusions solely based on the mean absolute values can also lead to misinterpretations.

Rat #2 – 'Carpe'

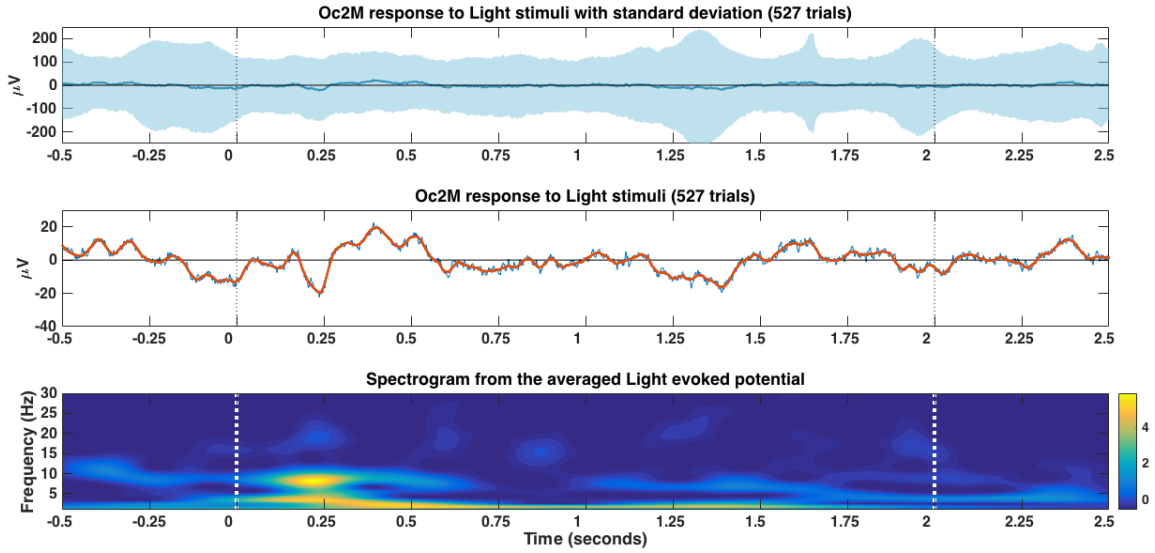

Fig. 3.17. Carpe's Oc2M response to light stimuli in the Stimbox protocol (n=527 trials).

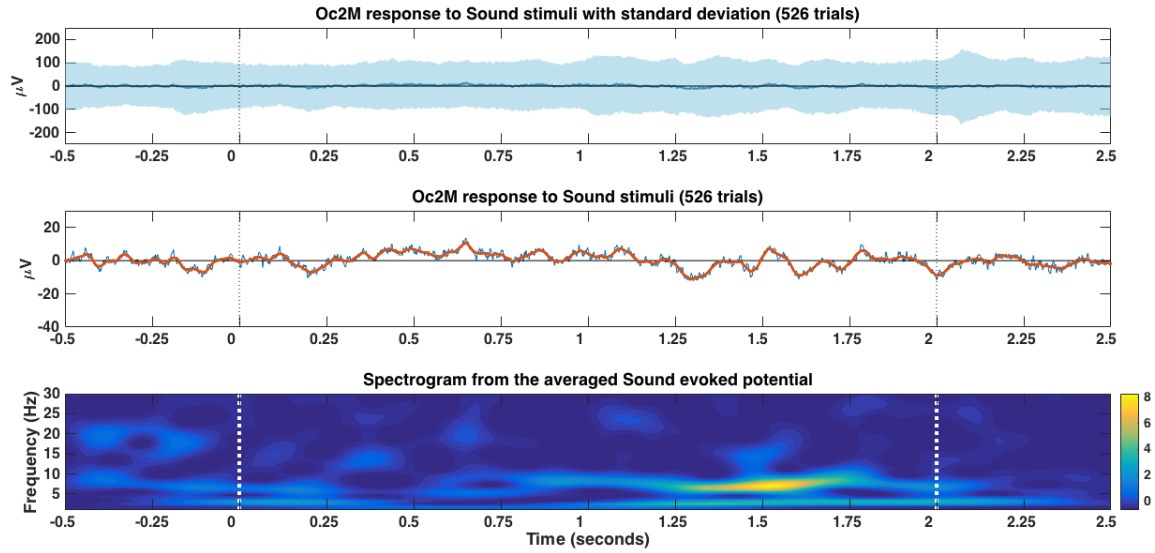

Fig. 3.18. Carpe's Oc2M response to sound stimuli in the Stimbox protocol (n=526 trials).

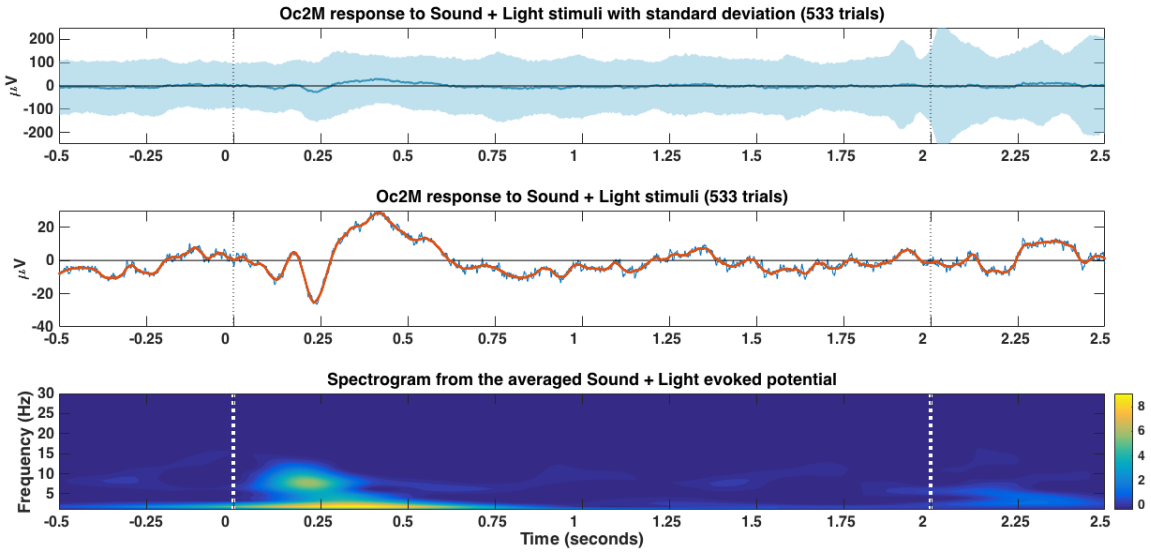

Fig. 3.19. Carpe's Oc2M response to sound + light stimuli in the Stimbox protocol (n=533 trials).

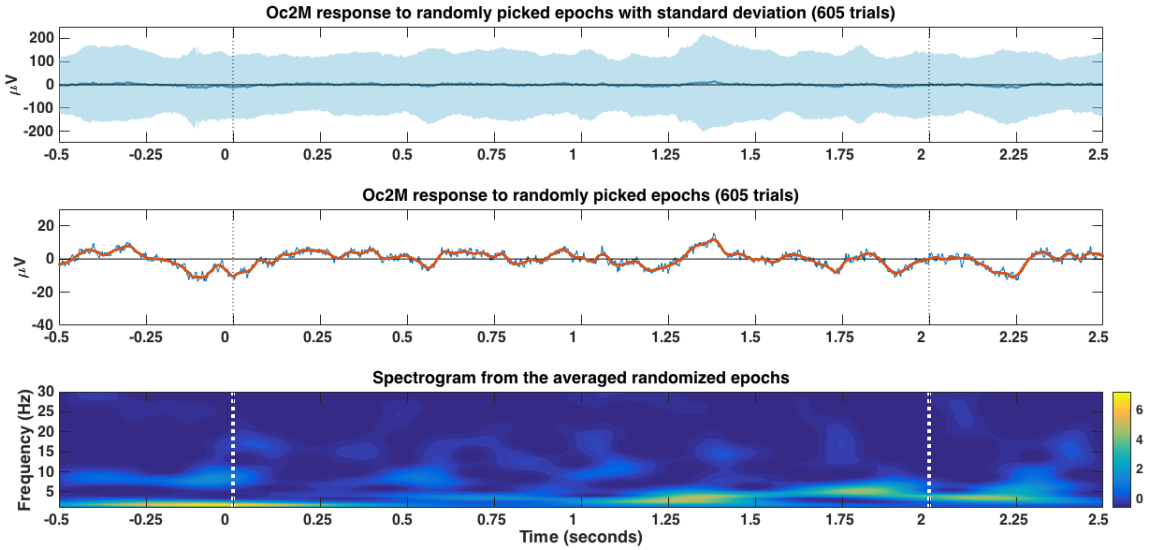

Fig. 3.20. Carpe's Oc2M response to randomly picked epochs in the Stimbox protocol (n=605 trials).

The four figures above correspond to the results of Oc2M recordings using the rat 'Carpe' under the Stimbox protocol. They highlight a pattern previously observed in Fausto: a response after stimulus onset in both light and sound + light conditions, whereas in the sound condition, no ERPs were identified. Besides, like in Fausto, LFP responses in light and sound + light conditions produced identical ERPs in time (the time point when the peak is detected) and shape (both averaged signals follow a similar trend, i.e. show the same voltage fluctuations).

However, one should be careful when doing comparisons between subjects

from these experiments. The data inputs that were used to compute Oc2M and Hippocampus LFP are quite different between the two rats. For instance, LFP data from Fausto's Oc2M is the result of the signal averaging of 12 tetrodes, while for Carpe's Oc2M just one tetrode was used. By averaging all electrodes within the same region, we are assuming that tetrodes placed at different sub-regions and layers will respond equally to sensory stimuli. Such is unlikely to happen (Lin et al., 2015), and the figure 6.4 (see section VI. Supplementary Figures) illustrate an example from one session, where two tetrodes placed at Oc2M exhibit different responses to sound + light stimulation. Nevertheless, in this case, the purpose of averaging was to find the overall output from these regions in response to stimulation.

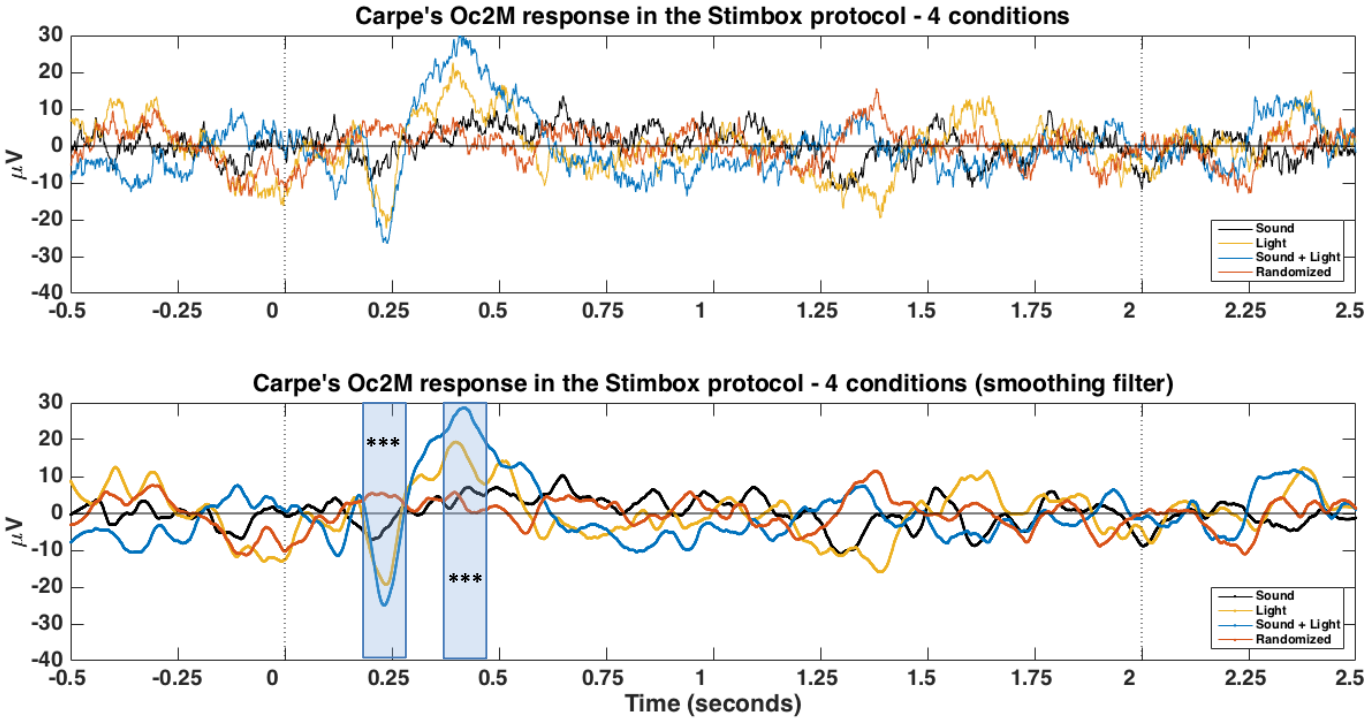

Fig. 3.21. Averaged LFP traces of Carpe's Oc2M responses to all sensory conditions in the Stimbox protocol.

(Top) Averaged raw traces from different conditions plotted together. **(Bottom)** Shows the same signals as above after applying a Savitsky-Golay filter to smooth the data. Two ERPs were identified and analyzed. The peak amplitude of the first ERP from the sound + light condition is at t=0.232 seconds (232 milliseconds after stimulus onset), and the time-window of analysis goes from t=0.182 seconds to t=0.282 seconds. In the second ERP analyzed, the peak amplitude of the signal from the sound + light condition is at t=0.420 seconds (420 milliseconds after stimulus onset), and the time-window of analysis ranges between t=0.370 seconds and t=0.470 seconds. An analysis of variance showed that the effect of sensory stimulation on Oc2M's LFP response was statically significant in the first ERP ($F_{(3,2187)} = 4.09$, $p = .006$) and the second ERP ($F_{(3,2187)} = 6.36$, $p < .001$).

A one-way ANOVA was conducted for each of the ERPs to compare the effect of different types of sensory stimulation on Oc2M's LFP responses. We found a statistically significant effect of sensory stimulation on Oc2M's responses at the p < .05 level in the first ($F_{(3,2187)}$ = 4.09, p = .006) and the second ERPs ($F_{(3,2187)}$ = 6.36, p < .001).

Compared Conditions	Difference between estimated group means	95% Confidence Interval for the true mean difference		P-Value
		Lower Bound	Upper Bound	
Light x Sound	-7.1	-22.2	8	0.621
Light x Mixed	2.6	-12.4	17.7	0.969
Light x Rand	-15.4	-30.1	-0.8	**0.034**
Sound x Mixed	9.7	-5.3	24.8	0.345
Sound x Rand	-8.3	-22.9	6.3	0.462
Mixed x Rand	-18.1	-32.6	-3.5	**.008**

Table 3.3 Pairwise multiple comparisons using the Tukey-Kramer test between each pair of stimulus condition relative to the first ERP in Carpe's Oc2M.

Compared Conditions	Difference between estimated group means	95% Confidence Interval for the true mean difference		P-Value
		Lower Bound	Upper Bound	
Light x Sound	10.2	-4	25.4	0.309
Light x Mixed	-10.3	-25.4	4.8	0.296
Light x Rand	11	-2.7	26.6	0.154
Sound x Mixed	-20.5	-35.6	-5.4	**.002**
Sound x Rand	1.8	-12.9	16.4	0.989
Mixed x Rand	22.3	7.7	36.9	**< .001**

Table 3.4 Pairwise multiple comparisons using the Tukey-Kramer test between each pair of stimulus condition relative to the second ERP in Carpe's Oc2M.

Post hoc comparisons using the Tukey-Kramer test showed that multimodal stimulation elicited the strongest LFP responses (first ERP: M = -13.29, SD = 4.14; second ERP: M = 24.94, SD = 4.15). It was the only sensory condition significantly different than the randomized condition in both ERPs (first ERP: M = 4.77, SD = 3.89; second ERP: M = 2.65, SD = 3.90). Additionally, in the first ERP, the only significant difference was found between light (M = -10.66, SD = 4.16) and randomized conditions. Whereas in the second ERP, only sound (M = 4.42, SD = 4.18) and sound + light conditions were found to be significantly different.

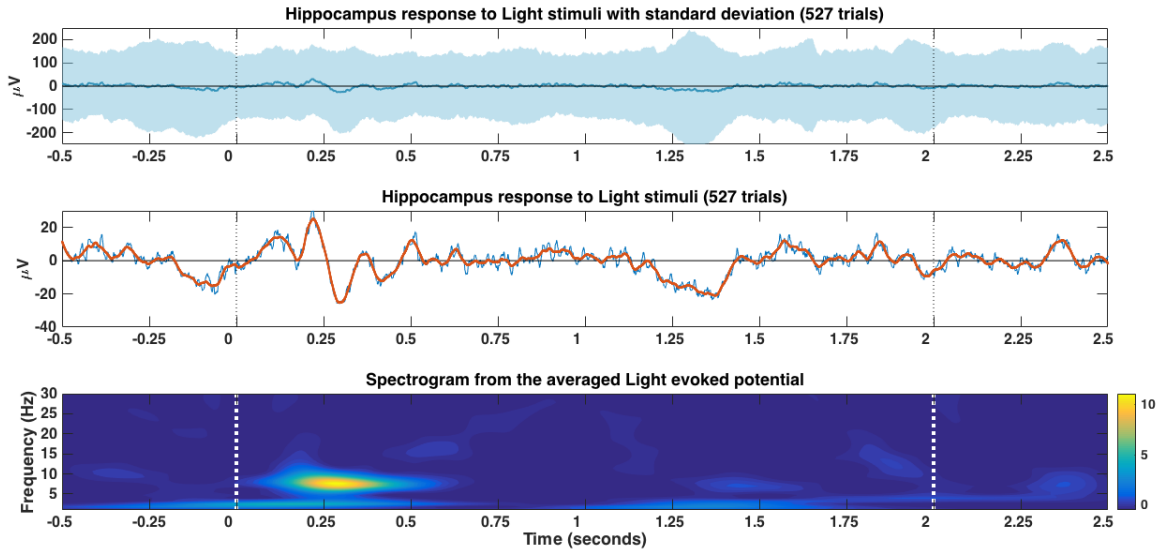

Fig. 3.22. Carpe's Hippocampus response to light stimuli in the Stimbox protocol (n=527 trials).

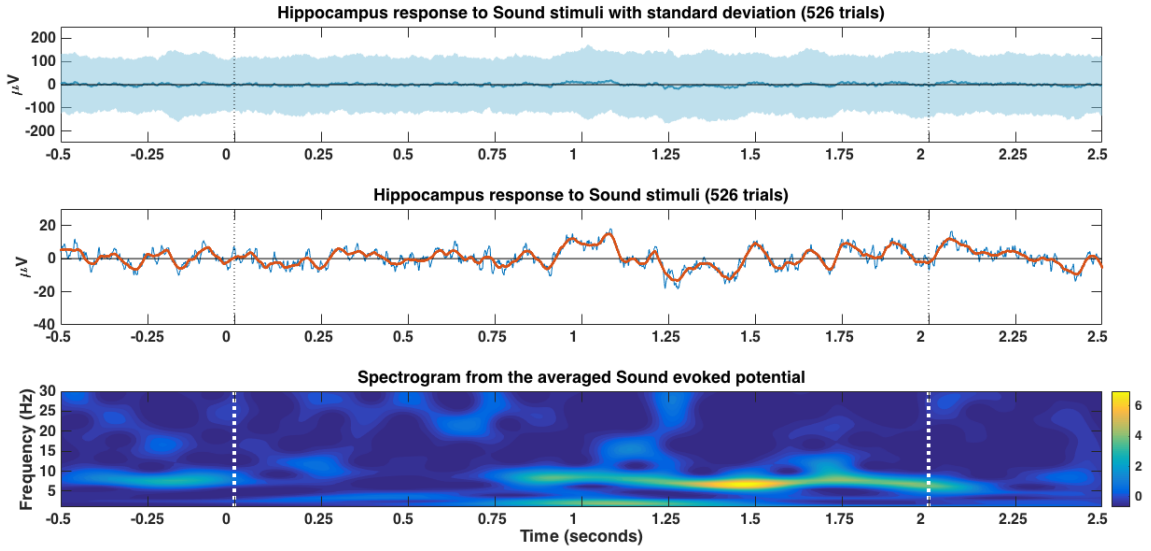

Fig. 3.23. Carpe's Hippocampus response to sound stimuli in the Stimbox protocol (n=526 trials).

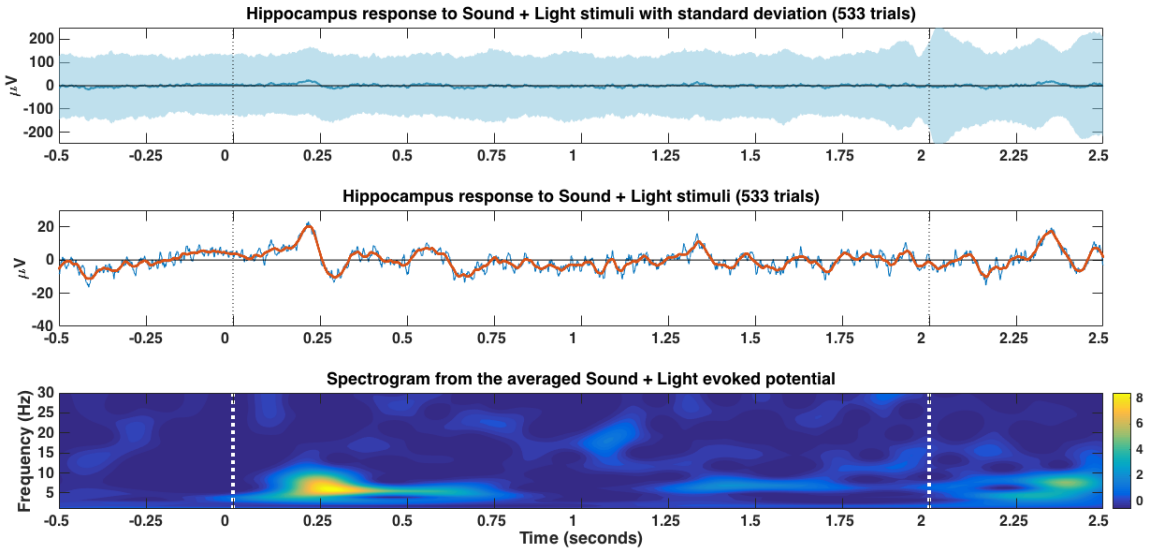

Fig. 3.24. Carpe's Hippocampus response to sound + light stimuli in the Stimbox protocol (n=533 trials).

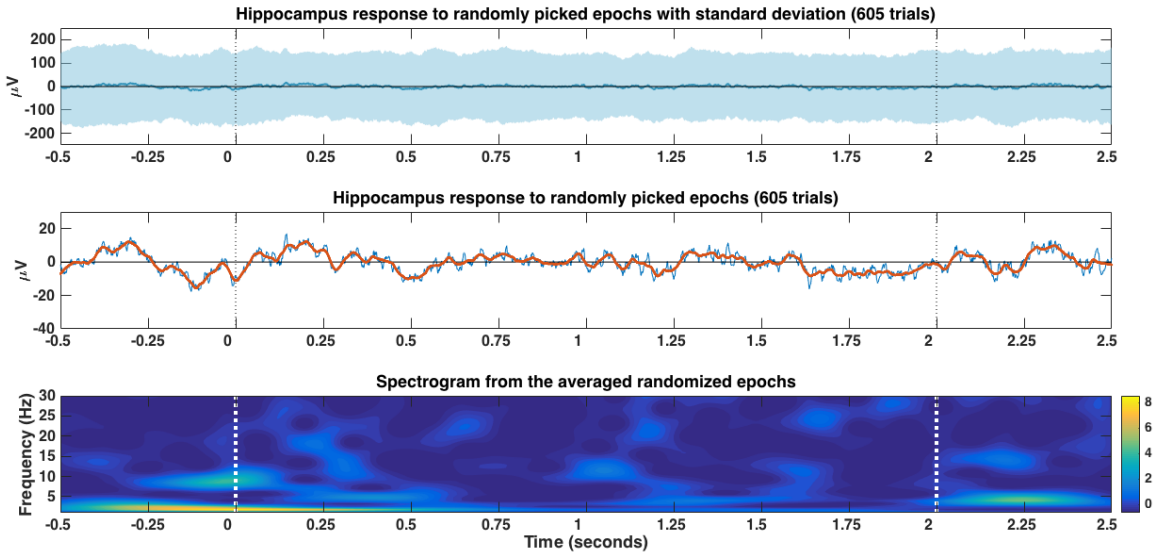

Fig. 3.25. Carpe's Hippocampus response to randomly picked epochs in the Stimbox protocol (n=605 trials).

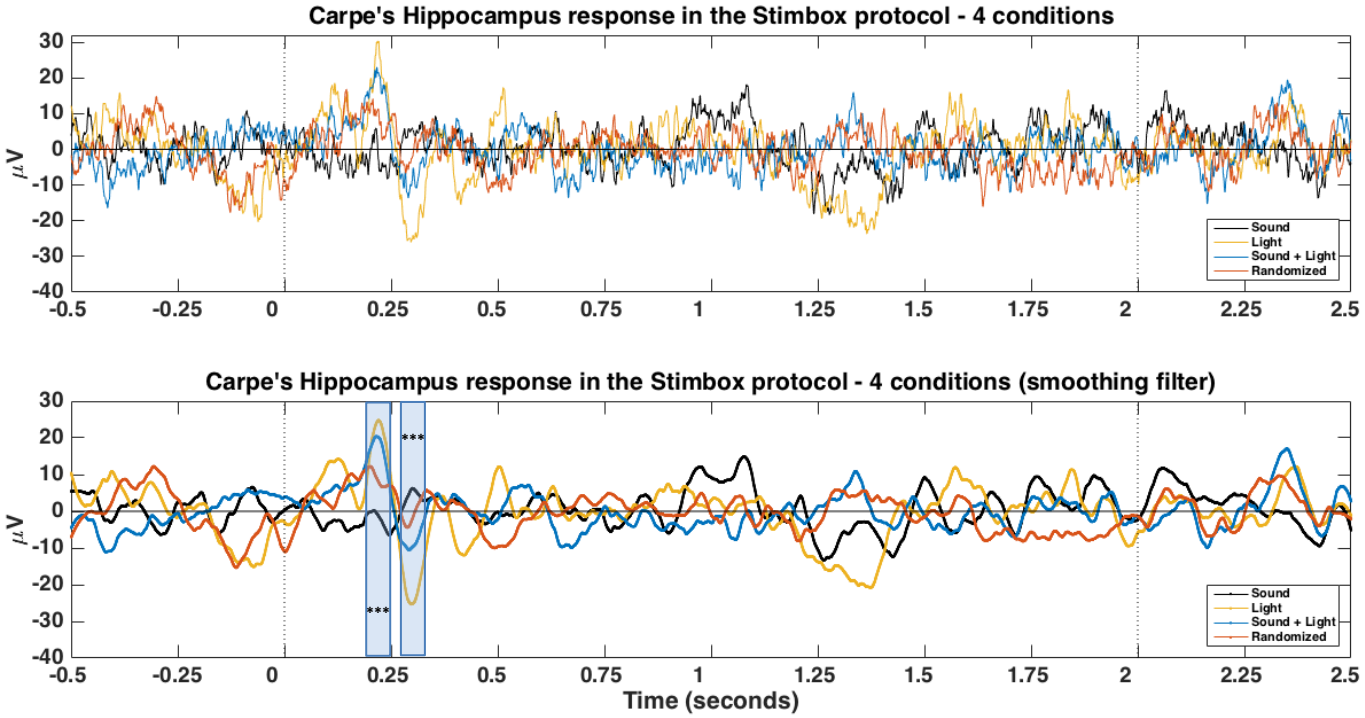

Fig. 3.26. Averaged LFP traces of Carpe's Hippocampus responses to all sensory conditions in the Stimbox protocol.

(Top) Averaged raw traces from different conditions plotted together. **(Bottom)** Shows the same signals as above after applying a Savitsky-Golay filter to smooth the data. Two ERPs were identified and analyzed. In order to fit the width of the ERP to the time-window of analysis, the window was defined by 60 milliseconds long, instead of the usual 100 milliseconds. The peak amplitude of the first ERP is at t=0.221 seconds (221 milliseconds after stimulus onset), and the time-window of analysis goes from t=0.191 seconds to t=0.251 seconds. In the second ERP analyzed, the peak amplitude of the signal is at t=0.298 seconds (298 milliseconds after stimulus onset), and the time-window of analysis ranges between t=0.268 seconds and t=0.328 seconds. An analysis of variance showed that the effect of sensory stimulation on Hippocampus's LFP response was statically significant in the first ERP ($F_{(3,2187)}$ = 3.86, p = .009) and the second ERP ($F_{(3,2187)}$ = 4.47, p = .003).

A one-way ANOVA was conducted for each of the ERPs to compare the effect of different types of sensory stimulation on Hippocampus' LFP responses. We found a statistically significant effect of sensory stimulation on Hippocampus's responses at the $p < .05$ level in the first ($F_{(3,2187)} = 3.86$, $p = .009$) and the second ERPs ($F_{(3,2187)} = 4.47$, $p = .003$).

Compared Conditions	Difference between estimated group means	95% Confidence Interval for the true mean difference		P-Value
		Lower Bound	Upper Bound	
Light x Sound	20.7	3.4	37.9	**0.011**
Light x Mixed	2.2	-15	19.4	0.987
Light x Rand	9.6	-7.1	26.3	0.450
Sound x Mixed	-18.5	-35.7	-1.3	0.029
Sound x Rand	-11.1	-27.7	5.6	0.321
Mixed x Rand	7.4	-9.2	24	0.662

Table 3.5 Pairwise multiple comparisons using the Tukey-Kramer test between each pair of stimulus condition relative to the first ERP in Carpe's Hippocampus.

Compared Conditions	Difference between estimated group means	95% Confidence Interval for the true mean difference		P-Value
		Lower Bound	Upper Bound	
Light x Sound	-24.6	-43.2	-6.1	**.003**
Light x Mixed	-12.7	-31.1	5.8	0.293
Light x Rand	-19.8	-37.7	-1.9	**0.023**
Sound x Mixed	11	-13.1	22.7	0.901
Sound x Rand	4.8	-13.1	22.7	0.901
Mixed x Rand	-7.2	-25	10.7	0.731

Table 3.6 Pairwise multiple comparisons using the Tukey-Kramer test between each pair of stimulus condition relative to the second ERP in Carpe's Hippocampus.

We found that the magnitude of the hippocampal LFP response to multimodal stimulation decreases in both ERPs, compared to the effect of light stimulation alone (fig. 3.26). The Tukey-Kramer test showed that only the light (M = 18.26, SD = 4.74) condition was significantly different than the sound (M = -2.40, SD = 4.75) condition in the first ERP. The second ERP shows the same significant difference between light (M = -20.57, SD = 5.10) and sound (M = 4.05, SD = 5.10) conditions, and also between light and randomized epochs (M = -0.76, SD = 4.76). Interestingly, we observed the opposite pattern in Carpe's Oc2M, where sound + light stimulus results in an increase of the response in comparison to light in isolation (fig. 3.25).

3.2.2. Multi and Single-Unit activity – Stimbox Protocol

In the following section we present the results of multiunit activity from different Oc2M tetrodes, recorded on different days, as well as the activity of a single-unit from Hippocampus. Neuronal responses from sensory cortex are highly variable. Even within the same population, cortical neurons differ in their neuronal tuning or in the overall firing-rate. We will show some examples of how neuronal populations recorded at different sites from one region (Oc2M), can exhibit significantly different responses to the same sensory cues. Aimed to illustrate such cortical neuronal variability, we selected a few tetrodes that captured clear distinct patterns of neural activity.

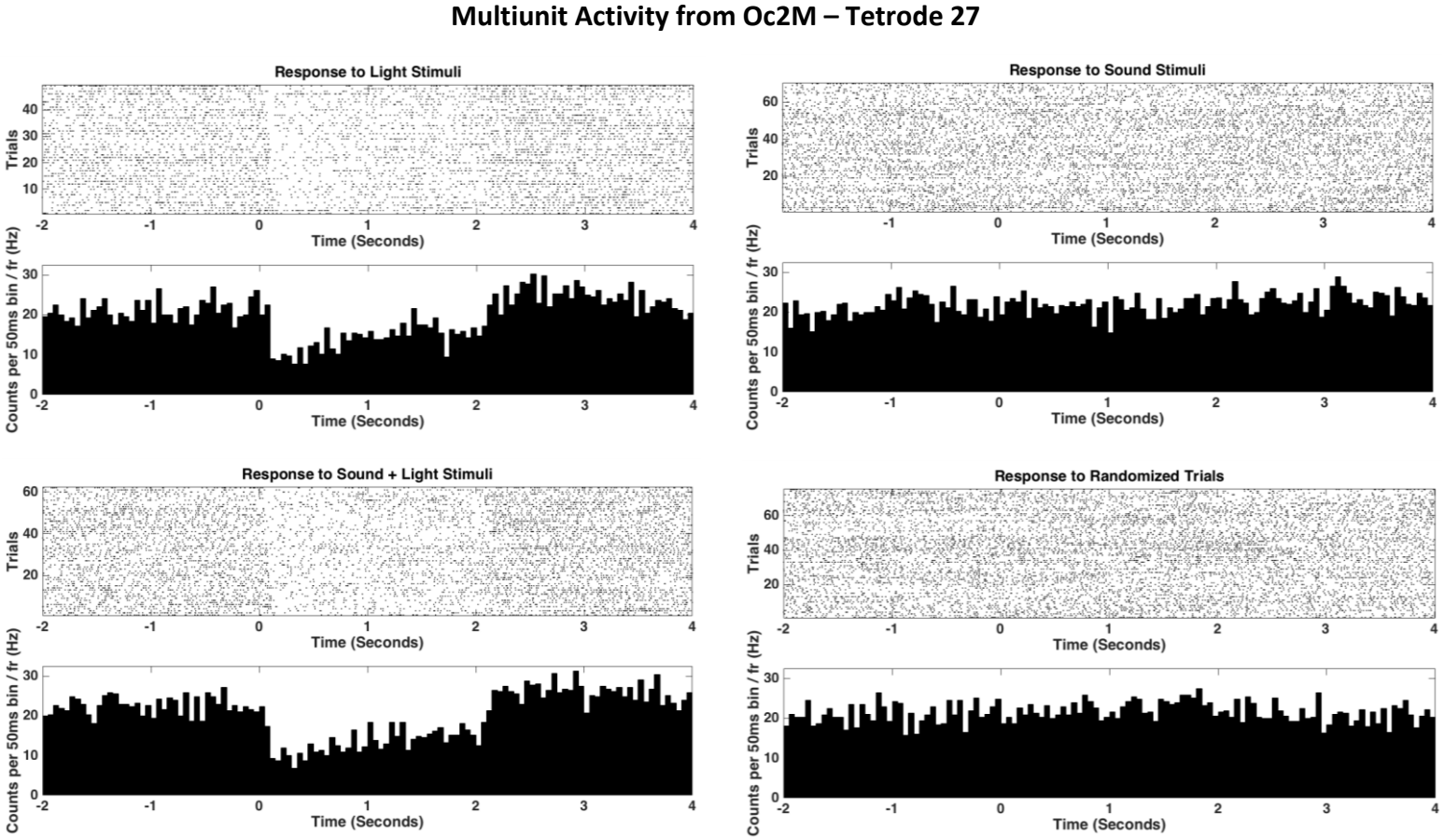

Fig. 3.27. Multiunit activity from Oc2M's tetrode 27 (rat Fausto - one session).

Each of the four plots corresponds, respectively, to a different sensory condition. Multiunit activity is here represented as a function of its firing rate. Results for each sensory condition are divided into two graphs.
(Top) Spike raster plot, where the spiking activity of the group of neurons recorded is displayed over time. The x-axis represents time (in seconds) and it goes from -2 seconds (i.e. 2 seconds before stimulus onset) to 4 seconds (i.e. 4 seconds after stimulus onset, and 2 seconds after stimulus offset). As shown in previous plots, stimulus is triggered at t= 0 seconds, and t = 2 seconds represents stimulus offset. The y-axis represents trials, where each row corresponds to the spiking activity on a given trial. As such, the presence of a dot in a given row and column, indicates that a neuron from this population, produced an action potential on that trial (y-axis row) at a specific time (x-axis column).
(Bottom) Peristimulus Time Histogram, where the number of spikes is quantified and sorted into bins of 50 milliseconds. The number of spike counts per bin is normalized to the overall firing rate, and corresponding values are represented in the y-axis. The x-axis (time in seconds) share the features already described of the respective raster plot.

Although neural activity is here classified as multiunit activity, the possibility that some of these plots (fig. 3.27 and following ones) are rather representing single-unit activity should not be excluded. However, during the clustering process, since cortical single-units were never fully isolated from remaining activity, we decided to classify all results from cortical neural activity as multiunit.

The raster plots in fig. 3.27 depicts the high firing rate of the recorded neurons, represented by the high density of dots (i.e. action potentials), over time and trials. Interestingly, comparing the different sensory conditions, we observe a strong effect elicited at stimulus onset (t = 0 seconds) in light and light + sound conditions. This effect is characterized by a decrease of the firing rate to about half, which slowly keeps increasing until stimulus offset. However, while stimulus is on, firing rate values never go above pre-stimulus (baseline) values. Additionally, it is possible to see in the raster plots of light and sound + light conditions that, as the number of trials progress, the decrease observed in the firing rate seems to appear earlier and earlier. It suggests that these neurons become quicker in responding to stimulation as the session develops.

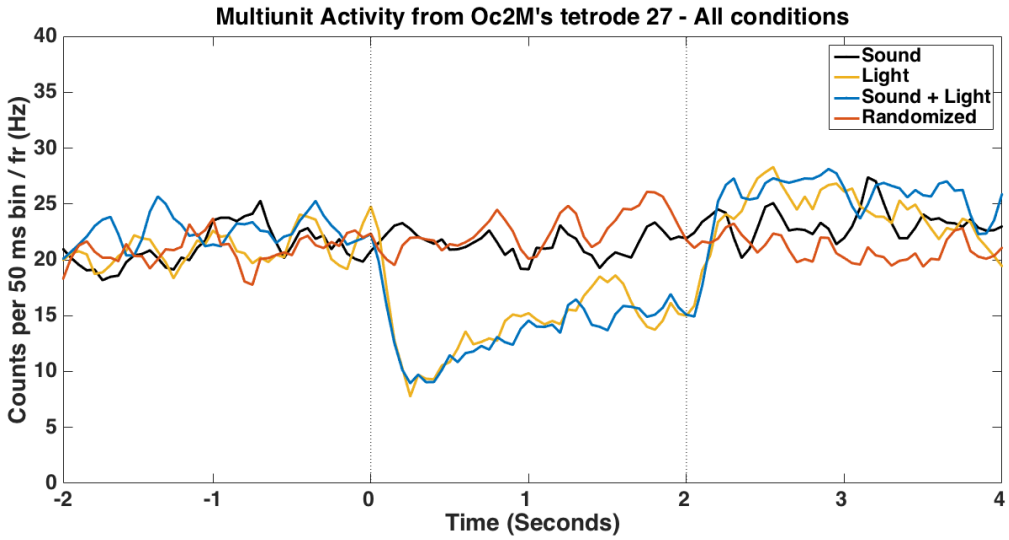

Fig. 3.28. Multiunit activity from Oc2M's tetrode 27 – All conditions overlapped.

The traces represent a fitting curve of the peristimulus time histogram, respectively, to each sensory condition from multiunit activity of tetrode 27. Values corresponding to each 50 milliseconds bin were used as input, and a Savitsky-Golay filter was then applied to smooth the data.

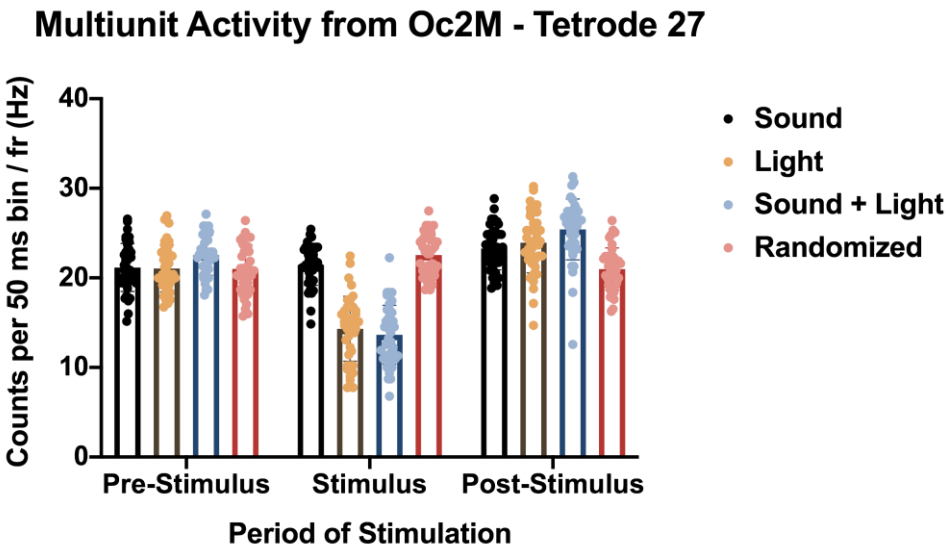

Fig. 3.29. Multiunit activity differences in terms of firing rate, according to sensory condition and period of stimulation (Tetrode 27).

Each bar represents the average of the counts of action potentials per 50 milliseconds bin (normalized to the firing rate), in a given sensory condition, at a given period of stimulation. 'Pre-Stimulus' corresponds to the 2 seconds period before stimulus onset, 'Stimulus' corresponds to the 2 seconds period of stimulation, and 'Post-Stimulus' corresponds to the 2 seconds of activity after stimulus offset. Each dot represents the value of a given bin, and together they show the dispersion around the mean.

We found a main effect of the period of stimulation ($F_{(1.942, 75.75)} = 93.41$, $p < .001$) and sensory condition ($F_{(2.795, 109)} = 17.94$, $p < .001$) on the multiunit activity of tetrode 27. Additionally, there was a significant interaction effect between period of stimulation and sensory condition ($F_{(4.056, 158.2)} = 67.53$, $p < .001$).

Post-hoc analyses suggested that sound cue had an impact on the recorded cortical population activity, but only after stimulus offset. The Tukey's multiple comparisons test showed that multiunit activity did not significantly change from pre-stimulus period (M = 21.16, SD = 2.67) to the stimulation period (M = 21.44, SD = 2.27). However, neural activity corresponding to the post-stimulus period (M = 23.28, SD = 2.38) displayed significant differences to baseline and stimulus periods. For instance, whereas multiunit activity in response to sound condition did not show significant differences to the randomized condition at pre-stimulus (M = 20.98, SD = 2.71) and stimulus (M = 22.53, SD = 2.26) periods, during the post-stimulus period, sound and randomized (M = 20.97, SD = 2.36) conditions were found to be different.

Significant effects were also found in light and sound + light conditions. Compared to baseline values (Light: M = 21.05, SD = 2.62; Sound + Light: M = 22.53, SD = 2.24), the firing rate of multiunit activity in both conditions significantly dropped upon stimulation (Light: M = 14.32, SD = 3.62; Sound + Light: M = 13.65, SD = 3.29). Additionally, such activity increased after stimulus offset (Light: M = 23.92, SD = 3.37; Sound + Light: M = 25.4, SD = 3.40) to values higher than its baseline. Overall, despite the clear effect of light and sound + light cues, the three types of stimulation showed significant differences between pre-stimulus and post-stimulus activity, something that was not observed in the control condition (i.e. randomly picked trials).

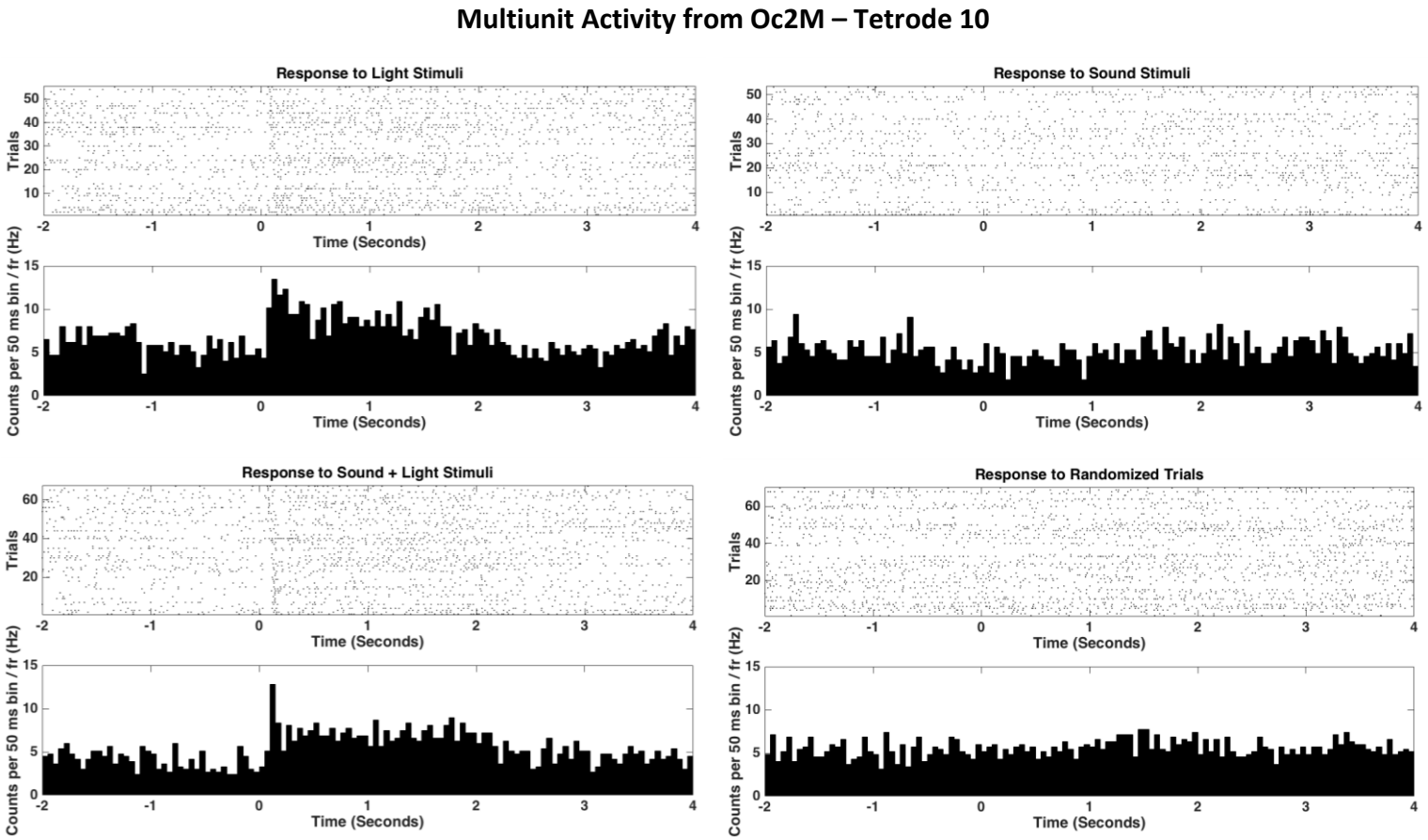

Fig. 3.30. Multiunit activity from Oc2M's tetrode 10 (rat Fausto - one session).

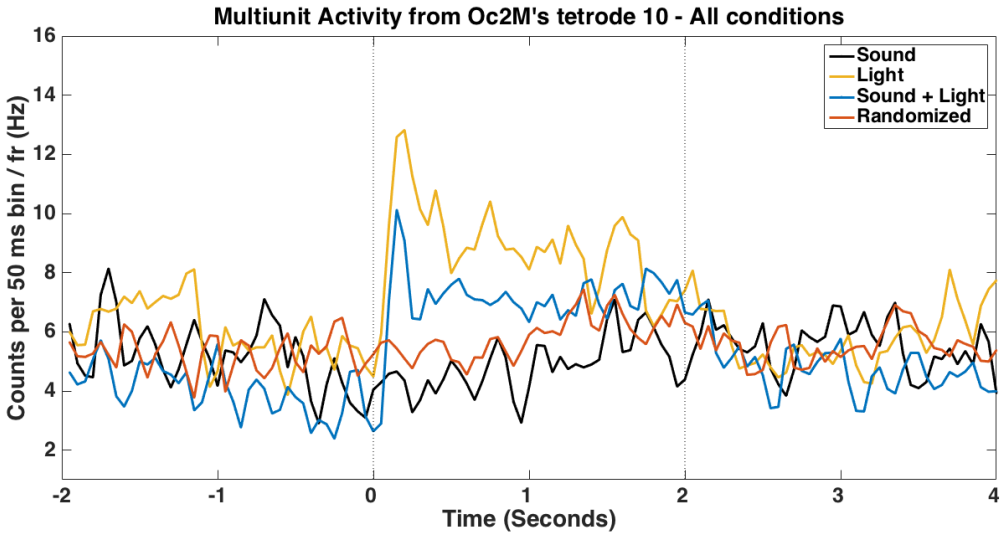

Fig. 3.31. Multiunit activity from Oc2M's tetrode 10 – All conditions overlapped.

The figs. 3.30 and 3.31 show that the neuronal population activity recorded from tetrode 10 is quite different than the one previously shown (tetrode 27). For instance, despite the differences after stimulus onset, the values of the normalized firing rate are also different. The baseline activity respective to tetrode 10 ranges within 3 and 8 counts per 50 milliseconds bins (figs. 3.30 and 3.31), less than half of the observed in tetrode 27 (figs. 3.28 and 3.29).

It was found a main effect of the period of stimulation ($F_{(1.994,\ 77.78)} = 54{,}98$, $p < .001$) and sensory condition ($F_{(2.871,\ 112)} = 41{,}64$, $p < .001$) on the multiunit activity of tetrode 10. A significant interaction effect was also found between period of stimulation and sensory condition ($F_{(4.784,\ 186.6)} = 25.8$, $p < .001$).

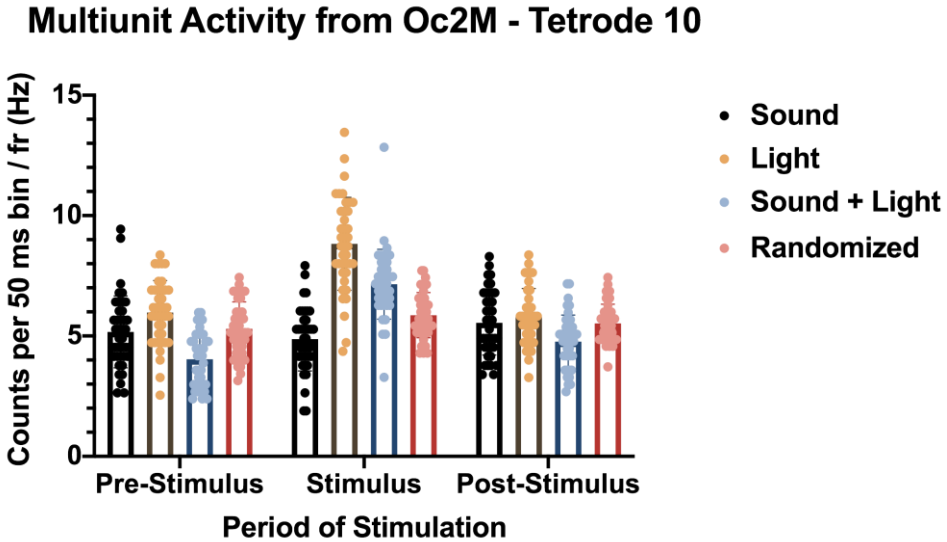

Fig. 3.32. Multiunit activity differences in terms of firing rate, according to sensory condition and period of stimulation (Tetrode 10).

Post hoc multiple comparisons showed a significant increase of the firing rate upon the presentation of light (M = 5.79, SD = 1.18) and sound + light (M = 7.15, SD = 1.45) cues. However, no differences were found in response to light between pre (M = 5.97, SD = 1.33) and post-stimulation (M = 8.83, SD = 1.93) periods, opposed to the sound + light condition where the firing rate is different between these two periods (Pre-stimulus: M = 4.03, SD = 1.15; Post-Stimulus: M = 4.77, SD = 1.10). Furthermore, no significant differences were found in response to sound between pre-stimulus (M = 5.17, SD = 1.49), stimulus (M = 4.87, SD = 1.32), and post-stimulus (M = 5.55, SD = 1.34) periods. The same was observed for randomly picked trials (Pre-stimulus: M = 5.3, SD = 1.12; Stimulus: M = 5.86, SD = 0.94; Post-Stimulus: M = 5.52, SD = 0.8). The neuronal ensemble recorded by tetrode 10 responded to light and sound + light stimulation. Yet, our results suggest that only multimodal stimulation had an effect on the period after stimulus offset, given the higher number of spikes captured in this period compared to baseline activity. On the other hand, the same was not found for unisensory stimulation, i.e. sound or light cues in isolation.

It is worth noting that the way statistical analyzes were designed, might fail to account for the full effect of the sensory conditions on neuron's firing rate. We divided time in three different periods and we looked for the existence of differences among several population means. In this case, the population mean corresponds to the mean of the firing rate[14], in a given sensory condition, at a given period. This raises a problem: by considering only the mean from each period, we are assuming that values are not supposed to change over time within that period. In other words, transients of activity present within a single period of stimulation might not be accounted for, since we are taking the average of the whole period. For example, the sound and light condition during stimulus presentation (blue bar, in fig. 3.32) presents a high value that, at first glance, looks like an outlier. However, the plot respective to the sound + light condition in fig. 3.30, shows that, that is actually the effect of stimulus triggering. Such resulted in an increase of the firing rate to more than double, followed by a fast

[14] Always in terms of the number of counts per 50 milliseconds bin, normalized to the overall firing rate.

decay. This subject will be further discussed in IV. Discussion section, as well as other possible tests suitable to capture and compare these transients of activity.

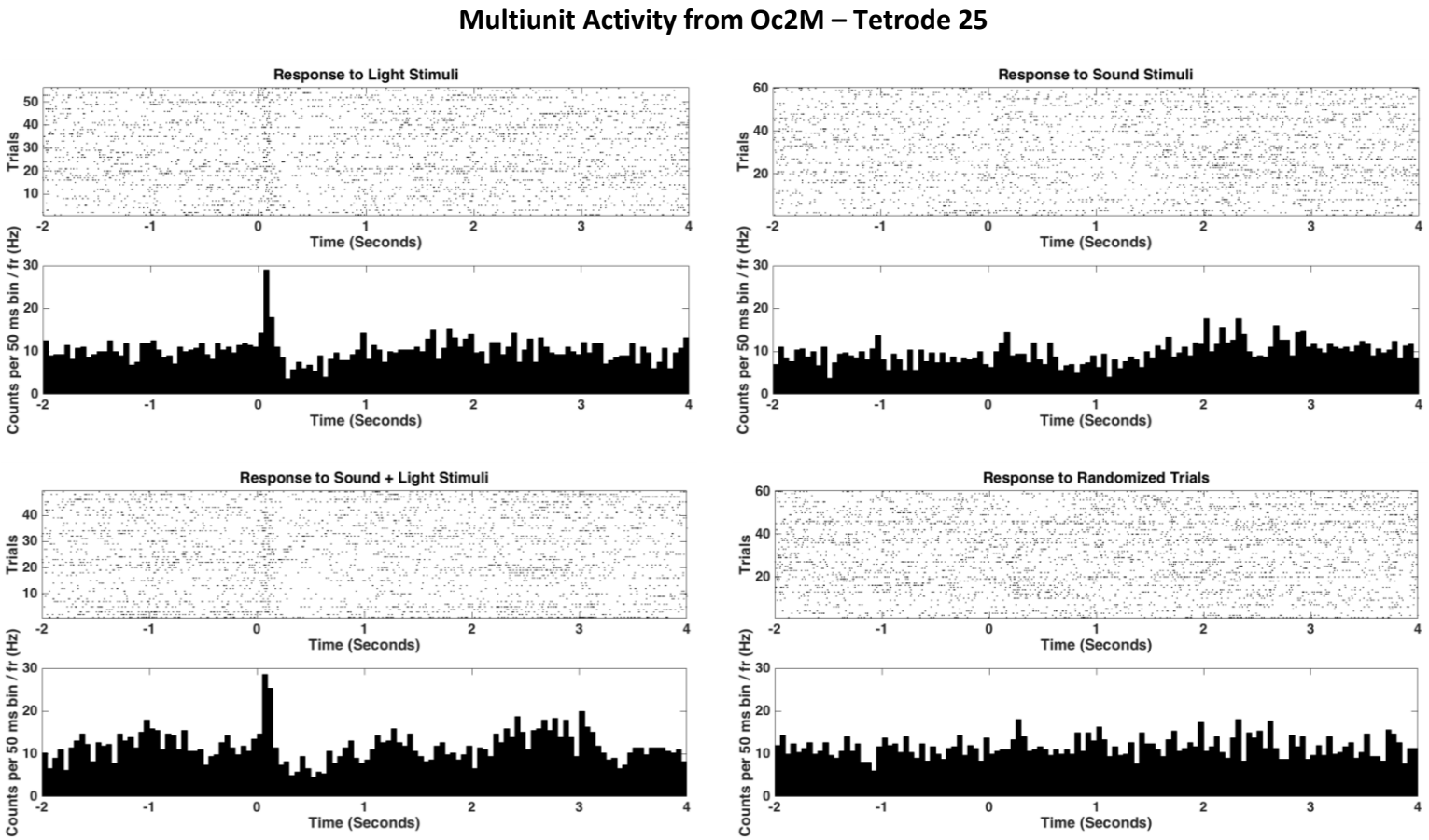

Fig. 3.33. Multiunit activity from Oc2M's tetrode 25 (rat Fausto - one session).

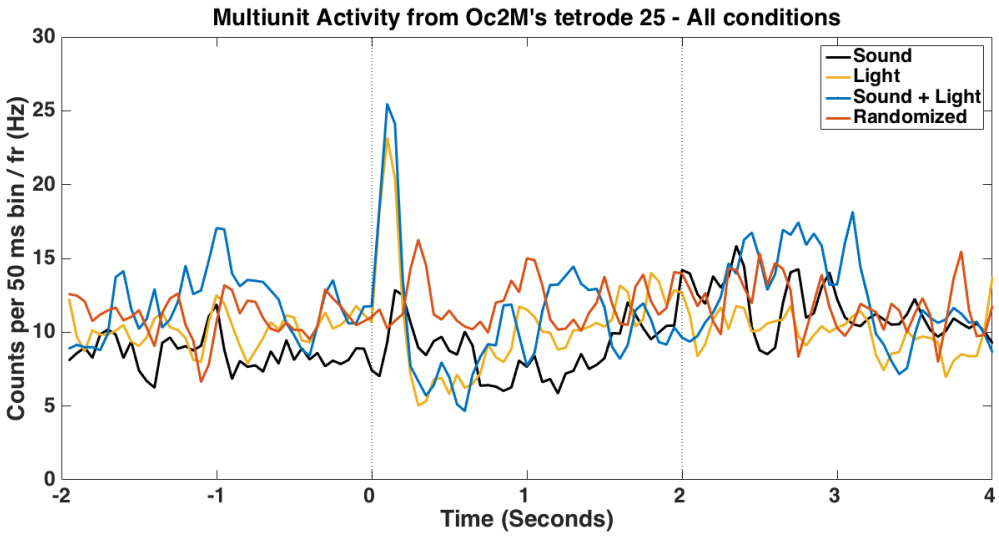

Fig. 3.34. Multiunit activity from Oc2M's tetrode 25 – All conditions overlapped.

Once again a strong response is observed after stimulus onset in the light and sound + light conditions. (Figs. 3.33 and 3.34). Interestingly, such effect is defined by the fast increase of neurons' firing rate, followed by a decrease to values lower than the pre-stimulus values of the respective sensory conditions. Besides, the values corresponded to this negative fluctuation are also lower than the ones detected in sound and randomized conditions, in pre-stimulus a stimulation periods.

A two-way ANOVA was conducted and we found a main effect of the period of stimulation ($F_{(1.991, 77.64)} = 3.763$, $p = .002$) and sensory condition ($F_{(2.714, 105.8)} = 19.98$, $p < .001$) on the multiunit activity of tetrode 25. A significant interaction effect was found between the period of stimulation and sensory condition ($F_{(3.388, 132.1)} = 4.617$, $p = .002$).

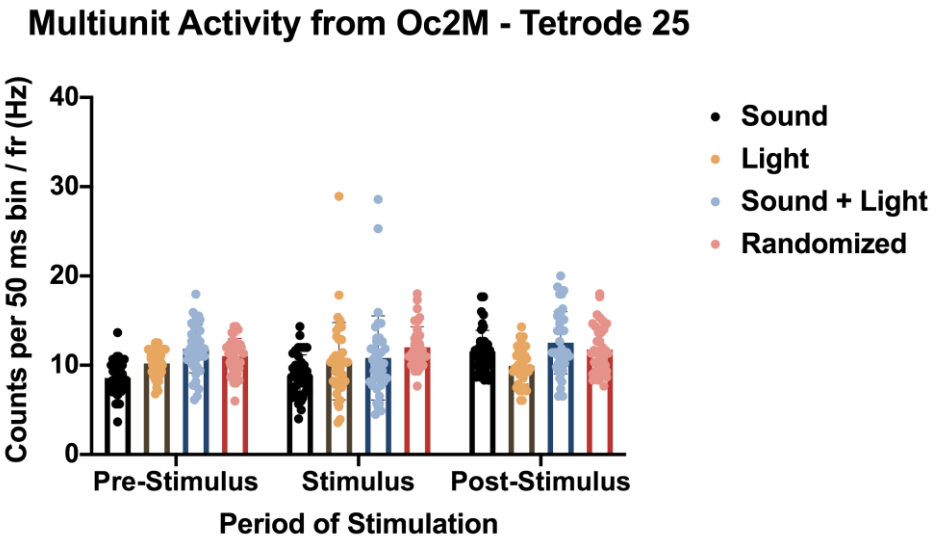

Fig. 3.35. Multiunit activity differences in terms of firing rate, according to sensory condition and period of stimulation (Tetrode 25).

In the light condition, no significant differences were found in the multiunit activity of tetrode 25 between the different stimulation periods (Pre-stimulus: M = 10.20, SD = 1.51; Stimulus: M = 10.46, SD = 4.33; Post-Stimulus: M = 9.93, SD = 2.04). The same result was found for the sound + light sensory condition (Pre-stimulus: M = 11.85, SD = 2.70; Stimulus: M = 10.82, SD = 4.71;

Post-Stimulus: M = 12.52, SD = 3.49). The lack of significant differences in these two conditions looks contradictory to the responses represented in figures 3.33 and 3.34. However, such results are expected under the light of the statistical methods used to compare conditions. As previously explained, we are comparing firing rate means from each stimulation period. Therefore, it is not surprising that the mean resulted from the stimulation epoch does not translate the response observed in the light and sound + light conditions (marked by an increase followed by a decrease, thus nulling each other).

Notably, even though multiunit activity did not significantly change between pre-stimulus (M = 8.58, SD = 1.86) and stimulus (M = 8.82, SD = 2.34) period, we found an increase of the overall firing rate after stimulus offset (M = 11.56, SD = 2.36), that was significantly different than pre-stimulus and stimulation periods. Despite the statistical quantification, a qualitative examination of the data suggests a modulation of the sound cue in this population of neurons, given its firing rate increase towards, and after, stimulus offset (figs. 3.33 and 3.34). An effect that is observed in the sound and sound + light conditions, but not seen when light is presented alone.

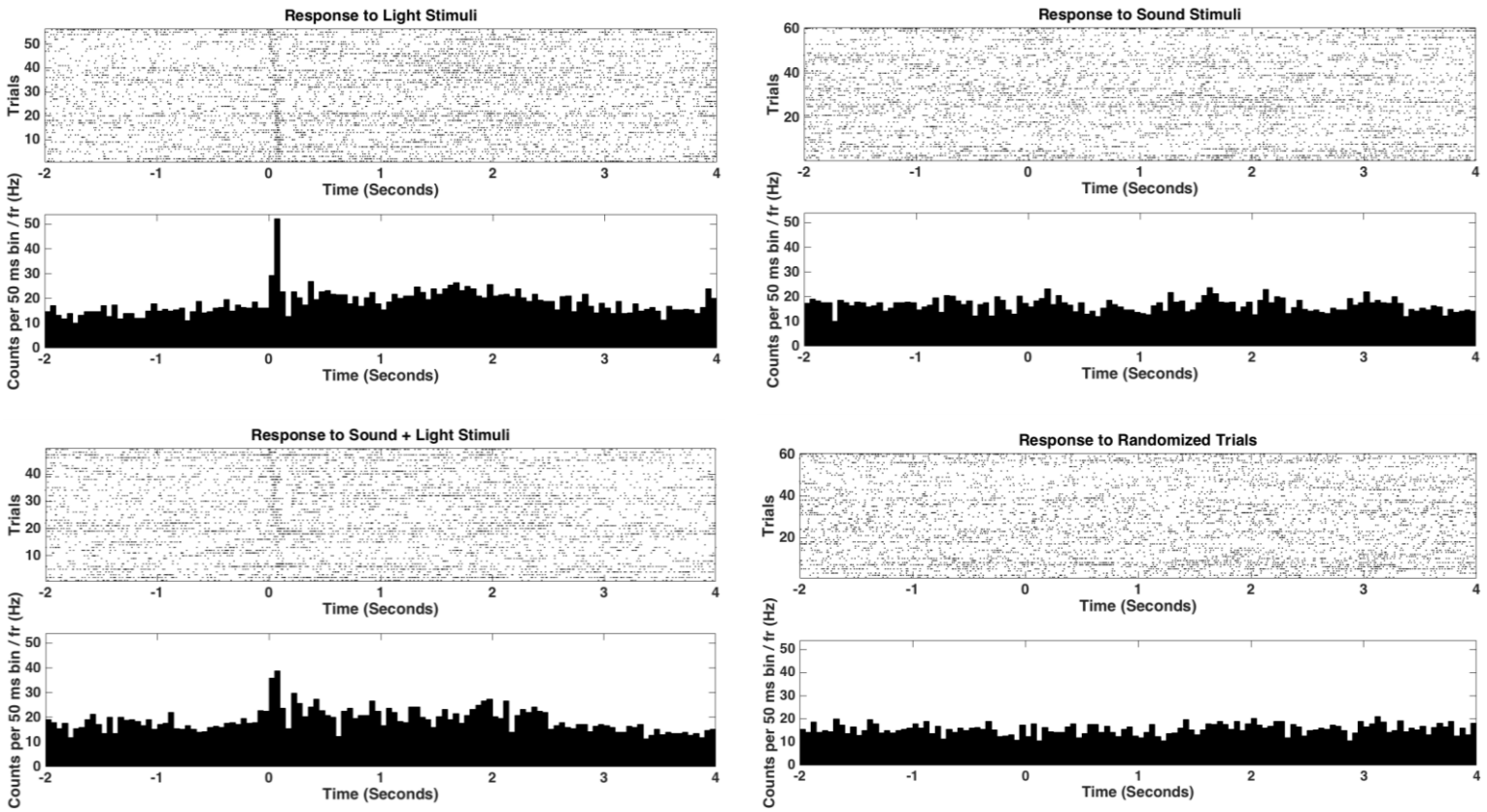

Fig. 3.36. Multiunit activity from Oc2M's tetrode 29 (rat Fausto - one session).

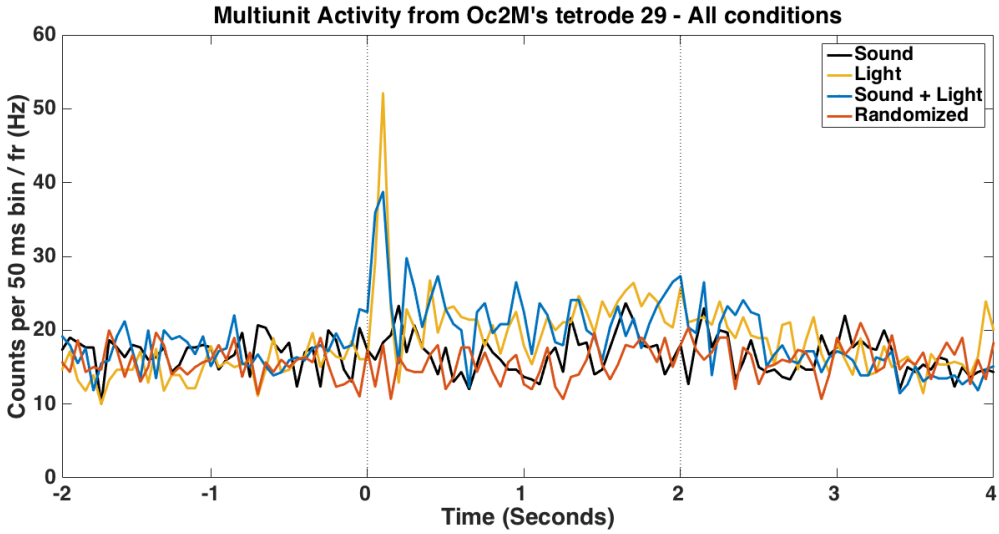

Fig. 3.37. Multiunit activity from Oc2M's tetrode 29 – All conditions overlapped.

We found a main effect of the period of stimulation ($F_{(1.874,\ 73.07)} = 30.12$, $p < .001$) and sensory condition ($F_{(2.710,\ 105.7)} = 24.07$, $p < .001$) on the multiunit

activity of tetrode 29. Additionally, there was a significant interaction effect between period of stimulation and sensory condition ($F_{(4.653, 181.5)} = 24.11$, $p < .001$).

Similar to Oc2M's tetrode 27 (fig. 3.27), the tetrode 29 also captured a population of neurons with an overall high firing rate. We can see it by the high-density presence of spikes in the raster plots, as also by the respective y-axis values in the peristimulus time histograms (fig. 3.36).

The recorded neural activity in this tetrode is characterized by a time-locked increase of the firing rate once light and sound + light cues are triggered. However, the response magnitudes found in the two conditions are quite different (figs. 3.36 and 3.37). Whereas sound and light cues presented simultaneously elicited an increase to around twice of baseline values, the light presentation alone evoked a response to nearly triple of the firing rate values before stimulus onset. Even though such large increase lasts only a few milliseconds, we see in light (M = 22.41, SD = 5.78) and sound + light (M = 22.51, SD = 4.98) conditions a followed sustained multiunit activity as long as the stimulus is on, with values significantly higher than in the pre-stimulus period of the respective conditions (Light Pre-stimulus: M = 15.02, SD = 2.17; Sound+Light Pre-stimulus: M = 17.35, SD = 2.51). Besides, during stimulus presentation, both multiunit activity in light and sound conditions were significantly higher than sound (M = 16.9, SD = 2.86) and randomized (M = 15.34, SD = 2.41) conditions.

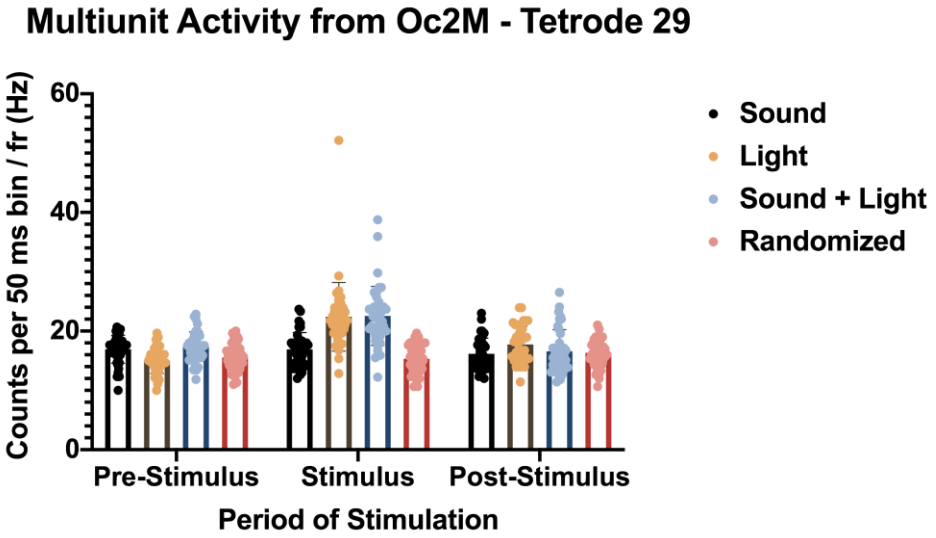

Fig. 3.38. Multiunit activity differences in terms of firing rate, according to sensory condition and period of stimulation (Tetrode 29).

Our analyses indicated that the presentation of a sound cue alone did not show significant differences on these neurons' activity among the different sensory conditions (Pre-stimulus: M = 16.94, SD = 2.35; Stimulus: M = 16.9, SD = 2.86; Post-Stimulus: M = 16.18, SD = 2.61). However, the statistically significant differences observed between sound, sound + light, and light conditions, during the time stimulus is on, suggests an effect of the sound when coupled with the light cue.

Note also the misalignment in the raster plots in the light and sound + light conditions, at the time stimulus is triggered. Such effect was described previously (fig. 3.27, tetrode 27), in which we see that, the increase of the firing rate in response to stimulus, appear earlier and earlier as the session progresses (even though in tetrode 27 the effect was characterized by a decrease in the firing rate, instead of an increase).

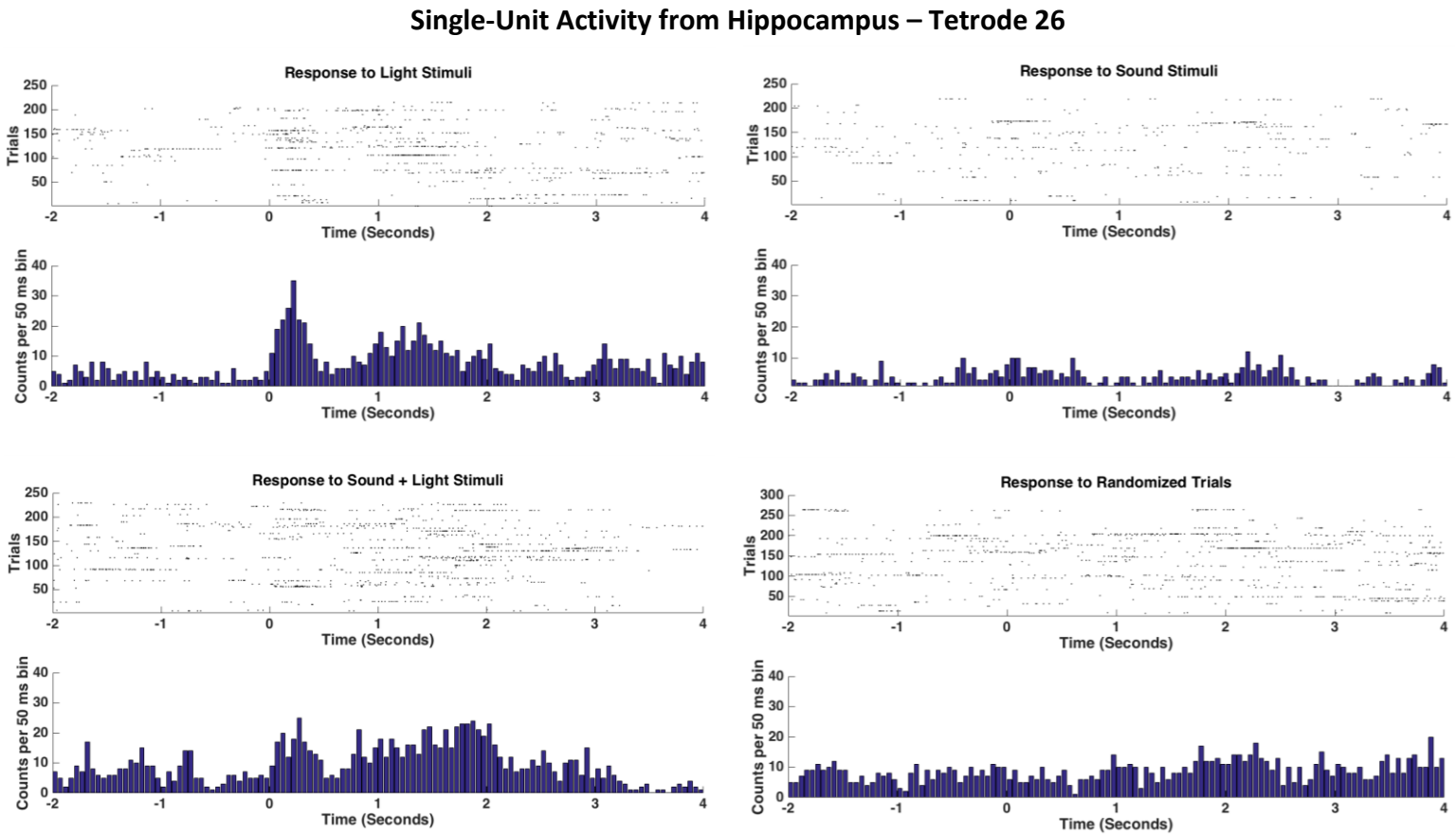

Fig. 3.39. Single-Unit activity from Hippocampus' tetrode 26 (rat Fausto - four sessions).

These plots correspond to the activity of a hippocampal neuron from four Stimbox sessions. The hippocampal tetrode 26 captured the activity of the same neuron across these four sessions. We concluded that based on the comparison of spike-clustering metrics across sessions (i.e. the same cluster could be found in all these sessions, sharing the same core features), and the fact that this tetrode was stuck at the time of these recording sessions.
Note also that the peristimulus time histograms are not normalized to the firing rate, meaning that each bar corresponds to the absolute value of spike counts (action potentials) in a given 50 milliseconds period.

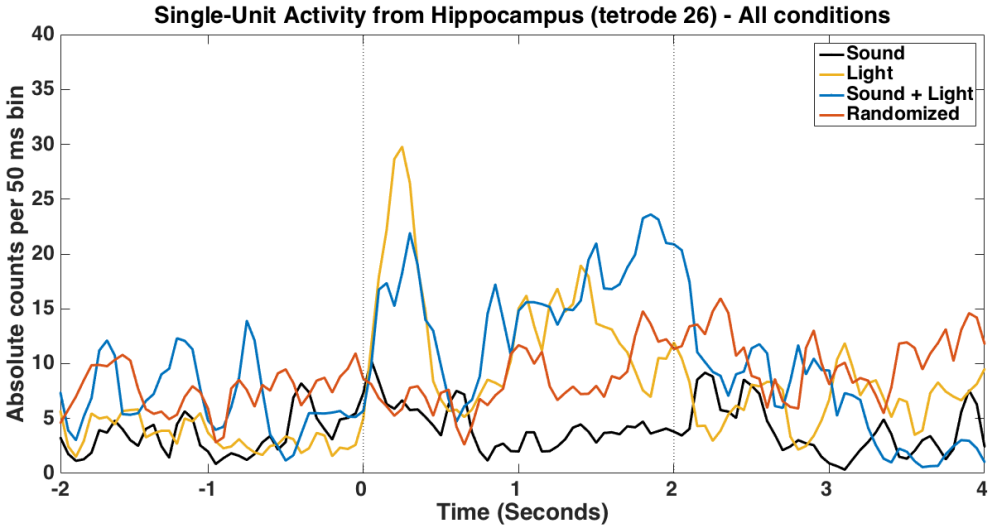

Fig. 3.40. Single-Unit activity from Hippocampus tetrode 26 – All conditions overlapped.

A two-way ANOVA test indicated that there was a main effect of the period of stimulation ($F_{(1.619,\ 63.15)} = 61.43$, $p < .001$) and sensory condition ($F_{(2.902,\ 113.2)} = 72.42$, $p < .001$) on the recorded hippocampal single-unit activity. A significant interaction effect was found between the period of stimulation and sensory condition ($F_{(3.695,\ 144.1)} = 24.36$, $p < .001$).

The raster plots in fig. 3.39 highlight the activity of a bursting pyramidal neuron. It is characterized by groups of high frequency spikes followed by quiescent periods. Some of these bursts occur independently of stimulus onset, as we can see from the differences of baseline values across sensory conditions. As such, one must be cautious when performing comparisons between sensory conditions.

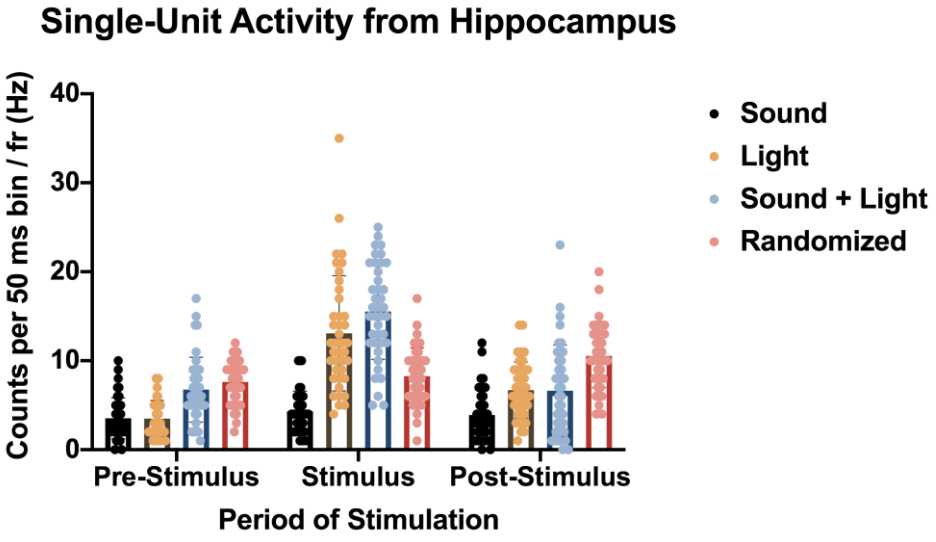

Fig. 3.41. Single-Unit activity differences in terms of firing rate, according to sensory condition and period of stimulation (Tetrode 26).

Once again we found significant differences in the light cue condition between the different stimulation periods (Pre-stimulus: M = 3.5, SD = 2.04; Stimulus: M = 13.08, SD = 6.47; Post-Stimulus: M = 6.7, SD = 3.15). On the contrary, no significant differences were found in the sound condition (Pre-stimulus: M = 3.53, SD = 2.32; Stimulus: M = 4.3, SD = 2.28; Post-Stimulus: M = 3.9, SD = 2.84). In the sound + light condition, the firing rate values during stimulation (M = 15.53, SD = 5.37) were found to be significantly higher than pre-stimulus (M = 6.75, SD = 3.64) and post-stimulus (M = 6.63, SD = 5.15) periods, although no differences were observed between pre and post-stimulus. Surprisingly, we found significant differences in the control condition (i.e. randomized) between pre-stimulus (M = 7.63, SD = 2.42) and post-stimulus (M = 10.55, SD = 3.57), as well between stimulus (M = 8.28, SD = 3.18) and post-stimulus.

Even though this neuron's activity corroborates the significant effects found in hippocampal LFP responses to light and sound + light cues, one must remember that this is just the example of one single neuron.

3.3. Ongoing Work

3.3.1. LFP responses according to speed

Here we present Oc2M LFP responses to sound trials according to the speed of the animal. We divided trials as stationary and non-stationary. We consider that the animal is motionless if speed values are not above 5 cm/second. On the other hand, we consider that the animal is moving if values cross this threshold (see section II. Methods for a detailed explanation).

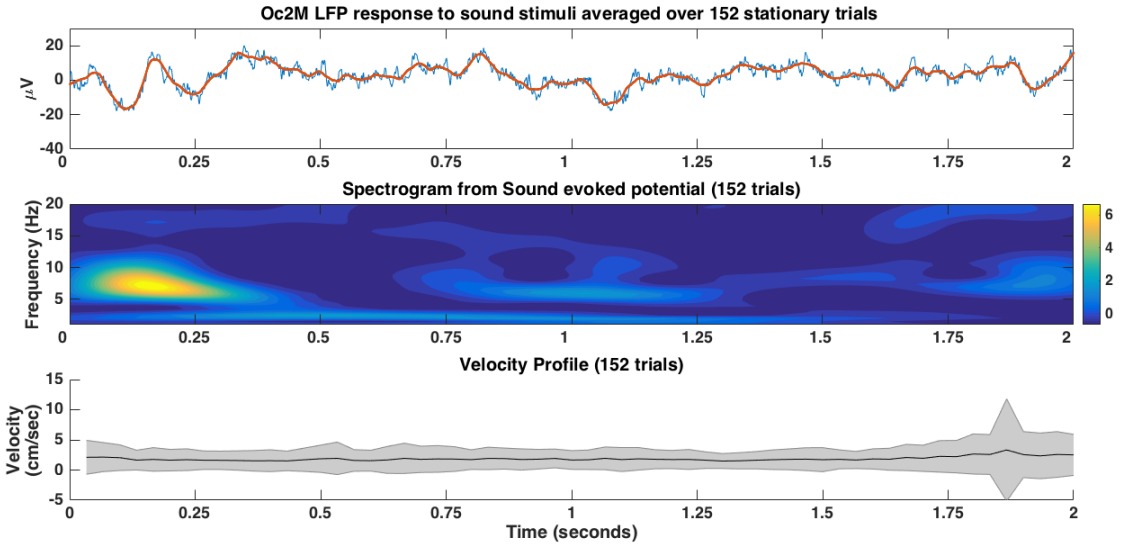

Fig. 3.42. Oc2M LFP response to sound stimuli while the rat is not moving.

As opposed to previous plots, the x-axes of the three plots range between t=0 seconds and t = 2 seconds, meaning that the full window is relative to the period of stimulation.

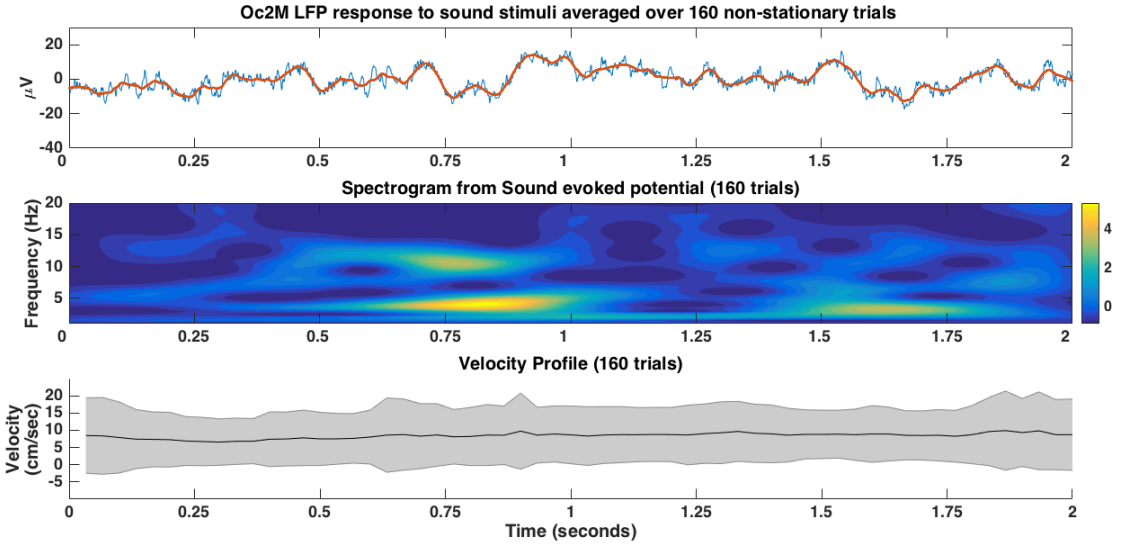

Fig. 3.43. Oc2M LFP response to sound stimuli while the rat is moving.

The figs. 3.42 and 3.43 represent just an exploratory test in which we try to address the possible confounding effects of movement on the LFP responses. Indeed, the responses between stationary and non-stationary trials are quite different. In the fig 3.40, we see a power increase right after stimulus onset, clearly distinguishable from the remaining activity of the epoch. However, when the animal is moving, such activity disappears and there is not a visible response that stands out along the signal. It is not possible yet to conclude whether such difference is significant and further analyses should contemplate the other sensory conditions.

3.3.2. Oc2M – Hippocampus Power Connectivity

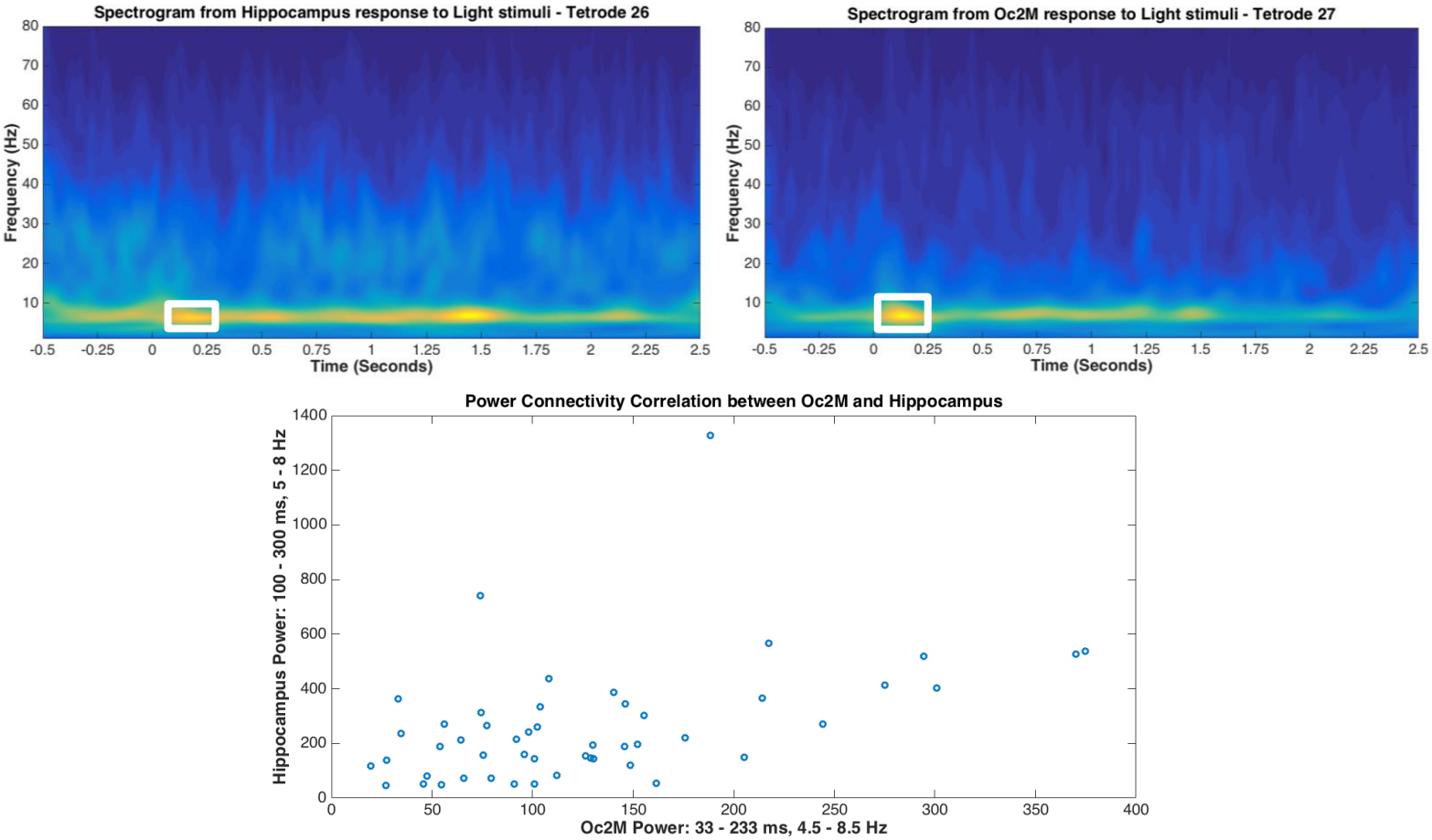

Fig. 3.44. Power connectivity between Hippocampus (tetrode 26) and Oc2M (tetrode27) during light stimulus epochs from one session.

(**Top**) Spectrograms from Hippocampus (left) and Oc2M (right) responses to light stimuli. We computed the spectrogram of each trial (0 to 80 Hz, and used a Morlet wavelet to convolute the signal looping over 90 frequencies) and then averaged them. The white rectangles represent the window of analysis chosen to look for power correlation between the two regions. (**Bottom**) Scatter plot where each dot represents the power values respective to each region, according the chosen time and frequency window. We found a positive statistically significant correlation between the two brain regions, $R_s = 0.50$, $p < .001$.

3.3.3. Oc2M – Hippocampus Phase Connectivity

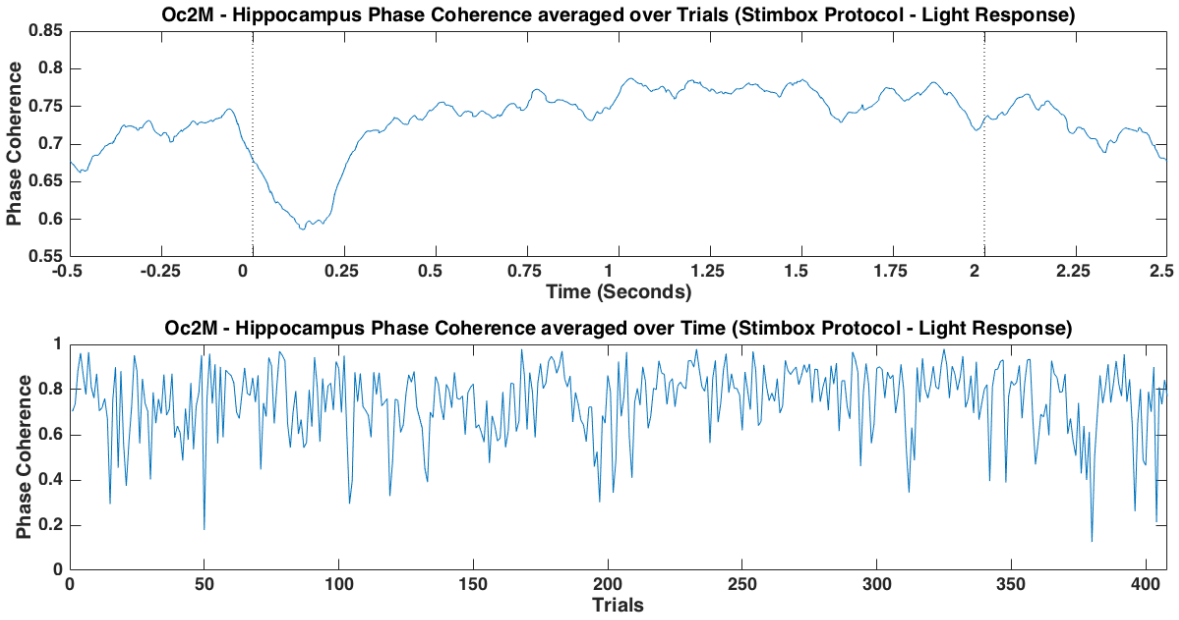

Fig. 3.45. Phase connectivity between Hippocampus and Oc2M during light stimulus epochs.

Phase connectivity was correlated over 408 trials, and Oc2M and Hippocampus LFP data resulted from the averaging of all tetrodes placed on site at the given sessions. We took the phase angle differences (real and complex values) between Oc2M and HIPP LFP signals, and each difference is represented as a unit vector in a polar coordinate system. (**Top**) We averaged unit vectors over trials and phase connectivity was measured by taking the magnitude (i.e. length) of the mean vector at each time point. (**Bottom**) Unit vectors were averaged over time (each trial) and phase connectivity was measured from the magnitude of the mean vector resulted from each trial.

The figure 3.45 (top) shows that, after light stimulus onset, we see a decrease in the phase synchronization between the two regions. Interestingly, the observed decrease occurs around the time of the identified ERPs observed on the LFP trace in response to light stimuli (see previous figures). In fact, both plots of fig. 3.45 show large synchrony values. One must be careful when interpreting these data. We should not conclude that Oc2M and Hippocampus are functionally connected solely based on these results. A better characterization regarding tetrodes' locations according to sub-regions is needed. Ideally, power and phase connectivity analyses would be implemented on datasets where the rat performed the SCTAT. A perceptual task where sensory information must be integrated, stored in memory, and retrieved when necessary.

IV. Discussion

We were able to successfully implement the SCTAT (2 conditions) in the first batch of animals, which corroborates previous evidence showing that rats can rely on memory to distinguish sound and visual cues in decision-making tasks (Gleiss & Kayser, 2012; David Raposo et al, 2014; Sakata, Yamamori, & Sakurai, 2004). The behavioral results from these rats were quite robust. They not only showed a linear performance progression over time, but they also maintained performance above chance levels during consecutive sessions. Besides, even after a long interruption period, the two rats were able to recall the task; having reached the desired performance levels within fewer sessions and with a shortened stimulus duration.

Nevertheless, it should be noted that only two out of six rats succeeded on learning the SCTAT. Even though reasons underlying such results are unknown to date, some hypotheses can be advanced to explain these findings. First, the two rats that learned the SCTAT (2 conditions) were the only ones that have been previously trained in the SCTAT (4 conditions). Despite that only sound cues were tested in the SCTAT – 4 conditions, the trajectory respective to the 1000 Hz tone was kept the same in the SCTAT – 2 conditions. Second, the first two rats were initially trained with two reward ports, each located right after the turn to a given trajectory (lateral arms), whereas the other four animals were trained with only one reward port, placed where trials start/finish. To effectively establish a behavior through operant conditioning, optimal stimulus-reward intervals must be implemented, since behavior becomes less efficient with longer intervals. As such, the considerable delay between the correct response (i.e. correct turn at decision point) and reward delivering, might have hindered the initial conditioning in the four followed rats. Third, compared to the first batch, these rats were much younger, and were not at 85% body weight when explored the maze for the first time. Finally, we did not reduce the number of trials per blocks according to a predefined criterion. For example, Kim et al. (2009) trained animals in a time interval discrimination task, where they gradually increased the

difficult of the task over blocks, defining a criterion of 80% of correct trials as the rule to upgrade to the next block. Although this principle was applied, to some extent, on the first two rats, the four next rats were never trained under this rule given the low number of trials presented. In fact, we had sometimes to vary the number of blocks within the same session, so that they could get confronted to both sensory cues.

LFP analysis demonstrates to be a reliable way of measuring neural activity, as it reflects the aggregate activity of a population of neurons based on their extracellular potentials. We have focused our LFP analyses on event-related potentials (ERPs), and compared time-dependent responses to different stimuli. The LFP activity from Oc2M and Hippocampus regions showed differences in response to sensory stimulation. These differences were observed not only across sensory conditions, but also between regions. However, results derived from ERPs analyses should always be carefully interpreted.

ERPs features, such as peak latency or magnitude, are arbitrarily defined components that are assumed to represent latent computational operations (Woodman, 2010). For instance, the time-locked responses observed in our experiments, might be interpreted as the process of sensory integration carried by Oc2M or Hippocampus, but we can't know if that is an effective characterization of the output signal. The extracted components of the signal are often found to vary, as they are greatly dependent on the behavioral state of the subject, tetrodes' locations, or type of stimulus, making difficult the attribution of an underlying meaning to the identified components. Furthermore, is very difficult to identify an ERP component at a single-trial level. There is the need to ensure a large sample of trials per condition so that the ERP can be revealed. However, even though averaging over trials increases signal-to-noise ratio[15], this strategy neglects possible features of the signal that could be present at the single-trial level (Rousselet & Pernet, 2011). Contrary to ERPs analysis in the time-domain, methods such as independent component analysis (ICA) or hierarchical

[15] It reduces noise contributions to the signal, as voltage fluctuations not related to the time-locked stimulus are attenuated.

Bayesian models, are found to be plausible solutions to account for the inter-trial variability in the data, and possible to be correlated it with behavior (Jung et al, 2001; Wu, Chen, Gao, & Brown, 2011).

Statistical comparisons between-subjects were not performed in our data. Both animals exhibited stronger responses to light stimulus than sound, an effect observed in Oc2M and Hippocampus. The voltage fluctuations defining the ERPs' responses were shown to be quite similar between animals. In fact, in both animals, the hippocampal LFP response preceded Oc2M's response by few milliseconds. Before drawing any conclusions from these observations, we should take into account the fact that the number of tetrodes contributing to each rat's LFP is very different. For example, Carpe had only confirmed one tetrode at Oc2M, so what we assumed as Oc2M's LFP activity is, in fact, the summation of extracellular potentials around the recording site of one single tetrode, which might not be representative of the whole region. On the other hand, Fausto's Oc2M activity resulted from an averaged signal of many tetrodes covering the full region. Although it gives an insight of the overall output, it might also hide specific sub-regions activity that contributes differently to stimuli responses (e.g. see figure 6.4, in Supplementary figures). Besides, even if both animals had been implanted with identical arrays and the same number of tetrodes, such would not guarantee similar responses in each tetrode. As Herreras (2016) points out, intracerebral LFP recordings do not ensure that the activity being recorded is generated by a source close to the tetrode. The obtained raw LFP signal usually captures the activity of different afferent pathways, located at different sites, elicited by different neuronal ensembles.

Phasic and tonic neuronal responses have been widely described in many types of neurons (Brischoux et al., 2009; Madrid et al., 2003; Pilkiw et al., 2017). Phasic firing refers to a short-lived response produced by a few action potentials usually right after stimulus onset, followed by accommodation. Tonic responses are characterized by a sustained action potential firing pattern during the course of the stimulus. Our results have showed that different populations of Oc2M

neurons can respond very differently to the same sensory cues. Instead of finding only tonic or phasic responses in a particular neuronal ensemble (e.g. see the example of figure 3.27, where Oc2M's neuronal activity is marked by a tonic increment activity until stimulus offset), mostly of recorded neurons showed combinations of tonic and phasic responses. Comparing light and sound sensory responses in isolation, light always elicited more prominent and robust responses in terms of firing rate. However, the fact that sound coupled with light stimulus resulted in responses differently than light alone, suggests that sound sensory information had a modulatory effect in the integration of both cues. For instance, recorded activity from Oc2M's tetrode 10 (figure 3.30) shows a tonic-decrement activity in the light sensory condition, whereas in the sound + light condition we see a firing pattern characterized by a phasic response at stimulus onset, followed by tonic-sustained activity until stimulus offset. To the best of our knowledge, this is the first study to highlight such diversified patterns of Oc2M neurons, in response to unisensory and multisensory stimulation.

Some of the recorded neurons showed superadditive, additive, and subadditive responses (for review, see Stein & Stanford, 2008), where a multisensory response is significantly different than the sum of responses resulted from unimodal stimulation. However, in the current Stimbox protocol, sound and light cues never changed in their location or intensity. As such, we can't test whether the 'space' rule, 'time' rule, and the principle of inverse effectiveness (Meredith & Stein, 1983; Stein et al, 1989), apply to Oc2M's neuronal populations. In order to test such principles, future experiments should contemplate more behavioral conditions, mixing the presentation of different stimulus intensity (e.g. light's brightness or sound's frequency) placed at different locations. Moreover, the possibility that Oc2M neuronal ensembles might integrate multisensory information in a Bayesian-optimal manner, can't be addressed using Stimbox experiments as performed here. To answer that question, we suggest the development of a behavioral task in which stimulus reliability varies across trials, and where animals are required to make decisions based on those sensory inputs. A task such as the SCTAT, or a modified version of

the Stimbox with operant conditioning, would help us unravel the underlying processes by which multisensory integration occurs, both at the neurophysiological and behavioral levels. Besides, it would elucidate us on how Oc2M integrates and conveys sensory information to Hippocampus during a contextual memory formation task. Since that our electrophysiological analyses were solely based in a passive-stimulation behavior protocol (i.e. Stimbox), we are not able yet to address whether rostral Oc2M neurons carry and compute locally previous sensory information (Akrami et al, 2018), or if they integrate sensory inputs that are accumulated elsewhere for decision-making processes (Licata et al, 2017).

Most of the observed single and multiunit responses displayed both phasic and tonic activity within the same period. Differences in responses were analyzed by comparing the means of each sensory condition at a given period (pre-stimulus, stimulus, post-stimulus). Averaging each defined epoch might not capture such transients of activity. Importantly, it can lead to a type II error, where the statistical test does not reject a false null hypothesis (i.e. we get a false negative result, in which we wrongly assume that there are no significant differences because the statistical test failed to capture such differences). To account for this problem, we propose for future analyses the resampling of the observed data in a permutation based-approach, where we can test for differences in the firing rate across sensory conditions as a function of time (Fujisawa et al, 2008). In this case, statistical significance is tested based on the data, instead of previous assumptions.

V. Conclusions

Animals' perception of the world results from a process called multisensory integration: the ability to simultaneously detect and combine information coming from multiple sensory systems. We explored the role of rat's Oc2M, a brain region traditionally considered as a secondary visual area, as a possible locus for convergence of sensory information, namely visual and sound information.

Our results showed that light stimuli elicited stronger responses in Oc2M compared to sound stimuli. However, the firing patterns of different populations of neurons recorded from Oc2M, revealed significant differences between multimodal (sound + light) and unimodal (sound or light) sensory stimulation. These findings suggest that sound had a modulatory effect in the neuronal computations carried by Oc2M neurons in the integration of both stimuli. Future experiments should contemplate simultaneous recordings of Oc2M and Hippocampus neuronal activity, while animals perform the sensory-cue trajectory association task (SCTAT). Such would help us to characterize the functional connectivity between Oc2M and Hippocampus, and unravel how Oc2M integrates sensory information in the service of memory. Furthermore, the implementation of techniques such chemogenetics (Ambruster et al., 2007) or optogenetics (Boyden et al., 2005) would allow us to modulate neurons' response (e.g. suppress their activity) in a region-specific manner (e.g. Oc2M). It opens up the possibility to causally study the role of Oc2M as a site of convergence to process sensory-relevant information.

VI. Supplementary Information

6.1. Figures

A

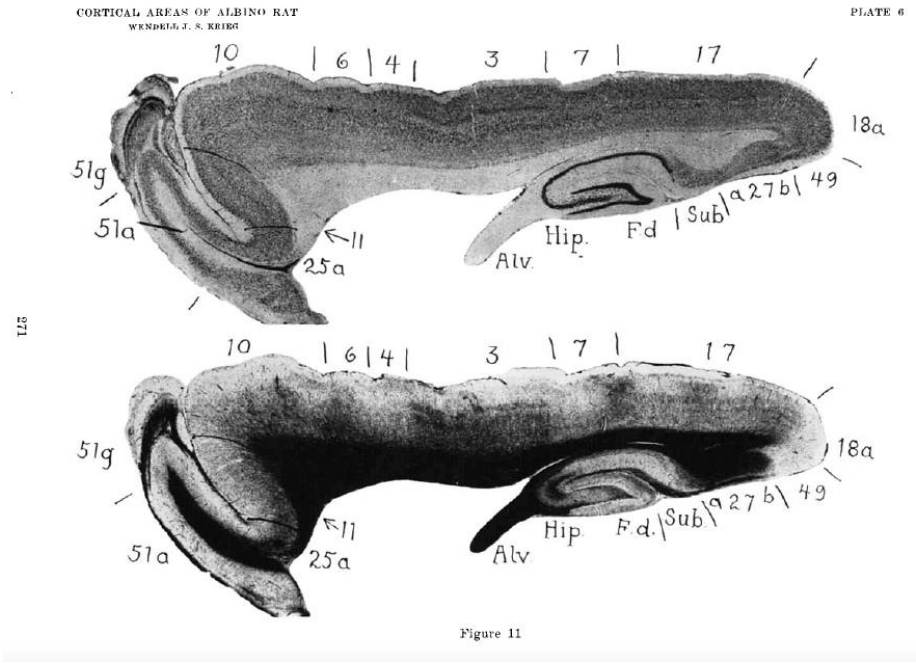

B

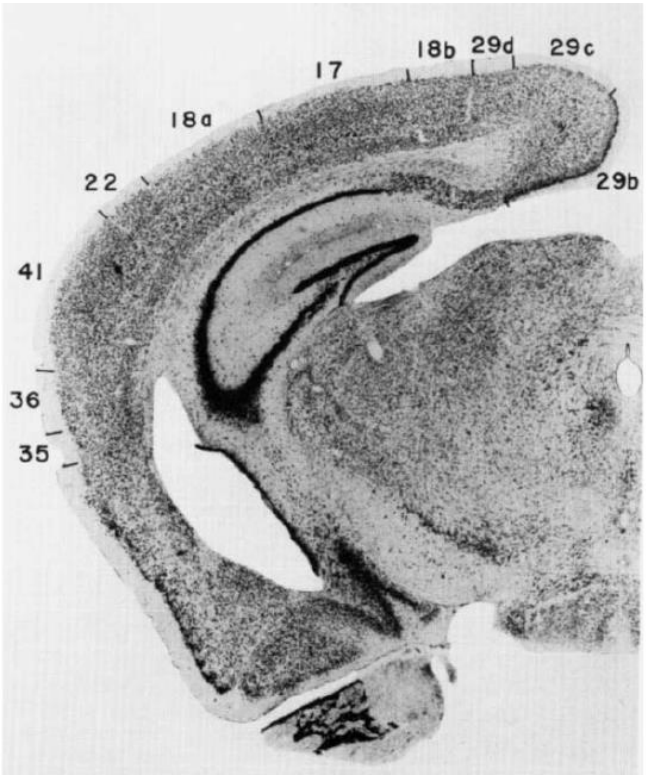

Fig. 6.1. Localization of brain regions overlapping with Oc2M according to different brain atlases.

(A) Krieg's area 7 (Krieg, 1946). **(B)** Caviness's area 18b and partially area 17.

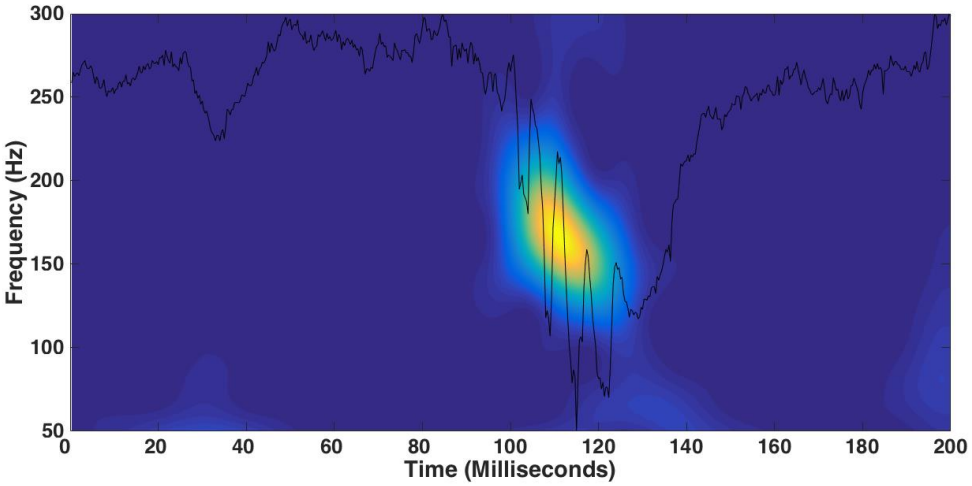

Fig. 6.2. Proof of concept of the Morlet wavelet convolution code.

Sharp-wave ripples (SPW-Rs) are characterized as hippocampal high-amplitude 120–250 Hz oscillations that last approximately between 40 – 120 milliseconds. We identified a SPW-R event in one of the datasets (black trace) and used the Morlet wavelet code to extract power-frequency information over time. The figure shows that, at the time of the SWP-R, the range of frequencies captured and the duration of the event match SWR's characteristics according to the literature.

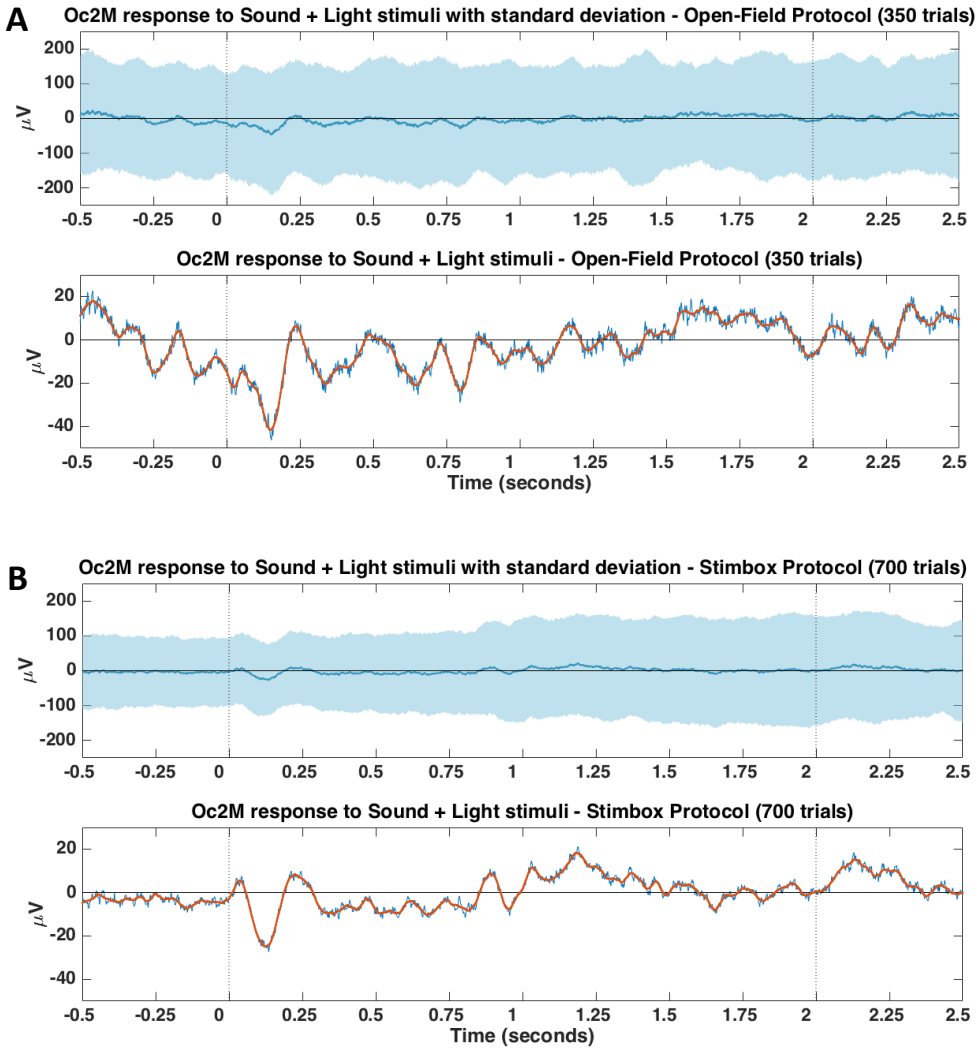

Fig. 6.3. Comparison of Oc2M responses (rat Fausto) to sound + light stimuli between Open-Field and Stimbox protocols.

(A) The plot on the top represents the averaged LFP signal with standard deviation, in response to sound + light stimulation under the Open-Field protocol. The plot on the bottom represents the same signal in a closed-up view, where a Savitsky-Golay filter (red) was applied to smooth the trace. **(B)** Represents the same features as in A, but the extracted signal corresponds to Oc2M responses under the Stimbox protocol.

Even though the same ERP component seems to be present in both protocols (peak amplitude at approximately t = 0.1 seconds), the response found in the Stimbox protocol is more robust than in the Open-Field. Such can be explained due to a lower signal-to-noise ratio in the Open-Field protocol because of the constant movement of the animal. In fact, if one compares standard deviation values, will find much larger values in the Open-Field than in the Stimbox (e.g. look at pre-stimulus period), which suggests noise contamination in the datasets in the context of ERPs analyses.

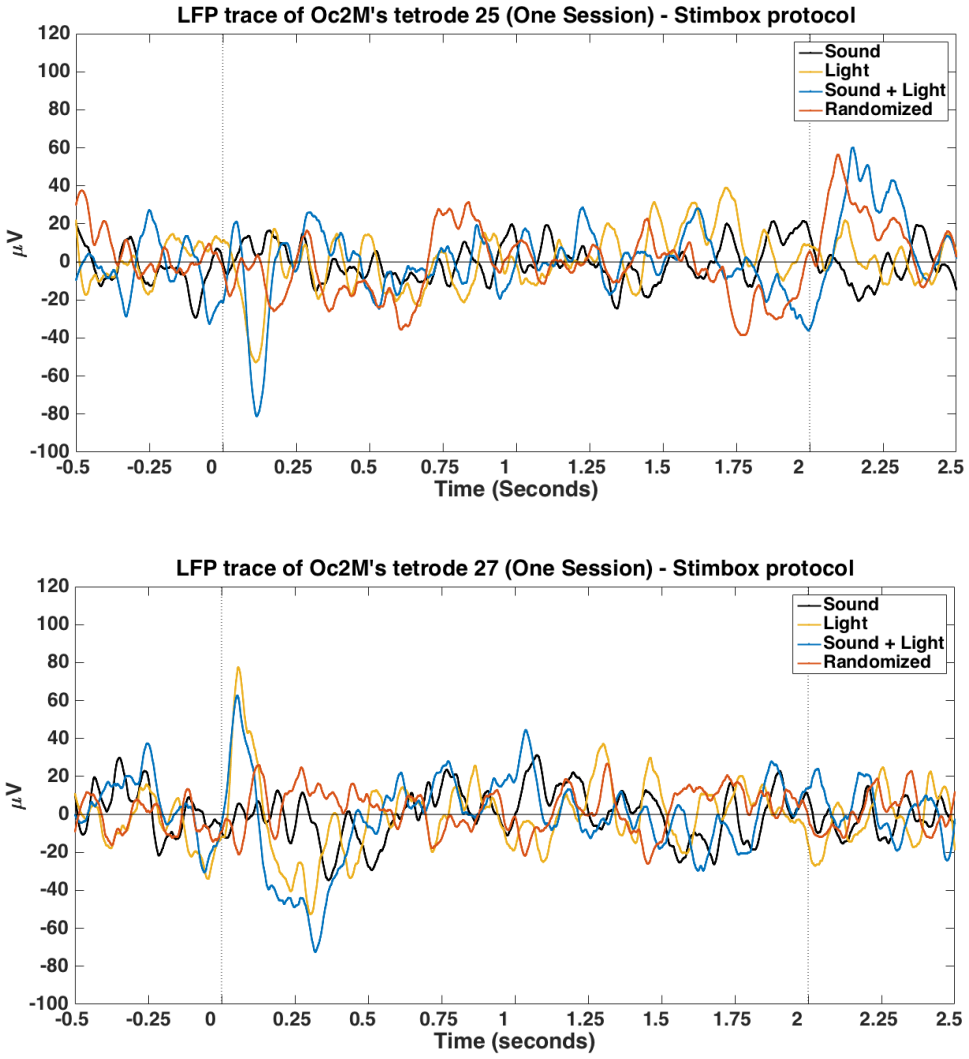

Fig. 6.4. Comparison of LFP traces between two different tetrodes placed at Oc2M.

The plots show the LFP responses recorded from two different tetrodes during one Stimbox session. It is possible to observe a prominent LFP response in the light and sound + light conditions in both tetrodes. However, the patterns are quite different. Whereas in tetrode 25 (**top**) we see a negative fluctuation of the signal after stimulus onset, the tetrode 27 (**bottom**) shows a positive and larger component after stimulus onset, followed by a decrease lower to baseline values.

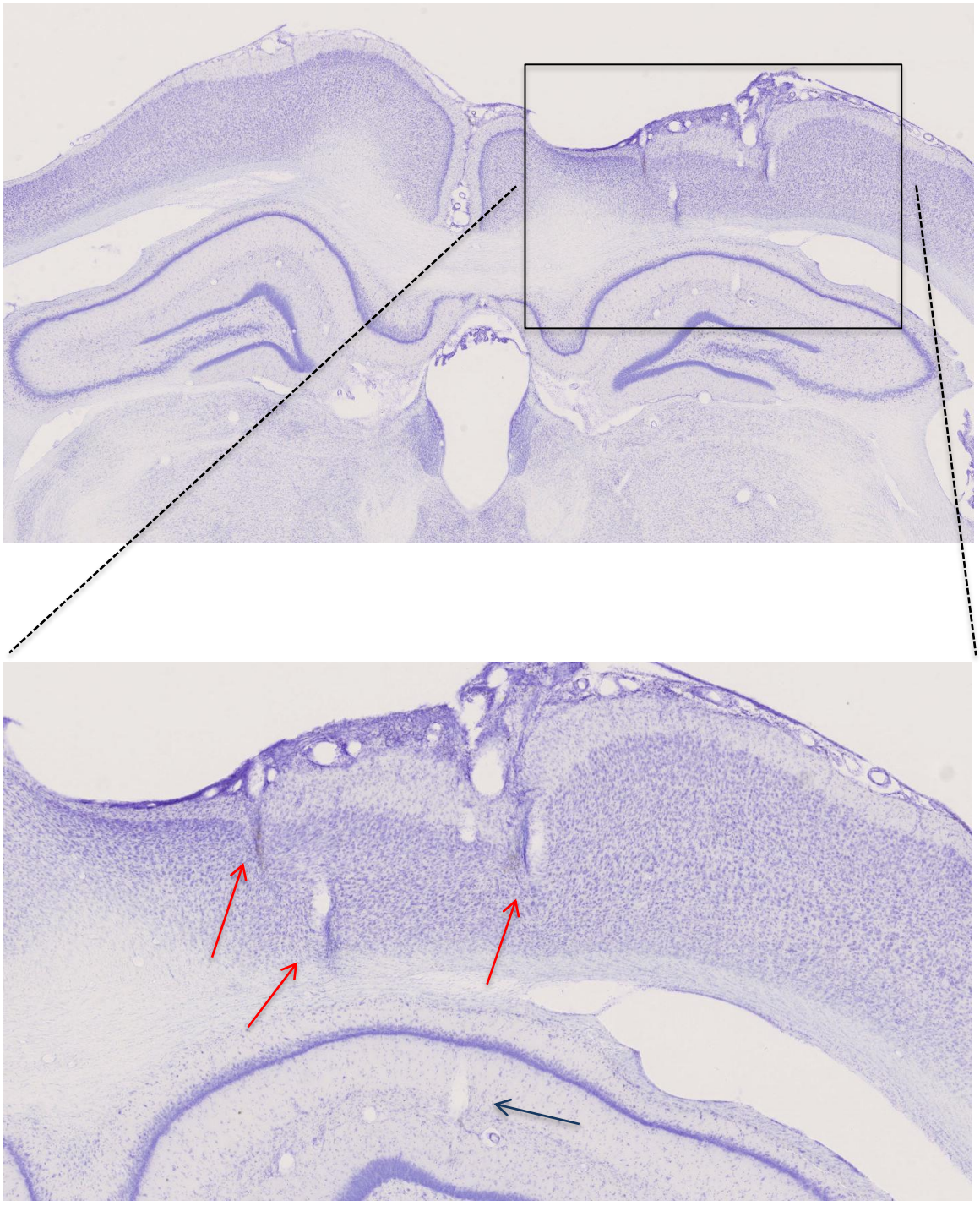

Fig. 6.5. Verification of representative tetrode tracks in Oc2M (red arrows) and Hippocampus (dark blue arrow).

6.2. Methods – Implant Surgery

The rat is first weighted and all injectable drugs are prepared accordingly beforehand (see table 4.1 for dosages and medical procedure). The anesthesia is induced in an induction box containing isoflurane and once the animal loses the righting reflex, an intraperitoneal injection of ketamine and xylazine is performed, followed by a subcutaneous injection of the anti-inflammatory Rymadil (Carprofen, see table 6.1). During the time between the isoflurane induction and the effects of ketamine + xylazine cocktail, the rat might start to recover some of the righting reflex. For that reason, the animal is put back again his home-cage and we wait until the anesthetics take effect.

The animal is moved to a heating pad and the surgical site is carefully shaved. After applying a lidocaine ointment (local anesthetic) inside the rat's ears, he is placed in the stereotaxic frame apparatus, connected to an isoflurane-delivering system through a mask, and ear bars are inserted into the ear canal. Ear bars placement is tested by gently trying to move rat's head along the different axes. Once we guarantee the animals is properly fixed in the frame and his paw withdrawal reflex is absent, eye ointment (Lacryvisc) is applied and a subcutaneous injection of Ringer's lactate solution is given (from then onwards administered each every hour until surgery is over).

The surgical field is cleaned with a 10% povidone-iodine followed by 70% ethanol in an alternate way. This is accomplished using a cotton swab by scrubbing the area in circles going from the center to the periphery (this procedure is repeated about 3/4 times). A surgical blade is then used for the sagittal incision starting at the midline of the inter-orbital line until the inter-aural line[16]. The skin is laterally retracted and the *periosteum* totally removed so we can get a good visibility of our stereotaxic landmarks (Bregma and Lambda) and a full exposure of our surgical field, preferentially cleaned and dried. An antibiotic (Baytril solution) is applied directly in the skull.

[16] Care must be taken when reaching the inter-aural line so that major muscle bleedings are avoided.

Medication	Procedure	Solutions Recipe
Ketamine + Xylazine cocktail	**Dosage: 3 ml/Kg** Administered intraperitoneally right after induction with isoflurane (i.e. if the rat weights 500g we give 1.5ml)	**1 ml** Ketamine **0.5 ml** Xylazine **1.5 ml** Saline solution
Rimadyl (Carprofen)	**Dosage: 0.5 ml/Kg** Administered subcutaneously at the beginning of the surgery (half-dose) and at the end (half-dose)	**0.1 ml** Carprofen **0.9 ml** Saline Solution
Baytril (Enrofloxacin)	Few drops are delivered directly on the surface of the skull once exposed (after skin retraction and periosteum removal)	
Ringer's lactate solution	5ml doses are subcutaneously injected each hour throughout the surgery in order to keep the animal hydrated	
Lacryvisc (Ophthalmic gel)	It prevents the eyes to dry out and is administered on an hourly-basis until surgery is over	

Table 6.1. Medication used in the implant surgery with respective doses and procedures.

Before any drilling we must ensure that the skull's surface is perfectly horizontal. A needle is incorporated in the stereotaxic probe holder and we compare the dorso-ventral values of Bregma and Lambda[17]. We do little adjustments to the head's animal position along the z-axis until Bregma and Lambda values match. A precision drill bit is then used to start delimiting the craniotomy site[18] relative to Bregma according to our hyperdrive's bundle size and respective brain targets' coordinates. Additionally, three lines were marked external to the craniotomy area[19] as a future reference for tetrodes placement over the brain in order to guarantee an accurate targeting.

[17] Such anatomical points are not always easy to identify so one might want to use a magnifier to help.
[18] The location and size of the craniotomy are defined taking into account not only the bundle array but also the amount of epoxy around it. Inevitably, this will cost an enlargement of our craniotomy over the margins of our target's coordinates.
[19] The references were the most medial coordinate (-1.4 mm), the most lateral (-3.1 mm) and the most anterior (-3.8 mm).

Six small screws are fixed to the skull close to the temporal crest, two on the side of the craniotomy and the other four on the left side. It is crucial that that screws are properly placed since that the future mechanical stability of the hyperdrive is greatly dependent on them. One additional screw hole is made posterior to the Lambda stereotaxic landmark that will be further used to fix a ground reference wire connected to the Electrode Interface Board (EIB). Only after all screws are in place (except for the ground), craniotomy can be finished followed by the removal of the meningeal membrane dura mater.

Once the brain gets exposed, two to three drops of mineral oil are applied and the hyperdrive can finally start be lowered having all tetrodes sticking out. Oc2M and Hippocampal tetrodes distances from the bundle were, respectively, 0.5 mm and 1.5 mm. Having the hyperdrive still a few centimeters above the target site, we grab the ground wire coming from the EIB and make sure it gets connected to the animal's skull by driving a last screw into the previously perforated hole (posterior to the lambdoid suture) with the wire inside it[20]. The hyperdrive can then continue to be lowered and, as it gets closer, one must try to align the tetrodes with the respective lines marked before. After ensuring that tetrodes entered the brain and epoxy is at the level of the bone's surface, the whole structure is secured to the screws with dental acrylic.

[20] Ground electrical conductance is then tested using a multimeter.

VII. References

Adrian, E.D. (1926). The impulses produced by sensory nerve-endings: Part 4. Impulses from Pain Receptors. *The Journal of Physiology, 62*(1), 33–51

Akrami, A., Kopec, C. D., Diamond, M. E., & Brody, C. D. (2018). Posterior parietal cortex represents sensory history and mediates its effects on behaviour. *Nature*, *554*(7692), 368–372. https://doi.org/10.1038/nature25510

Alais, D., & Burr, D. (2004). Ventriloquist Effect Results from Near-Optimal Bimodal Integration. *Current Biology*, *14*(3), 257–262. https://doi.org/10.1016/S0960-9822(04)00043-0

Anastasio, T. J., Patton, P. E., & Belkacem-Boussaid, K. (2000). Using Bayes' rule to model multisensory enhancement in the superior colliculus. *Neural Computation*, *12*(5), 1165–1187. https://doi.org/10.1162/089976600300015547

Armbruster, B. N., Li, X., Pausch, M. H., Herlitze, S., & Roth, B. L. (2007). Evolving the lock to fit the key to create a family of G protein-coupled receptors potently activated by an inert ligand. *Proceedings of the National Academy of Sciences*, *104*(12), 5163–5168. https://doi.org/10.1073/pnas.0700293104

Atiani, S., David, S. V., Elgueda, D., Locastro, M., Radtke-Schuller, S., Shamma, S. A., & Fritz, J. B. (2014). Emergent selectivity for task-relevant stimuli in higher-order auditory cortex. *Neuron*, *82*(2), 486–499. https://doi.org/10.1016/j.neuron.2014.02.029

Boyden, E. S., Zhang, F., Bamberg, E., Nagel, G., & Deisseroth, K. (2005). Millisecond-timescale, genetically targeted optical control of neural activity. *Nature Neuroscience*, *8*(9), 1263–1268. https://doi.org/10.1038/nn1525

Botvinick, M., & Cohen, J. (1998). Rubber hands "feel" touch that eyes see. *Nature, 391*(6669), 756. https://doi.org/10.1038/35784

Brischoux, F., Chakraborty, S., Brierley, D. I., & Ungless, M. A. (2009). Phasic

excitation of dopamine neurons in ventral VTA by noxious stimuli. *Proceedings of the National Academy of Sciences of the United States of America*, *106*(12), 4894–4899. https://doi.org/10.1073/pnas.0811507106

Buchholz, V. N., Goonetilleke, S. C., Medendorp, W. P., & Corneil, B. D. (2012). Greater benefits of multisensory integration during complex sensorimotor transformations. *Journal of Neurophysiology*, *107*(11), 3135–3143. https://doi.org/10.1152/jn.01188.2011

Burnett, L. R., Stein, B. E., Chaponis, D., & Wallace, M. T. (2004). Superior colliculus lesions preferentially disrupt multisensory orientation. *Neuroscience*, *124*(3), 535–547. https://doi.org/10.1016/j.neuroscience.2003.12.026

Buzsáki, G. (2015). Hippocampal sharp wave-ripple: A cognitive biomarker for episodic memory and planning. *Hippocampus*, *25*(10), 1073–1188. https://doi.org/10.1002/hipo.22488

Buzsáki, G., & Silva, F. L. (2012). High frequency oscillations in the intact brain. *Progress in neurobiology*, *98*(3), 241–249. doi:10.1016/j.pneurobio.2012.02.004

Cappe, C., Murray, M. M., Barone, P., & Rouiller, E. M. (2010). Multisensory facilitation of behavior in monkeys: Effects of stimulus intensity. *Journal of Cognitive Neuroscience*, *22*(12), 2850–2863. https://doi.org/10.1162/jocn.2010.21423

Caras, M. L., & Sanes, D. H. (2017). Top-down modulation of sensory cortex gates perceptual learning. *Proceedings of the National Academy of Sciences*, *114*(37), 9972–9977. https://doi.org/10.1073/pnas.1712305114

Caviness, V. S. (1975). Architectonic map of neocortex of the normal mouse. *Journal of Comparative Neurology*, *164*(2), 247–263. https://doi.org/10.1002/cne.901640207

Chen, L. L., & Nakamura, K. (1998). Head-centered representation and spatial

memory in rat posterior parietal cortex. *Psychobiology*, *26*(2), 119–127. https://doi.org/10.3758/BF03330599

Cherry, E. C. (1953). Some experiments on the recognition of speech with one and with two ears. *The Journal of the Acoustical Society of America*, *25*, 975–979. https://doi.org/http://dx.doi.org/10.1121/1.1907229

Churchland, A. K., Kiani, R., Chaudhuri, R., Wang, X. J., Pouget, A., & Shadlen, M. N. (2011). Variance as a Signature of Neural Computations during Decision Making. *Neuron*, *69*(4), 818–831. https://doi.org/10.1016/j.neuron.2010.12.037

Clayton N. S. & Dickinson A. (1998). Episodic-like memory during cache recovery by scrub jays. *Nature*, *395*, 272–274.

Colonius, H., & Diederich, A. (2002). A maximum-likelihood approach to modeling multisensory enhancement. In T. G. Dietterich, S. Becker, & Z. Ghahramani (Eds.), *Advances in neural information processing systems 14* (pp. 181-187). Cambridge, MA: the MIT Press

Diederich, A., Colonius, H., Bockhorst, D., & Tabeling, S. (2003). Visual-tactile spatial interaction in saccade generation. *Experimental Brain Research*, *148*(3), 328–337. https://doi.org/10.1007/s00221-002-1302-7

Dossani, R. H., Missios, S., & Nanda, A. (2015). The Legacy of Henry Molaison (1926-2008) and the Impact of His Bilateral Mesial Temporal Lobe Surgery on the Study of Human Memory. *World Neurosurgery*, *84*(4), 1127–1135. https://doi.org/10.1016/j.wneu.2015.04.031

Downer, J. D., Niwa, M., & Sutter, M. L. (2015). Task Engagement Selectively Modulates Neural Correlations in Primary Auditory Cortex. *Journal of Neuroscience*, *35*(19), 7565–7574. https://doi.org/10.1523/jneurosci.4094-14.2015

Doyle, M. C., & Snowden, R. J. (2001). Identification of visual stimuli is improved by accompanying auditory stimuli: The role of eye movements and sound location. *Perception*, *30*(7), 795–810. https://doi.org/10.1068/p3126

Elliott, M. T., Wing, A. M., & Welchman, A. E. (2010). Multisensory cues improve sensorimotor synchronisation. *European Journal of Neuroscience*, *31*(10), 1828–1835. https://doi.org/10.1111/j.1460-9568.2010.07205.x

Eramudugolla, R., Henderson, R., & Mattingley, J. B. (2011). Effects of audio-visual integration on the detection of masked speech and non-speech sounds. *Brain and Cognition*, *75*(1), 60–66. https://doi.org/10.1016/j.bandc.2010.09.005

Ergorul, C., & Eichenbaum, H. (2004). The hippocampus and memory for "what", "where", and "when". *Learning & Memory*, *11*, 397–405. https://doi.org/10.1101/lm.73304

Ernst, M. O., & Banks, M. S. (2002). Humans integrate visual and haptic information in a. *Nature*, *415*, 429–433.

Espinoza, S., Pinto-Hamuy, T., Passig, C., Carreño, F., Marchant, F., & Urzúa, C. (1999). Deficit in the water-maze after lesions in the anteromedial extrastriate cortex in rats. *Physiology and Behavior*, *66*(3), 493–496. https://doi.org/10.1016/S0031-9384(98)00315-1

Fairhall, S. L., & MacAluso, E. (2009). Spatial attention can modulate audiovisual integration at multiple cortical and subcortical sites. *European Journal of Neuroscience*, *29*(6), 1247–1257. https://doi.org/10.1111/j.1460-9568.2009.06688.x

Faisal, A., Selen, L. P. J., & Wolpert, D. M. (2009). UKPMC Funders Group Noise in the nervous system. *Learning*, *9*(4), 292–303. https://doi.org/10.1038/nrn2258.Noise

Ferbinteanu, J., & Shapiro, M. L. (2003). Prospective and retrospective memory coding in the hippocampus. *Neuron*, *40*(6), 1227–1239. https://doi.org/10.1016/S0896-6273(03)00752-9

Fetsch, C. R., Pouget, A., Deangelis, G. C., & Angelaki, D. E. (2012). Neural correlates of reliability-based cue weighting during multisensory integration. *Nature Neuroscience*, *15*(1), 146–154. https://doi.org/10.1038/nn.2983

Frank, L. M., Brown, E. N., & Wilson, M. (2000). Trajectory encoding in the hippocampus and entorhinal cortex. *Neuron*, *27*(1), 169–178. https://doi.org/10.1016/S0896-6273(00)00018-0

Frassinetti, F., Bolognini, N., & Làdavas, E. (2002). Enhancement of visual perception by crossmodal visuo-auditory interaction. *Experimental Brain Research*, *147*(3), 332–343. https://doi.org/10.1007/s00221-002-1262-y

Fujisawa, S., Amarasingham, A., Harrison, M. T., & Buzsáki, G. (2008). Behavior-dependent short-term assembly dynamics in the medial prefrontal cortex. *Nature Neuroscience*, *11*(7), 823–833. https://doi.org/10.1038/nn.2134

Ghazanfar, A. A., & Schroeder, C. E. (2006). Is neocortex essentially multisensory? *Trends in Cognitive Sciences*, *10*(6), 278–285. https://doi.org/10.1016/j.tics.2006.04.008

Gleiss, S., & Kayser, C. (2012). Audio-Visual Detection Benefits in the Rat. *PLoS ONE*, *7*(9). https://doi.org/10.1371/journal.pone.0045677

Gu, Y., Angelaki, D. E., & DeAngelis, G. C. (2008). Neural correlates of multisensory cue integration in macaque MSTd. *Nature Neuroscience*, *11*(10), 1201–1210. https://doi.org/10.1038/nn.2191

Hafting, T., Fyhn, M., Molden, S., Moser, M. B., & Moser, E. I. (2005). Microstructure of a spatial map in the entorhinal cortex. *Nature*, *436*(7052), 801–806. https://doi.org/10.1038/nature03721

Hanks, T. D., Kopec, C. D., Brunton, B. W., Duan, C. A., Erlich, J. C., & Brody, C. D. (2015). Distinct relationships of parietal and prefrontal cortices to evidence accumulation. *Nature*, *520*(7546), 220–223. https://doi.org/10.1038/nature14066

Herreras, O. (2016). Local field potentials: Myths and misunderstandings. *Frontiers in Neural Circuits*, *10*(DEC), 1–16. https://doi.org/10.3389/fncir.2016.00101

Hill, D. N., Mehta, S. B., & Kleinfeld, D. (2011). Quality metrics to accompany spike sorting of extracellular signals. *Journal of Neuroscience*, *31*(24), 8699–8705. https://doi.org/10.1523/JNEUROSCI.0971-11.2011

Hill, D. N., Mehta, S. B., & Kleinfeld, D. (2012). *UltraMegaSort2000 Manual*. 1–46. Retrieved from papers3://publication/uuid/6DF76942-B9EB-4542-A961-75B0F02F3F77

Hirokawa, J., Bosch, M., Sakata, S., Sakurai, Y., & Yamamori, T. (2008). Functional role of the secondary visual cortex in multisensory facilitation in rats. *Neuroscience*, *153*(4), 1402–1417. https://doi.org/10.1016/j.neuroscience.2008.01.011

Jung, T., Makeig, S., Westerfield, M., Townsend, J., Courchesne, E., & Sejnowski, T. J. (2001). *Analysis and Visualization of Single-Trial Event-Related Potentials*. *185*(June), 166–185.

Kandel E R, Schwartz J H, Jessell T M, Siegelbaum S A, Hudspeth A J. (2013). Sensory Coding. In Principles of Neural Science pp 449–74. New York, New York: McGraw-Hill

Keefe, J. O. (1976). Units in the Hippocampus Moving Rat. *Experimental Neurology*, *51*(1), 78–109.

Kim, J., Jung, A. H., Byun, J., Jo, S., & Jung, M. W. (2009). Inactivation of medial prefrontal cortex impairs time interval discrimination in rats. *Frontiers in Behavioral Neuroscience*, *3*(NOV), 1–9. https://doi.org/10.3389/neuro.08.038.2009

Körding, K. (2007). Decision theory: what "should" the nervous system do? *Science*, 318, 606-610.

Krieg, W.J.S. (1946) Connections of Cerebral Cortex. I. The Albino Rat. A. Topography of the Cortical Areas. *Journal of Comparative Neurology, 84*, 221-275. https://doi.org/10.1002/cne.900840302

Le Merre, P., Esmaeili, V., Charrière, E., Galan, K., Salin, P. A., Petersen, C. C. H., & Crochet, S. (2018). Reward-Based Learning Drives Rapid Sensory Signals in Medial Prefrontal Cortex and Dorsal Hippocampus Necessary for Goal-Directed Behavior. *Neuron*, *97*(1), 83-91.e5. https://doi.org/10.1016/j.neuron.2017.11.031

Lehmann, S., & Murray, M. M. (2005). The role of multisensory memories in unisensory object discrimination. *Cognitive Brain Research*, *24*(2), 326–334. https://doi.org/10.1016/j.cogbrainres.2005.02.005

Liang, M., Mouraux, A., & Iannetti, G. D. (2013). Bypassing primary sensory cortices-a direct thalamocortical pathway for transmitting salient sensory information. *Cerebral Cortex*, *23*(1), 1–11. https://doi.org/10.1093/cercor/bhr363

Licata, A. M., Kaufman, M. T., Raposo, D., Ryan, M. B., Sheppard, J. P., & Churchland, A. K. (2017). Posterior Parietal Cortex Guides Visual Decisions in Rats. *The Journal of Neuroscience*, *37*(19), 4954–4966. https://doi.org/10.1523/jneurosci.0105-17.2017

Lin, I.C., Okun, M., Carandini, M., & Harris, K.D. (2015). The nature of shared cortical variability. *Neuron*, *87*, 644–656. https://doi.org/10.1016/j.neuron.2015.06.035

Liu, B., Lin, Y., Gao, X., & Dang, J. (2013). Correlation between audio-visual enhancement of speech in different noise environments and SNR: A combined behavioral and electrophysiological study. *Neuroscience*, *247*, 145–151. https://doi.org/10.1016/j.neuroscience.2013.05.007

London, M., Roth, A., Beeren, L., Häusser, M., & Latham, P. E. (2010). Sensitivity to perturbations in vivo implies high noise and suggests rate coding in cortex. *Nature*, *466*(7302), 123–127. https://doi.org/10.1038/nature09086

Lovelace, C. T., Stein, B. E., & Wallace, M. T. (2003). An irrelevant light enhances auditory detection in humans: A psychophysical analysis of multisensory

integration in stimulus detection. *Cognitive Brain Research*, *17*(2), 447–453. https://doi.org/10.1016/S0926-6410(03)00160-5

Lyamzin, D., & Benucci, A. (2019). The mouse posterior parietal cortex: Anatomy and functions. *Neuroscience Research*, *140*, 14–22. https://doi.org/10.1016/j.neures.2018.10.008

Ma, W. J., Beck, J. M., Latham, P. E., & Pouget, A. (2006). Bayesian inference with probabilistic population codes. *Nature Neuroscience*, *9*(11), 1432–1438. https://doi.org/10.1038/nn1790

Macleod, A. & Summerfield, Q. (1987). Quantifying the contribution of vision to speech perception in noise. *British Journal of Audiology*, *21*(2), 131-141

Madrid, R., Sanhueza, M., Alvarez, O., & Bacigalupo, J. (2003). Tonic and phasic receptor neurons in the vertebrate olfactory epithelium. *Biophysical Journal*, *84*(6), 4167–4181. https://doi.org/10.1016/S0006-3495(03)75141-8

Makino, H., & Komiyama, T. (2015). Learning enhances the relative impact of top-down processing in the visual cortex. *Nature Neuroscience*, *18*(8), 1116–1122. https://doi.org/10.1038/nn.4061

Matusz, P. J., Thelen, A., Amrein, S., Geiser, E., Anken, J., & Murray, M. M. (2015). The role of auditory cortices in the retrieval of single-trial auditory-visual object memories. *European Journal of Neuroscience*, *41*(5), 699–708. https://doi.org/10.1111/ejn.12804

Matusz, P. J., Wallace, M. T., & Murray, M. M. (2017). A multisensory perspective on object memory. *Neuropsychologia*, *105*(April), 243–252. https://doi.org/10.1016/j.neuropsychologia.2017.04.008

McGurk, H., & MacDonald, J. (1976). Hearing lips and seeing voices. *Nature,* *264*(5588), 746–748. doi:10.1038/264746a0

Megginson, L. C. (1963). “Lessons from Europe for American Business.” *Southwestern Social Science Quarterly,* *44*(1): 3-13

Meredith, M. A., & Stein, B. E. (1986). Visual, auditory, and somatosensory convergence on cells in superior colliculus results in multisensory integration. *Journal of Neurophysiology*, *56*(3), 640–662. https://doi.org/10.1152/jn.1986.56.3.640

Meredith, M., & Stein, B. (1983). Interactions among converging sensory inputs in the superior colliculus. *Science*, *221*(4608), 389–391. https://doi.org/10.1126/science.6867718

Milner, B., & Scoville, W. B. (1957). Loss of recent memory after bilateral hippocampal lesions. *Journal of Neurology, Neurosurgery and Psychiatry*, *20*(11), 11–22.

Mohan, H., de Haan, R., Mansvelder, H. D., & de Kock, C. P. J. (2018). The posterior parietal cortex as integrative hub for whisker sensorimotor information. *Neuroscience*, *368*, 240–245. https://doi.org/10.1016/j.neuroscience.2017.06.020

Moreno-Bote, R. (2014). Poisson-Like Spiking in Circuits with Probabilistic Synapses. *PLoS Computational Biology*, *10*(7). https://doi.org/10.1371/journal.pcbi.1003522

Moser, M.-B., Rowland, D. C., & Moser, E. I. (2015). Place cells, grid cells, and memory. *Cold Spring Harbor Perspectives in Medicine*, *5*(1), a021808. https://doi.org/10.1101/cshperspect.a021808

Murray, M. M., Foxe, J. J., & Wylie, G. R. (2005). The brain uses single-trial multisensory memories to discriminate without awareness. *NeuroImage*, *27*(2), 473–478. https://doi.org/10.1016/j.neuroimage.2005.04.016

Nakamura, K. (1999). Auditory spatial discriminatory and mnemonic neurons in rat posterior parietal cortex. *Journal of Neurophysiology*, *82*(5), 2503–2517.

Noel, J. P., Modi, K., Wallace, M. T., & Van der Stoep, N. (2018). Audiovisual integration in depth: multisensory binding and gain as a function of distance. *Experimental Brain Research*, *236*(7), 1939–1951.

https://doi.org/10.1007/s00221-018-5274-7

O'Keefe, J., & Dostrovsky, J. (1971). Short Communications The hippocampus as a spatial map: Preliminary evidence from unit activity in the freely moving rat. *Brain Research*, *34*, 171–175.

Odegaard, B., Wozny, D. R., & Shams, L. (2015). Biases in Visual, Auditory, and Audiovisual Perception of Space. *PLoS Computational Biology*, *11*(12), 1–23. https://doi.org/10.1371/journal.pcbi.1004649

Ohshiro, T., Angelaki, D. E., & Deangelis, G. C. (2011). A normalization model of multisensory integration. *Nature Neuroscience*, *14*(6), 775–782. https://doi.org/10.1038/nn.2815

Olivarria, J. & Montero, V.M. (1981). Reciprocal connections between the striate cortex and extrastriate cortical visual areas in the rat. *Brain Research, 217*(2), 358–363. doi:10.1016/0006-8993(81)90011-1

Palomero-Gallagher, N. & Zilles, K. (2004). Isocortex. In *The Rat Nervous System* (pp. 728-747). San Diego, California: Elsevier Academic Press

Pilkiw, M., Insel, N., Cui, Y., Finney, C., Morrissey, M. D., & Takehara-Nishiuchi, K. (2017). Phasic and tonic neuron ensemble codes for stimulus-environment conjunctions in the lateral entorhinal cortex. *ELife*, *6*, 1–22. https://doi.org/10.7554/eLife.28611

Pinto-Hamuy, T., Montero, V. M., & Torrealba, F. (2004). Neurotoxic lesion of anteromedial/posterior parietal cortex disrupts spatial maze memory in blind rats. *Behavioural Brain Research*, *153*(2), 465–470. https://doi.org/10.1016/j.bbr.2004.01.003

Polley, D. B. (2006). Perceptual Learning Directs Auditory Cortical Map Reorganization through Top-Down Influences. *Journal of Neuroscience*, *26*(18), 4970–4982. https://doi.org/10.1523/jneurosci.3771-05.2006

Pons, T.P., Garraghty, P.E., Friedman, D.P., & Mishkin, M. (1987). Physiological

evidence for serial processing in somatosensory cortex. *Science, 237*, 417–420

Raij, T., Karhu, J., Kičić, D., Lioumis, P., Julkunen, P., Lin, F. H., … Belliveau, J. W. (2008). Parallel input makes the brain run faster. *NeuroImage*, *40*(4), 1792–1797. https://doi.org/10.1016/j.neuroimage.2008.01.055

Raposo, D., Sheppard, J. P., Schrater, P. R., & Churchland, A. K. (2012). Multisensory Decision-Making in Rats and Humans. *Journal of Neuroscience*, *32*(11), 3726–3735. https://doi.org/10.1523/jneurosci.4998-11.2012

Raposo, David, Kaufman, M. T., & Churchland, A. K. (2014). A category-free neural population supports evolving demands during decision-making. *Nature Neuroscience*, *17*(12), 1784–1792. https://doi.org/10.1038/nn.3865

Redish, A. D. (1999). Route Navigation: Taxon and Praxic Strategies. In *Beyond the cognitive map: From place cells to episodic memory* (pp. 35-45). Cambridge, Massachusetts: the MIT Press

Romo, R., & de Lafuente, V. (2013). Conversion of sensory signals into perceptual decisions. *Progress in Neurobiology*, *103*, 41–75. https://doi.org/10.1016/j.pneurobio.2012.03.007

Ross, L. A., Saint-Amour, D., Leavitt, V. M., Javitt, D. C., & Foxe, J. J. (2007). Do you see what I am saying? Exploring visual enhancement of speech comprehension in noisy environments. *Cerebral Cortex*, *17*(5), 1147–1153. https://doi.org/10.1093/cercor/bhl024

Rousselet, G. A., & Pernet, C. R. (2011). Quantifying the time course of visual object processing using ERPs: It's time to up the game. *Frontiers in Psychology*, *2*(MAY), 1–6. https://doi.org/10.3389/fpsyg.2011.00107

Sakata, S., Yamamori, T., & Sakurai, Y. (2004). Behavioral studies of auditory-visual spatial recognition and integration in rats. *Experimental Brain Research*, *159*(4), 409–417. https://doi.org/10.1007/s00221-004-1962-6

Sánchez, R. F., Montero, V. M., Espinoza, S. G., Díaz, E., Canitrot, M., & Pinto-

Hamuy, T. (1997). Visuospatial discrimination deficit in rats after ibotenate lesions in anteromedial visual cortex. *Physiology and Behavior*, *62*(5), 989–994. https://doi.org/10.1016/S0031-9384(97)00201-1

Sargolini, F., Fyhn, M., Hafting, T., McNaughton, B. L., Witter, M. P., Moser, M. B., & Moser, E. I. (2006). Conjunctive representation of position, direction, and velocity in entorhinal cortex. *Science*, *312*(5774), 758–762. https://doi.org/10.1126/science.1125572

Schiffino, F. L., Zhou, V., & Holland, P. C. (2014). Posterior parietal cortex is critical for the encoding, consolidation, and retrieval of a memory that guides attention for learning. *European Journal of Neuroscience*, *39*(4), 640–649. https://doi.org/10.1111/ejn.12417

Schröger, E., & Widmann, A. (1998). Speeded responses to audiovisual signal changes result from bimodal integration. *Psychophysiology*, *35*(6), 755–759. https://doi.org/10.1017/S0048577298980714

Seilheimer, R. L., Rosenberg, A., & Angelaki, D. E. (2014). Models and processes of multisensory cue combination. *Current Opinion in Neurobiology*, *25*, 38–46. https://doi.org/10.1016/j.conb.2013.11.008

Seitz, A. R., Kim, R., & Shams, L. (2006). Sound Facilitates Visual Learning. *Current Biology*, *16*(14), 1422–1427. https://doi.org/10.1016/j.cub.2006.05.048

Sekuler, R., Sekuler, A.B. & Lau, R. (1997). Sound alters visual motion perception. *Nature, 385*, 308. https://doi.org/10.1038/385308a0

Shams, L., & Seitz, A. R. (2008). Benefits of multisensory learning. *Trends in Cognitive Sciences*, *12*(11), 411–417. https://doi.org/10.1016/j.tics.2008.07.006

Sheppard, J. P., Raposo, D., & Churchland, A. K. (2013). Dynamic weighting of multisensory stimuli shapes decision-making in rats and humans. *Journal of Vision*, *13*(6), 4–4. https://doi.org/10.1167/13.6.4

Siemann, J. K., Muller, C. L., Bamberger, G., Allison, J. D., Veenstra-VanderWeele,

J., & Wallace, M. T. (2015). A novel behavioral paradigm to assess multisensory processing in mice. *Frontiers in Behavioral Neuroscience*, *8*(January), 1–10. https://doi.org/10.3389/fnbeh.2014.00456

Squire, L., Bloom, F., Spitzer, N., Du Lac, S., Ghosh, A., & Berg, D. (2008). Sensory Systems. In *Fundamental Neuroscience* (pp. 535-637). San Diego, California: Elsevier Academic Press

Solstad, T. (2008). Representation of Geometric Borders in the Entorhinal Cortex. *Science (New York, N.Y.)*, *1865*(5909), 1–5. https://doi.org/10.1126/science.1166466

Stanford, T. R., & Stein, B. E. (2007). Superadditivity in multisensory integration: Putting the computation in context. *NeuroReport*, *18*(8), 787–792. https://doi.org/10.1097/WNR.0b013e3280c1e315

Stein, B. E., Burr, D., Constantinidis, C., Laurienti, P. J., Alex Meredith, M., Perrault, T. J., … Lewkowicz, D. J. (2010). Semantic confusion regarding the development of multisensory integration: A practical solution. *European Journal of Neuroscience*, *31*(10), 1713–1720. https://doi.org/10.1111/j.1460-9568.2010.07206.x

Stein, B. E., Meredith, M. A., Huneycutt, W. S., & McDade, L. (1989). Behavioral indices of multisensory integration: Orientation to visual cues is affected by auditory stimuli. *Journal of Cognitive Neuroscience, 1*(1), 12-24. http://dx.doi.org/10.1162/jocn.1989.1.1.12

Stein, B. E., & Stanford, T. R. (2008). Multisensory integration: Current issues from the perspective of the single neuron. *Nature Reviews Neuroscience*, *9*(4), 255–266. https://doi.org/10.1038/nrn2331

Stevenson, R. A., Bushmakin, M., Kim, S., Wallace, M. T., Puce, A., & James, T. W. (2012). Inverse effectiveness and multisensory interactions in visual event-related potentials with audiovisual speech. *Brain Topography*, *25*(3), 308–326. https://doi.org/10.1007/s10548-012-0220-7

Sumby, W. H., & Pollack, I. (1954). Visual contribution to speech intelligibility in noise. *The Journal of the Acoustical Society of America*, *26*(2), 212–215.

Talsma, D., Doty, T. J., & Woldorff, M. G. (2007). Selective attention and audiovisual integration: Is attending to both modalities a prerequisite for early integration? *Cerebral Cortex*, *17*(3), 679–690. https://doi.org/10.1093/cercor/bhk016

Thelen, A., Talsma, D., & Murray, M. M. (2015). Single-trial multisensory memories affect later auditory and visual object discrimination. *Cognition*, *138*, 148–160. https://doi.org/10.1016/j.cognition.2015.02.003

Tolhurst, D. J., Movshon, J. A., & Dean, A. F. (1983). The statistical reliability of signals in single neurons in cat and monkey visual cortex. *Vision Research*, *23*(8), 775–785. https://doi.org/10.1016/0042-6989(83)90200-6

van Ee, R., van Boxtel, J. J. A., Parker, A. L., & Alais, D. (2009). Multisensory Congruency as a Mechanism for Attentional Control over Perceptual Selection. *Journal of Neuroscience*, *29*(37), 11641–11649. https://doi.org/10.1523/jneurosci.0873-09.2009

Wallace, M. T., & Stein, B. E. (1996). Chapter 21 Sensory organization of the superior colliculus in cat and monkey. *Progress in Brain Research*, *112*(C), 301–311. https://doi.org/10.1016/S0079-6123(08)63337-3

Woodman, G. F. (2010) A brief introduction to the use of event-related potentials in studies of perception and attention. *Attention, Perception, & Psychophysics, 72*, 2031–46. https://doi.org/10.3758/BF03196680

Wu, W., Chen, Z., Gao, S., & Brown, E. N. (2011). A hierarchical Bayesian approach for learning sparse spatio-temporal decompositions of multichannel EEG. *NeuroImage*, *56*(4), 1929–1945. https://doi.org/10.1016/j.neuroimage.2011.03.032

Yamashita, T., & Petersen, C. C. H. (2016). Target-specific membrane potential dynamics of neocortical projection neurons during goal-directed behavior.

ELife, *5*(JUN2016), 1–11. https://doi.org/10.7554/eLife.15798

Yan, Y., Rasch, M. J., Chen, M., Xiang, X., Huang, M., Wu, S., & Li, W. (2014). Perceptual training continuously refines neuronal population codes in primary visual cortex. *Nature Neuroscience*, *17*(10), 1380–1387. https://doi.org/10.1038/nn.3805

Zhou, W., & Crystal, J. D. (2009). Evidence for remembering when events occurred in a rodent model of episodic memory. *Proceedings of the National Academy of Sciences of the United States of America*, *106*(23), 9525–9529. https://doi.org/10.1073/pnas.0904360106